Università degli Studi del Piemonte Orientale “Amedeo Avogadro”
Department of Health Sciences
PhD Program in Food, Health and Longevity
XXXVI Cycle

3D *In Vitro* Model of Osteosarcoma: Advantages and Limitations of Two Distinct Approaches

S.S.D. MED/50

Candidate:
Ksenia Menshikh

Supervisor:
Prof. Lia Rimondini, DDS
Co-Supervisor:
Prof. Janis Locs
Coordinator:
Prof. Antonia Follenzi

a.a. 2023/2024

Contents

Description of the MSCA ITN Project PREMUROSA

The work presented in this thesis is part of the PREMUROSA project – Marie Skłodowska-Curie Actions (MSCA) Innovative Training Network (ITN) funded by the EU Framework Programme for Research and Innovation Horizon 2020 (GA no. 860462). The project's consortium is composed of 13 early-stage researchers (ESRs), 9 academic and 4 non-academic members, and 6 industrial partner organizations. The project is coordinated by the University of Eastern Piedmont (Università degli studi del Piemonte Orientale Amedeo Avogadro, UPO), where I am employed as a PhD candidate and as ESR5 of the PREMUROSA project. The Center on Autoimmune and Allergic Diseases (CAAD, Novara, Italy) is a research infrastructure of UPO and is the main location of my research activities. CAAD is an interdisciplinary centre where research groups of UPO from different scientific fields collaborate and benefit from high-level equipment. Representatives of academic, non-academic and public sectors are hosted at CAAD.

PREMUROSA – 'Precision medicine for musculoskeletal regeneration, prosthetics and active ageing' – aims at "developing a new generation of scientists equipped with an integrated vision of the whole value chain in musculoskeletal regeneration technologies and able to boost the necessary innovations to achieve precision principles in developing innovative devices and optimized clinical applications". The project's scope was conceptualized with the Latin-derived term "*premurosa*" meaning "to take care with care". The training program offered by PREMUROSA is a comprehensive combination of courses and workshops hosted locally at partner institutions and as yearly summer schools. In addition, each ESR benefits from secondments to different partner institutions widening their research experience by getting hands-on with various equipment and facing different working approaches and cultures.

As ESR 5, I benefited from 3 secondment periods. At the Faculty of Technology and Metallurgy of the University of Belgrade (Belgrade, Serbia) under the supervision of Prof. Bojana Obradovic, I worked on the application of perfusion conditions to the alginate-based osteosarcoma *in vitro* model using bioreactor systems. At CÚRAM of the University of Galway (Galway, Ireland) under the supervision of Prof. Abhay Pandit, I investigated the potential of 3D-printed calcium phosphate scaffolds to simulate bone microenvironment. Finally, at EU CORE Consulting (Turin, Italy) under the supervision of Irene Liverani, I received full training on the preparation of the postdoctoral project proposal.

The primary objective of the PREMUROSA consortium is to develop a thorough comprehension of the intricate relationship between the properties of biomaterials, cell response in conventional and advanced *in vitro* models, and the distinct attributes of each patient. Currently, the approach to treating musculoskeletal disorders focuses on prosthetic rehabilitation or regenerative surgeries like biomaterial implantation. In both cases, the inflammatory and regenerative reactions of specific tissues, combined with the suitability of the implanted material, significantly influence the final treatment results. By tackling these intricacies, PREMUROSA strives to redefine and enhance the benchmarks of care in musculoskeletal regeneration.

Abstract

In the realm of anti-cancer drug development, three-dimensional (3D) cell culture models *in vitro* have emerged as promising alternatives to conventional two-dimensional (2D) monolayer and animal models due to their physiological relevance and potential for personalized medicine. However, existing models primarily focus on soft tissue cancers, neglecting the complexities of hard tissue cancers such as osteosarcoma.

This thesis aims to address this gap by developing a robust, tuneable, and reproducible *in vitro* model of primary bone cancer – osteosarcoma – that mimics the complexity of bone tissue and the heterogeneity of the tumour microenvironment while integrating mechanical stimuli that are characteristic of the musculoskeletal system.

The main objectives include optimizing cell spheroid generation methods, developing a synthetic scaffold mimicking bone tissue, evaluating the scaffold cytocompatibility and performance in dynamic culture systems, and assembling a tri-culture 3D *in vitro* model applicable for drug testing.

Chapter 1 discusses the importance of a cell spheroid-based approach as the first step from 2D to 3D and presents a method for their generation applicable to the osteosarcoma cell line of choice. Chapter 2 focuses on the development of freeze-dried alginate-based porous scaffolds, their characterization, application, and limitations. Chapter 3 investigates 3D-printed tricalcium phosphate scaffolds via material characterization and biological evaluation with emphasis on primary human bone-marrow-derived mesenchymal stem cells, as well as evaluates scaffold performance in various bioreactor systems. Chapter 4 discusses the assembly of the described components into a tri-culture 3D *in vitro* model in a perfusion bioreactor, culminating in the testing of an anticancer compound.

Through interdisciplinary collaborations and innovative approaches, this thesis contributes to the advancement of *in vitro* modelling of skeletal diseases on the example of osteosarcoma, offering an approach for designing a platform aimed at more accurate drug screening and personalized treatment strategies.

Sommario

Nel campo dello sviluppo di farmaci antitumorali, i modelli di colture cellulari tridimensionali (3D) *in vitro* sono emersi come alternative promettenti ai convenzionali modelli bidimensionali (2D) e animali grazie alla loro rilevanza fisiologica e al potenziale nel campo della medicina personalizzata. Tuttavia, i modelli esistenti si concentrano principalmente sui tumori dei tessuti molli, trascurando le complessità dei tumori dei tessuti duri come l'osteosarcoma.

Questa tesi mira a colmare questo divario sviluppando un modello *in vitro* robusto, modulabile e riproducibile di cancro osseo primario – l'osteosarcoma – che imita la complessità del tessuto osseo e l'eterogeneità del microambiente tumorale integrando stimoli meccanici caratteristici dell'apparato muscolo-scheletrico.

Gli obiettivi principali includono l'ottimizzazione dei metodi di generazione di sferoidi cellulari, lo sviluppo di una matrice sintetica che imita il tessuto osseo, la valutazione della citocompatibilità e delle prestazioni della matrice stessa nei sistemi di coltura dinamica e l'assemblaggio di un modello *in vitro* 3D tri-colturale applicabile per la valutazione di farmaci antitumorali.

Il Capitolo 1 discute l'importanza dell'approccio basato su sferoidi cellulari come primo passo dal 2D al 3D e presenta un metodo per la loro generazione applicabile alla linea cellulare di osteosarcoma scelta. Il Capitolo 2 si concentra sullo sviluppo di scaffolds porosi a base di alginato liofilizzato, sulla loro caratterizzazione, applicazione ed eventuali limitazioni. Il Capitolo 3 analizza gli scaffolds di fosfato tricalcico stampati in 3D attraverso la caratterizzazione dei materiali e la loro valutazione biologica, con particolare attenzione alle cellule staminali mesenchimali primarie derivate dal midollo osseo umano, oltre a valutare le prestazioni degli scaffold in vari sistemi a bioreattore. Il Capitolo 4 discute l'assemblaggio dei componenti descritti in un modello *in vitro* 3D tri-colturale in un bioreattore a perfusione, culminando nella sperimentazione di un composto antitumorale usato correntemente in clinica.

Attraverso collaborazioni interdisciplinari e approcci innovativi, questa tesi contribuisce al progresso della modellizzazione *in vitro* delle malattie scheletriche sull'esempio dell'osteosarcoma, offrendo un approccio innovativo per la progettazione di una piattaforma mirata per uno screening farmacologico più accurato e per nuove strategie di trattamento personalizzate.

General Introduction

In modern drug development, the journey from the emergency of a new therapeutic substance until its actual approval is nothing but lengthy and expensive. Approximately 75% of the investment is the cost of failure in this field, ½ of which is caused by lack of efficacy and ¼ – by excess toxicity (Ewart et al., 2022). Mostly, these statistics are driven by the flaws of the standard testing pipeline: conventional *in vitro* models → animal studies → clinical trials. *In vitro* models are presented by oversimplified two-dimensional (2D) cell monolayers, while animal models do not fully recapitulate the pathophysiology of the disease – thus, the reliability of testing and efficiency of sorting out "weak" candidates in these first stages is relatively low. As a result, nine of ten candidates entering clinical trials fail (Sun et al., 2022). These economic circumstances form the need for reliable testing methods as well as advanced test models. In the context of anti-cancer drug development, three-dimensional (3D) cell culture models are becoming widely used as test systems thanks to their similarity with physiological conditions of tumour growth and their potential to bridge the *in vitro/in vivo* gap (Pinto et al., 2020). Moreover, the use of a 3D spheroid or organoid model grown from patient-derived cells is known to be a promising approach for finding a personalized treatment strategy – therapy that would work best for the patient (Al-Aloosi et al., 2024; Gray et al., 2023). Due to a high number of incidences of such types of malignancies as lung, prostate and breast cancer (IARC, 2022), most studies focus mainly on modelling soft tissue cancer. However, there is a tendency for such cancers to metastasize to bones, and primary bone cancer itself poses a burden to society affecting adolescents and elderly people and being a poorly diagnosed and aggressive cancer (Zhao et al., 2021). Bone, unlike soft tissues, possesses remarkable stiffness and high mineral content, and mimicking the complexity of this tissue along with the heterogeneity of the tumour microenvironment remains an unconquered challenge (De Luca et al., 2018).

The **goal** of this thesis is to develop a robust, tuneable and reproducible *in vitro* model of primary bone cancer – osteosarcoma – that mimics the complexity of bone tissue and heterogeneity of the tumour microenvironment and implements the mechanical stimuli characteristic of the musculoskeletal system.

The **main objectives** of the thesis are:

- To optimize the method of cell spheroids generation – the basic "building block" of modern *in vitro* models of cancer representing the tumour unit – applicable to the osteosarcoma cell line of choice;
- To develop and characterize synthetic scaffold simulating bone tissue from the points of its microstructural and mechanical features, including its compatibility with perfusion culture conditions;
- To evaluate the scaffold from the biological perspective via testing it towards multiple cell types-representatives of bone tumour microenvironment;
- To assemble an *in vitro* co-culture 3D model with the use of the scaffold and perfusion conditions and perform a preliminary assessment of the model's application for testing anti-cancer drugs.

The thesis is structured as follows. **Chapter 1** starts with a review of primary and metastatic bone cancer and the reasons underlying the stagnation of survival rate. Later on, it discusses the importance of spheroids as basic "building blocks" of advanced *in vitro* models of cancer, as well as their fundamental role in anti-cancer drug efficacy testing as a better alternative to conventional 2D monolayer models. In this chapter, possibilities of spheroid generation are described, and the experimental part focuses on the method applicable to the chosen osteosarcoma cell line. Additionally, it finds a solution to the common challenge in cell spheroid generation: not all cell lines form cell aggregates stable enough to be handled during the following application and analysis due to poor extracellular matrix (ECM) production. Finally, Chapter 1 outlines various techniques of cell spheroid characterization from the point of mechanical features and biological functions. The established methods of controllable spheroids generation and their application in biomaterials cytocompatibility studies are described in the manuscript "Bifunctional Mesoporous Glasses for Bone Tissue Engineering: Biological Effects of Doping with Cerium and Polyphenols in 2D and 3D *In Vitro* Models" published in *Biomaterials and Biosystems* journal of Elsevier publisher group (https://doi.org/10.1016/j.bbiosy.2024.100095).

Chapter 2 starts with an introduction focused on the key characteristics of the bone tumour environment: the complexity of bone tissue itself, the diversity of cell types and their interactions, and the peculiarities of the tumour matrix. It also briefly covers mechanical stimuli that play an important role in the fate of the cells residing in bone tissue. Overall, these features are observed as parameters to consider during the development of scaffold for simulating bone tissue in bone cancer models. In more detail, outer and inner mechanical stimuli in the context of bone cancer are described in the review article "Biomechanical Aspects in Bone Tumor Engineering" published in *Tissue Engineering, Part B: Reviews* journal of Mary Ann Liebert publisher group (https://doi.org/10.1089/ten.teb.2023.0106). The experimental part of Chapter 2 is dedicated to the development and application of freeze-dried alginate-based porous scaffolds. All the steps of the production contain controllable parameters – and, on the one hand, it opens up opportunities to obtain the desired characteristics such as porosity and rehydration rate, but on the other hand, may result in poor reproducibility. In Chapter 2 I discuss these parameters, and by varying several of them I obtain a number of scaffold types, which I eventually characterize. Material characterization is followed by biological evaluation employing *in vitro* tests with various cell types, including osteosarcoma cell spheroids. Finally, I introduce the perfusion bioreactor system as a source of efficient mass transport and mechanical stimuli and assess the excellence of the obtained alginate-based freeze-dried scaffolds from the point of application in a dynamic culture. This part of the work was done in collaboration with the research group led by Prof. Bojana Obradovic during my secondment to the Faculty of Technology and Metallurgy of the University of Belgrade (Belgrade, Serbia).

In **Chapter 3**, I move to a different approach. While the previous chapter is focused on the "soft scaffold-based" *in vitro* model, Chapter 3 is dedicated to the "hard scaffold-based" approach. With the use of one of the most widely utilized calcium phosphate – tricalcium phosphate – and 3D-printing technology, I aim to increase the reproducibility of the scaffolds, their mechanical stability and, thus, better performance in dynamic culture systems with constant medium flow. In addition to a comprehensive material characterization, I test the 3D-printed tricalcium phosphate scaffolds in various cell types-representatives of bone tumour

microenvironment. Such evaluation is of particular importance: even though calcium phosphates have long been the biomaterials of choice in the fields of dentistry and bone tissue engineering, their use *in vitro* should be carried out with caution. The pitfalls of direct-contact testing of calcium phosphates *in vitro* were extensively discussed in the manuscript "Challenging Applicability of ISO 10993-5 for Calcium Phosphate Biomaterials Evaluation: Towards More Accurate *In Vitro* Cytotoxicity Assessment" published in *Biomaterials Advances* of Elsevier publishers (https://doi.org/10.1016/j.bioadv.2024.213866). The main role of the investigated tricalcium phosphate scaffolds is to provide a suitable matrix for mesenchymal stem cells used for building a bone-like environment. Due to this reason, in Chapter 3 I paid special attention to the behaviour of primary human bone-marrow-derived mesenchymal stem cells on the scaffolds in prolonged cultured periods by analysing their transcriptome. Additionally, the performance of the scaffolds was evaluated in three different bioreactor systems. This part of the study was performed in collaboration with Prof. Jonathan Massera and Virginia Alessandra Gobbo of Tampere University (Tampere, Finland), and with the research group of Prof. Abhay Pandit during my secondment to CÚRAM of the University of Galway (Galway, Ireland).

Finally, **Chapter 4** serves to discuss the assembling of the "building blocks" described in the previous chapters into an advanced tri-culture 3D *in vitro* model in perfusion bioreactor. Consisting of stable osteosarcoma cell spheroids, tricalcium phosphate scaffolds pre-cultured with bone marrow-derived stem cells, and endothelial cells, the tri-culture models are arranged in the selected perfusion system and analysed after being cultured in static and dynamic conditions. In conclusion, the system is applied for testing a widely known anticancer compound.

References

Al-Aloosi, M., Prechtl, A. M., Chatterjee, P., Bernard, B., Kemp, C. J., Rosati, R., Diaz, R. L., Appleyard, L. R., Pereira, S., Rajewski, A., McDonald, A., Gordon, E. J., & Grandori, C. (2024). Case report: ex vivo tumor organoid drug testing identifies therapeutic options for stage IV ovarian carcinoma. *Frontiers in Oncology*, *13*. https://doi.org/10.3389/fonc.2023.1267650

De Luca, A., Raimondi, L., Salamanna, F., Carina, V., Costa, V., Bellavia, D., Alessandro, R., Fini, M., & Giavaresi, G. (2018). Relevance of 3d culture systems to study osteosarcoma environment. *Journal of Experimental and Clinical Cancer Research*, *37*(1), 1–15. https://doi.org/10.1186/s13046-017-0663-5

Ewart, L., Apostolou, A., Briggs, S. A., Carman, C. V., Chaff, J. T., Heng, A. R., Jadalannagari, S., Janardhanan, J., Jang, K.-J., Joshipura, S. R., Kadam, M. M., Kanellias, M., Kujala, V. J., Kulkarni, G., Le, C. Y., Lucchesi, C., Manatakis, D. V., Maniar, K. K., Quinn, M. E., … Levner, D. (2022). Performance assessment and economic analysis of a human Liver-Chip for predictive toxicology. *Communications Medicine*, *2*(1), 154. https://doi.org/10.1038/s43856-022-00209-1

Gray, H. J., Chatterjee, P., Rosati, R., Appleyard, L. R., Durenberger, G. J., Diaz, R. L., Swan, H. A., Peretti, D., Pollastro, M., Ainge, T., Kapeli, K., Pereira, S., Margossian, A. L., Banda, K., Goff, B. A., Swisher, E. M., Bernard, B., Kemp, C. J., & Grandori, C. (2023). Extraordinary clinical response to ibrutinib in low-grade ovarian cancer guided by organoid drug testing. *Npj Precision Oncology*, *7*(1), 45. https://doi.org/10.1038/s41698-023-00379-8

IARC. (2022). *Cancer Today*. https://gco.iarc.fr/today/en

Pinto, B., Henriques, A. C., Silva, P. M. A., & Bousbaa, H. (2020). Three-dimensional spheroids as in vitro preclinical models for cancer research. *Pharmaceutics*, *12*(12), 1–38. https://doi.org/10.3390/pharmaceutics12121186

Sun, D., Gao, W., Hu, H., & Zhou, S. (2022). Why 90% of clinical drug development fails and how to improve it? *Acta Pharmaceutica Sinica B*, *12*(7), 3049–3062. https://doi.org/10.1016/j.apsb.2022.02.002

Zhao, X., Wu, Q., Gong, X., Liu, J., & Ma, Y. (2021). Osteosarcoma: a review of current and future therapeutic approaches. In *BioMedical Engineering Online* (Vol. 20, Issue 1). BioMed Central Ltd. https://doi.org/10.1186/s12938-021-00860-0

1. Mimicking bone tumour environment *in vitro*: a step-by-step approach

1.1. Introduction

1.1.1. Primary bone cancer

Rare [0.2% of all malignancies (Forsyth & Hogendoorn, 2022)], yet aggressive, primary bone cancer tends to metastasize in the lungs, being a huge burden to society. Osteosarcoma is the most common type of primary bone cancer, followed by chondrosarcoma and Ewing sarcoma by number of incidences. Osteosarcoma is found among children and older people thus having a bimodal age distribution in the human population (Zhao et al., 2021). At a young age, bone remodelling is most active, and the imbalance of osteoclasts and osteoblasts responsible for bone resorption and formation, respectively, can serve as a favourable condition for the development of cancer. Osteosarcoma develops in the metaphyses of rapidly growing long bones such as the femur or lower leg (Jafari et al., 2020). Osteosarcoma can lead to pathological bone resorption as well as excessive bone growth. The osteolytic state is characterized by an imbalance between osteoblasts' and osteoclasts' activity when the latter is being pushed by tumour-derived or induced osteoclast activating factors. At the same time, the growth factors and calcium ions released in the process of bone resorption promote the following tumour progression. This positive feedback loop in the interaction of bone cancer cells with normal bone cells is described as a "vicious cycle" (Roodman & Silbermann, 2015). In brief, bone cancer cells release proteins that stimulate osteoblasts to produce a receptor activator of nuclear factor kappa-B ligand (RANKL). RANKL activates osteoclasts and thus enhances the destruction of bone tissue. One of the consequences of tissue degradation is the release of entrapped growth factors which have a positive effect on tumour progression and trigger further destruction of the bone (Buenrostro et al., 2016).

The aetiology of osteosarcoma is not fully understood. Nowadays, mesenchymal stem cells are thought to be the source of future tumour development, but also the tumour can be, for example, of osteoblastic or chondroblastic origin. Of the several genes whose expression is altered in osteosarcoma, RB1 and TP53 are the most frequent ones (De Luca et al., 2018). During tumour development, the whole bone tissue environment plays a role. Osteosarcoma is considered one of the most complex cancers in terms of molecular aberration. It is frequently marked that extracellular vesicles, acidic environment, and hypoxia are the key factors of osteosarcoma well-being (Yang et al., 2020).

Unfortunately, in the vast majority of cases it is diagnosed in the progressive stage due to the pain it causes or, less likely, occasionally. Modern osteosarcoma therapy strategies include surgical resection of the primary tumour alongside chemotherapy – doxorubicin (adriamycin), high-dose methotrexate, cisplatin, and ifosfamide (Harris & Hawkins, 2022). Resection is complicated and may lead to local recurrence, for sarcomas are of mesenchymal origin, and the tumour does not have a clear margin, unlike carcinomas (Brookes et al., 2021). A positive outcome may be reached by the application of Raman spectroscopy for single-cell live imaging of osteosarcoma or alternative precision techniques (D'Acunto et al., 2019). The

5-year survival rate in patients undergoing only surgical intervention is 10–20%, and it rises to 50–70% in case the tumour is localised and treated by chemotherapy (Hegyi et al., 2011). Metastase occurrence brings the survival rate down to 20–30% (Munoz-Garcia et al., 2021). Several potential targeted therapies for osteosarcoma are in development. In fact, novel drugs against osteosarcoma are expected and highly needed. It seems that molecular abnormalities currently explored in the field could be used as potential drug targets, including the deregulation of the p53 pathway as well as stem-cell-related signalling (Lindsey et al., 2017).

1.1.2. Bone metastases

It is a well-known fact in oncology that a tumour is capable of metastasizing. How do metastases occur? More than a century ago, Stephen Paget promoted the theory that metastasis formation is like a seed reaching favourable conditions for its growth (Fidler, 2003). Cells, like seeds, are being spread in large numbers and get into different organs and parts of the body, but only those of them that get into a suitable "soil" will give rise to metastases. The hypothesis is called 'seed and soil', where circulating cancer cells are the 'seeds' and the microenvironment is the 'soil'. We are now familiar with the process much better and at the moment we know several key stages of how metastases develop: carcinogenesis, growth of the primary tumour, neovascularization, invasion of tumour cells and their access to the circulatory system, survival during circulation, extravasation into the microvascular system of distant organs (bones in this case) and growth in them (Jafari et al., 2020).

If cancer cells have managed to spread in the body, there are organs and tissues in which the likelihood of unwanted "settling" of cells is higher than in others. Bones are just such organs, and they are most often subject to metastasis. There is also the concept of osteotropic types of cancer, which include such common oncopathologies as breast cancer, prostate cancer, and lung cancer. Bone metastasis has been found in 70% of people who died from breast cancer or prostate cancer. Unfortunately, there are no clinical signs or symptoms when distant metastases first emerge, and even in cases where a patient is in remission, solitary disseminated tumour cells may already be present in the bone tissue. While disseminated tumour cells possess a brief life span and typically do not progress into new, far-off solid tumours, cells with adequate proliferative capacity to effectively colonise bone can result in metastases (Buijs & van der Pluijm, 2009). High-tech imaging techniques, such as positron emission tomography, are used to diagnose bone metastases and arrange subsequent therapy. When these techniques are not feasible, a biopsy is required. To differentiate between chondrosarcoma, post-radiation osteosarcoma, osteomyelitis, etc., a biopsy is also required. Treatment of metastases consists of the use of radiotherapy in combination with other methods, for instance, immunotherapy. Since metastases change the bone tissue at a qualitative level, deteriorating the density and hardness, invading the nearest soft tissues and causing pain, patients often require surgical intervention (Marazzi et al., 2020).

It should be emphasized that there is a change in the balance between osteogenesis and bone resorption noticed during the progression of bone metastases: similarly, such disbalance is associated with the emergency of OS. There is a slight correlation between the type of cancer and the direction in which the balance will shift – towards the uncontrolled formation of bone tissue or its excessive destruction. But more often than this, these processes coexist.

1.1.3. Challenges in osteosarcoma therapy development

Since the 1980s, there has been little change in the 5-year overall survival and recurrence rates for localised OS, even if the number of limb-salvage surgeries has increased due to improvements in surgical methods and early detection. The lack of better treatment choices over the past 40 years has contributed to this stagnation (Tippett et al., 2023). In clinical trials examining novel medicines (immunotherapies such as mifamurtide, IL-2 or PD-1 inhibitors and tyrosine kinase inhibitors), the survival rate for patients has grown, although only a little, despite intense attempts to improve the prognosis for patients with OS, particularly those with overt metastases. It appears that further basic biology research and the development of medications targeting novel molecular pathways and processes (distinct from those targeted in clinical trials nowadays) will be necessary to achieve the long-sought significant increases in patient survival. The pursuit of this objective will be accelerated by optimal clinical trial design (Harris & Hawkins, 2022).

Before clinical trials and even before animal models, *in vitro* modelling needs attention. According to recent literature observations, current cell models for finding drug targets in chemoresistant osteosarcoma may point at the wrong molecular mechanisms. It is suggested, that for such *in vitro* tests, a panel of cell lines representing various types of osteosarcoma as well as cross-resistance to common therapeutic substances are needed, and the studies should investigate a clearly stated strategy of exposure to chemotherapy (Tippett et al., 2023). These will then need to be followed by carefully planned animal experiments (mostly – mouse and dog models) and phase II clinical trials, which should identify promising candidate therapies for phase III trial evaluation (Harris & Hawkins, 2022).

1.1.4. 3D *in vitro* models in disease modelling and drug discovery

Currently, most *in vitro* cell studies are conducted in 2D culture conditions, limiting the diversity of cell physiology compared to *in vivo* conditions caused by forced adaptation of cells to artificial plain surfaces and depriving them of essential cell-cell and cell-matrix contacts. Cultivating cells as monolayers – on plastic or glass – alters their metabolism, functionality, and phenotypic characteristics (Zschenker et al., 2012). As a result, cells cultured via standard methods lack the heterogeneity seen in the three-dimensional structure of tumours. To study tumour cell biology effectively, it is preferable to use a culture system that replicates the *in vivo* tumour microenvironment. Despite the primary obstacle to incorporating the third dimension into preclinical testing – the absence of standardised techniques for the characterization of 3D disease tissue models, – 3D cell cultures in cancer research offer a more accurate mimicry of tumour cell behaviour *in vivo*, making them superior to 2D systems for identifying therapeutic targets (Brancato et al., 2020). Transitioning to 3D cell culture systems aims to model tumour tissue architecture and nutrient movement more closely to physiological conditions, and, as a consequence, results in a significant difference in cell response to various treatments compared to monolayer cultures (Baek, Seo, Kim, et al., 2016; Baek, Seo, Lee, et al., 2016; Hoarau-Véchot et al., 2018).

The *in vivo* microenvironment of bone cancer, including cells, extracellular matrix (ECM), signalling molecules, and biomechanical forces, is a complex system with unknown contributions of each factor influencing cell behaviour and acting synergistically or nullifying

one other. Thus, simulating such a system *in vitro* seems an insurmountable challenge. To approach this challenge, the research community performs an act similar to reverse engineering – by disassembling the known *in vivo* systems and rebuilding them in controlled laboratory conditions unit by unit. One of such units has long been cancer cell spheroid – the first step on the way from 2D to 3D.

1.1.5. Cell spheroid as a fundamental building block

Cell spheroids have been in use for more than 50 years (Jubelin et al., 2022). Comparably economical, this approach enables to mimic several important features of avascular tumours such as an abundance of cell-cell and cell-ECM interactions, a gradient of oxygen and nutrients throughout the spheroid volume and altered gene expression and cell signalling (Pinto et al., 2020). Spheroid-based *in vitro* models are reproducible, and a correctly chosen method of spheroid generation is able to lead to homogenous results – spheroids of the same shape and size. Numerous methods for spheroids generation are available nowadays in a wide range: from cheap and demanding to more expensive ones allowing high-throughput analysis, from hanging drop method and ultra-low attachment plates to spinner flasks and matrix encapsulation (Pinto et al., 2020). Based on the size of the spheroid – which usually depends on the initial cell seeding number and the type of the cells used, – it is possible to control key features of the spheroid, such as its invasiveness and response to tested drugs. Moreover, the size will dictate the presence of 3 "zones" in the spheroid: the outer layer composed of proliferating cells, the middle layer of quiescent cells, and the necrotic core composed of cells lacking nutrients and gases due to permeation gradient throughout the spheroid volume (Jubelin et al., 2022). In a study employing spheroids formed out of 12 different cell lines including osteosarcoma, it was shown that the spheroids exceeding 200 μm in diameter formed a necrotic core. As for their functionality, the cytotoxicity assay of widely used anticancer agent doxorubicin resulted in a much higher IC50 in comparison to monolayer 2D culture (Baek, Seo, Kim, et al., 2016). The same research group performed the study using another well-known anticancer drug – cisplatin (Baek, Seo, Lee, et al., 2016). They underline that for some cell lines, even though judging from metabolic activity assays the cells were affected by the drug, visually the spheroids did not seem altered.

In the context of osteosarcoma, the following cell lines are frequently used: Saos-2, MG-63 and U2OS. Despite being of similar origin, the functional characteristics of the above-mentioned cell lines differ. For instance, according to the research by Mohseny and co-authors, MG-63 cells may differentiate along the chondroblasts lineage, while it is possible to trigger adipogenic differentiation of U2OS cells. Tumour formation was not observed after a first or second round of injection of MG-63 cells in mice. In contrast, tumour formation was observed after the second injection of U2OS cell suspension. Also, in that case, invasion, osteoid production and weak angiogenesis took place (Mohseny et al., 2011). In another study, an osteoblastic characterization of U2OS, Saos-2 and MG-63 cells was performed. While MG-63 profiling revealed that the cells were heterogenic and had both mature and immature osteoblastic features, U2OS cells appeared to be negative for the majority of osteoblastic markers and positive for type IV collagen and cartilage markers like collagen II, IX and X (Pautke et al., 2004). Moreover, different osteosarcoma cell lines show distinct susceptibility

to ferroptosis – an iron-dependent form of cell death – which correlates with their mesenchymal phenotype (Panczyszyn et al., 2024). Overall, these data indicate heterogeneity of osteosarcoma cell lines in terms of their functionality.

1.1.6. From spheroids to organoids

While cell spheroids are usually stable cell aggregates comprised of one type of cells, organoids are more advanced structures: they can be either composed of various types of cells, embedded in a matrix, or both. To understand how to advance cell spheroids used for bone tumour engineering applications – which cell type to introduce – it is essential to untangle the complex cell-cell interactions present in the bone tumour microenvironment.

The cells of various types, except for tumour cells, reside in tumour stroma and comprise less than 5% of the total cell number (Chow et al., 2021). Stroma was found to have a considerable effect on tumour growth, progress, and metastasis. More precisely, stromal cells secrete cytokines which affect tumour cell proliferation and drug resistance (Cortini et al., 2019). Cells that are part of the osteosarcoma cell microenvironment should be perceived in the context of bone tissue.

The main cell types that constitute the bone cancer microenvironment are bone cells (osteoblasts, osteoclasts, osteocytes), stromal cells (mesenchymal cells, fibroblasts), vascular cells (endothelial, pericytes), and immune cells. Cancer cells take advantage of the surroundings by exploiting other cells in the process of tumour development and progression. Crosstalk of cancer and normal cells is particularly interesting: it can be conducted directly via intracellular communication or indirectly by paracrine signalling and also via different soluble factors among which are growth factors such as TGF, VEGF, FGF, chemokines, cytokines and others (C. F. Monteiro et al., 2019). The interaction of bone cancer cells with normal bone cells is no exception; moreover, it is organized as a “vicious cycle” already described above (Buenrostro et al., 2016). The interplay between tumour cells and mesenchymal stromal/stem cells (MSCs) is of particular interest due to the evidence that MSCs may play a role in both tumour growth inhibition and progression (Freeman et al., 2022).

It is well established that the gradient of chemokines and/or cytokines, including SDF-1, MIF, and TGF-β, draws MSCs to the wound site. Additionally, MSCs may be drawn to the tumour's development because the tumour and its surrounding tissue can be identified as a "never-healing wound," which may draw MSCs through related signalling pathways (Papaccio et al., 2017; Zheng et al., 2018).

The release of VEGF to boost cancer growth and metastasis is one of the roles played by MSCs at the tumour site. Tu et al. constructed a basic *in vitro* model utilising osteosarcoma cells and MSCs. Conventionally cultivated MSCs from femur fracture were supplemented with the conditioned medium following the culturing of Saos-2 and U2OS osteosarcoma cells (Tu et al., 2014).

Numerous studies have also demonstrated that MSCs have the opposite effect on the formation of tumours. When MG-63 osteosarcoma cells were cultivated in a medium conditioned with MSCs, there was a noticeable suppression of the cells' migration and proliferation. Then, it was thought that TGF-β was involved in the initiation of autophagy processes in osteosarcoma cells (Gauthaman et al., 2012). However, it is important to note that

MSCs from the human umbilical cord were used in the study to limit cancer growth, and it is well known that the secretion profile of these cells differs from MSCs from other sources, such as bone marrow (Han et al., 2022).

The inclusion of MSCs increases the stemness of cancer cells, hence they must be taken into account for designing *in vitro* cancer models. Enhanced drug resistance results from the promoted cancer cell stemness, which is brought about by a number of variables, including IL-6 (Zheng et al., 2018). For example, Freeman et al. employed an *in vitro* model based on direct co-culture of osteosarcoma cells and MSCs in the form of spheroid for the first time in this setting, mimicking various stages of osteosarcoma progression (Freeman et al., 2022).

In summary, considering the design of *in vitro* models that suggest the formation of a bone-like microenvironment, it would be possible to have MSCs that are not differentiated. This would allow osteosarcoma and MSCs to interact and promote cancer invasiveness, stemness, and proliferation.

1.2. Aim

In this Chapter, I aim to define the method of controllable spheroid generation and optimize it for the chosen osteosarcoma cell line. As an essential component of the advanced *in vitro* osteosarcoma model, the cell spheroid should possess sufficient mechanical properties, heterogeneity of cell population and functional potential. For these reasons, I do not limit the experimental part of the present Chapter to the generation of the spheroids but extend it to the characterization of the spheroid by quantitative analysis of bright-field microscopy monitoring, metabolic activity assay, nanoindentation analysis, scanning electron microscopy and migration assay. On the examples of the spheroids, I also demonstrate an approach to quantitative live/dead assay. In addition, I complement this part of the thesis with gene expression analysis to demonstrate the upregulation of several key genes in the resulting 3D model in comparison to cells cultured in 2D.

1.3. Materials and Methods

1.3.1. Materials

Low-glucose, as well as high-glucose Dulbecco's modified Eagle's medium (DMEM), fetal bovine serum (FBS), trypsin EDTA 1X, ethanol (EtOH, BioUltra, ≥ 99.8%, molecular biology grade, CAS: 64-17-5), phosphate-buffered saline (PBS, ready-to-use tablets, Ref. N. P4417-100TAB), resazurin sodium salt (Ref. N. R7017-5G, CAS: 62758-13-8), alginic acid sodium salt (medium viscosity Cat. No. A2033-250G), paraformaldehyde (Reagent grade, crystalline, Ref. N. P6148-1KG, CAS: 30525-89-4), hexamethyldisilazane (HMDS, Alfa Aesar, Waltham, USA) and collagen (PureCol® EZ Gel, 5 mg/mL) were purchased from Sigma-Aldrich, USA. Penicillin-streptomycin (PS) and fluorescent live/dead assay (LIVE/DEAD, L3224) were purchased from Invitrogen, USA. Multiwell plates (Ref. N. 30024) were purchased from SPL Life Sciences, Korea. Certified Molecular Biology Agarose

(Cat. No. 1613100), iScript™ cDNA Synthesis Kit and master mix for quantitative real-time PCR (SsoAdvanced Universal SYBR Green Supermix) were purchased from Bio-Rad Laboratories, USA. Primers for qPCR were designed using PrimerQuest™ Tool and synthesized by Integrated DNA Technologies (IDT, USA). was purchased from Bio-Rad Laboratories, USA. Cell lines used for the research have the following specifications: human bone marrow-derived stem cells (hBMSCs, hTERT-BMSC clone Y201, isolated from bone marrow and immortalized through hTERT lentiviral vectors (James et al., 2015)) were kindly provided by Prof. P. Genever, University of York; human umbilical vein cell line (EA.hy926, CRL2922) and human osteosarcoma cell line (U2OS, HTB96) were purchased in American Type Culture Collection, Manassas, VA, USA.

1.3.2. Cell culture and spheroid generation

Human bone marrow-derived stem cells (hBMSCs Y201) were cultivated in low-glucose DMEM supplemented with 15% FBS and 1% PS. Human osteosarcoma cells (U2OS) were cultivated in high-glucose DMEM supplemented with 10% FBS and 1% PS. All cell lines were cultivated at 37 ºC in the humidified atmosphere containing 5% CO_2. Before experiments, cells were cultivated until 80-90% confluence, detached by trypsin-EDTA solution, harvested, and used for experiments.

For spheroid generation, firstly, wells of a 48-well plate were coated with 1.5% agarose solution in sterile conditions and let solidify and sterilize at room temperature (RT) under UV exposure for 2 h. Then, hBMSCs and U2OS cells were seeded in the amount of $1x10^5$ cells per well of the agarose-coated plate – as monocultures or in proportions of 1:3 and 3:1. Cells were incubated in standard conditions with medium (relevant for each cell line or 1:1 mix) being changed every 2 or 3 days. Self-aggregation of the spheroids was monitored by light microscopy.

1.3.3. Cell viability assays

To assess the metabolic activity of cells, the dye resazurin, better known as alamarBlue™, was used. The choice of the dye was dictated by its sensitivity, absence of cytotoxicity, and the ability to use it for both quantitative and qualitative analysis over a long period. Resazurin is a water-soluble non-fluorescent violet dye. When added to metabolically active cells, resazurin acts as an electron acceptor and transforms into a reduced form - resorufin. In opposite to violet-coloured non-fluorescent resazurin, resorufin is pink and fluorescent. On the $1^{st,}$ 3^{rd} and 7^{th} days, the medium was removed from each well and replaced with alamarBlue™ solution in fresh culture medium. Plates were incubated in the dark for 3 h, and then 100 µl were transferred into a black opaque 96-well plate and read with a spectrophotometer (Spark®, Tecan Trading AG, CH) using the following set-up: fluorescence excitation wavelength 560 nm, emission reading 590 nm. Results were presented in relative fluorescent units (RFU).

To assess the spatial arrangement of live and dead cells, a standard method of staining with Calcein AM and Ethidium homodimer-1 was used. The stained spheroids were analysed with the help of a multiphoton microscope (TCS SP8 MP Multiphoton Microscope, Leica, Japan). The images taken through the volume of the spheroid along the z-axis with the use of different lasers were analysed in ImageJ (version 1.54d) using a script for batch folder analysis

(Menshikh, 2024). The principle of image analysis is presented in Figure 1-1. In brief, the images were separated by channels (green for live cells and red for dead cells), converted to binary, and then the area of stained cells was calculated. The ratio of live cell area to dead cell area was calculated for each spheroid analysed.

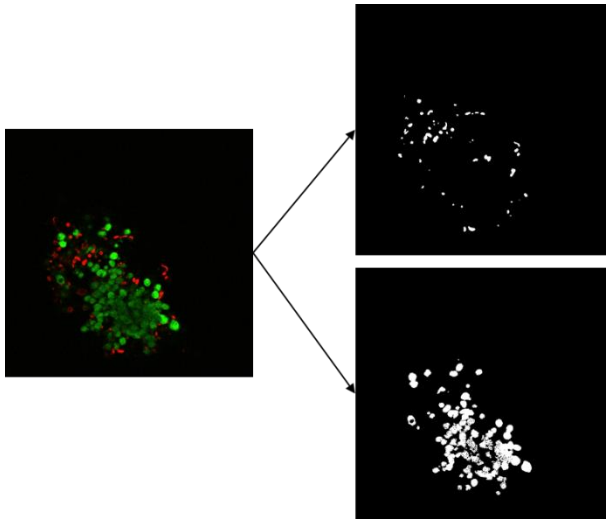

Figure 1-1 – The principle of the image analysis done with the use of ImageJ 1.54d macro script. The two-channel image is separated into green (live cells) and red (dead cells), converted to binary, and the area of stained cells is calculated.

1.3.4. Spheroid migration assay

To estimate the invasion potential of the spheroids, a cell spheroid migration assay was set up. For this, the mature spheroids were transferred from a non-adhesive agarose-coated plate to a 24 multi-well plate and let adhere overnight. Phase-contrast light microscopy images of spheroids were collected, and results were analysed in the ImageJ software with the use of a free toolset for cell invasion analysis (Analyse Spheroid Cell Invasion In 3D Matrix, RRID: SCR_021204).

1.3.5. Nanoindentation

For mechanical characterization, the spheroids were transferred from the agarose-coated plate to the cell culture petri dish and allowed to attach overnight. In the case when the spheroids did not attach, they were placed onto the thin layer of 5 mg/mL collagen solution applied on the dish surface. Stably attached spheroids were washed with PBS and fixed with 4% paraformaldehyde solution at RT for 20 mins. Cells were washed with PBS three times to eluate the fixative reagent and left in PBS at 4 ºC until the analysis.

Each spheroid was indented by the probe (stiffness of 3.9 N/m and tip radius of 50.5 µm) 25 times as a 5x5 matrix scan (with dX and dY equal to 5 µm) with Piuma Nanoindenter (Optics11 Life, NL). Measurement was performed in PBS to minimize attraction forces between the material and the tip, as well as to prevent the spheroid from drying out. The view of the measurement procedure is shown in Figure 1-2. Optimization of the obtained data was

done by indentation model on the relevant range with the use of DataViewer Software (v2.5.7, Optics11 Life, NL).

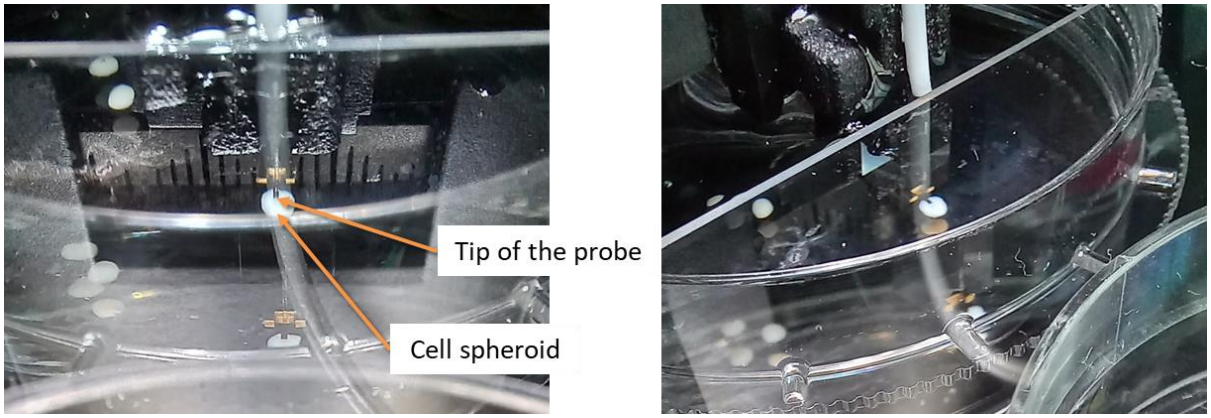

Figure 1-2 – An example of the process of spheroid nanoindentation.

1.3.6. Scanning electron microscopy

Cell spheroid morphology at the end of the experiment was analysed with scanning electron microscopy (SEM). Briefly, cells were fixed with 2.5% glutaraldehyde overnight at 4 ºC, dehydrated by the ethanol scale (50%, 70%, 90%, 96% and 100%, 30 min each) and immersed in HMDS to preserve intact morphology of cells. After complete evaporation of HMDS, specimens were mounted onto aluminium stubs using conductive carbon tape to undergo surface metallization with gold (DII-29019SCTR Smart Coater, Jeol, Japan), and were observed with SEM (JSM-IT500, JEOL, Japan).

1.3.7. Gene expression analysis

The U2OS monoculture spheroids and U2OS monolayer were compared in the context of the expression of VEGF, TP53 and RB1 genes. Total RNA was extracted using TRIzol™ extraction following the manufacturer's recommendations. The gene expression was analysed on the synthesized cDNA (iScript™ cDNA Synthesis Kit, Bio-Rad Laboratories, USA) with a mix for quantitative real-time PCR (SsoAdvanced Universal SYBR Green Supermix, Bio-Rad Laboratories, USA). GAPDH was used as a housekeeping gene. The sequences of forward and reverse primers are listed in Table 1-1.

Table 1-1– Forward and reverse primer sequences.

Gene	Forward primer	Reverse primer
GAPDH	5'- GTA TGA CAA CAG CCT CAA GAT -3'	5'- GTC CTT CCA CGA TAC CAA AG -3'
RB1	5'- AGC CTA TCT CCG GCT AAA TA -3'	5'- GTC CAA ATG CCT GTC TCT C -3'
VEGF	5'- ACC AGA GGA AAG TGG TGT -3'	5'- CAT GAG CTC CAC AGT CAA G -3'
TP53	5'- TGT ACC ACC ATC CAC TAC A -3'	5'- TGT TCC GTC CCA GTA GAT TA -3'

1.3.8. Statistical analysis

Each group of samples was represented by three replicates. Results are shown as mean value ± standard deviation, where applicable. Comparison between groups within experimental time points was performed in Prism (v8, GraphPad Software, USA) using one-way ANOVA with Tukey correction for multiple comparisons, preceded by normal distribution Shapiro–Wilk's test and homoscedasticity Levene's median test. For each comparison performed, the difference was determined as significant for $p < 0.05$.

1.4. Results and Discussion

1.4.1. Spheroid formation and gene expression

First, the ability of osteosarcoma U2OS cells to form stable spheroids was evaluated. Bright-field microscopy observation revealed that the cells tended to disaggregate with time – independently from the initial cell seeding density. Figure 1-3 shows the spheroids of different sizes on the 1st, 2nd and 3rd day after formation of the cell aggregates. During the culture medium exchange, it was also noticed that not all spheroids could stand spontaneous mechanical disruption caused by the pipette tip. This inability of U2OS cells to form stable cell spheroids appropriate for follow-up handling can indeed be met in the literature: it is reported that the formed spheroids are frequently found to be loose, without clear edges (Baek, Seo, Kim, et al., 2016; Panczyszyn et al., 2024).

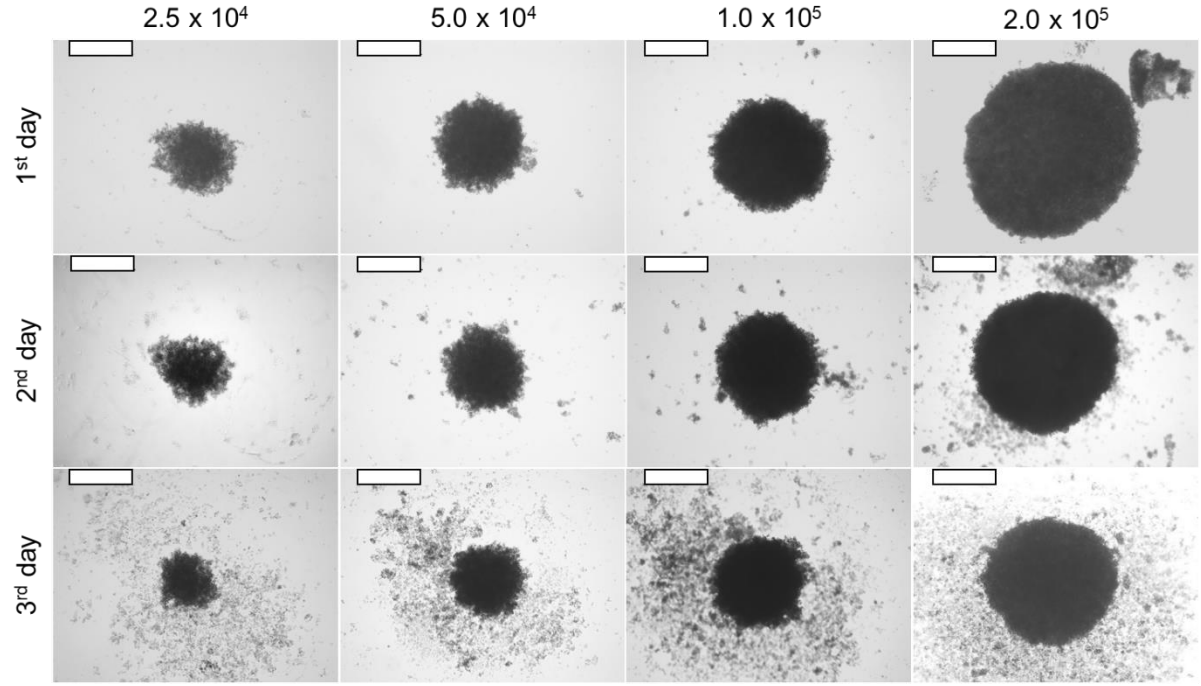

Figure 1-3 – U2OS cell spheroid disaggregation monitoring for 3 days after spheroid maturation. Spheroid formed from various cell numbers are presented. Bright-field microscopy, scale bar 500 µm.

However, even such a poor formation of a spheroid was found to be able to slightly alter the gene expression (Figure 1-4). Vascular endothelial growth factor A, encoded by the VEGF gene, is crucial for angiogenesis, vasculogenesis, and endothelial cell growth. While not a primary treatment target in osteosarcoma, VEGF expression shows potential in prognosis, despite inconsistent correlation with disease stage (Assi et al., 2021; Bajpai et al., 2009; Ren & Gu, 2017; Yu et al., 2014; Zamborsky et al., 2019). The TP53 gene encodes the tumor suppressor protein p53, involved in diverse cellular stress responses. In osteosarcoma, downregulation of TP53 is associated with lower 3-year overall and disease-free survival rates (Zamborsky et al., 2019). The RB1 gene encodes the tumour suppressor retinoblastoma-associated protein, regulating the G1/S cell cycle transition. RB1 dysregulation is implicated in osteosarcoma progression and metastasis (Ren & Gu, 2017). In comparison to U2OS cells cultured in monolayer, there was a slight upregulation of VEGF, and slight downregulation of RB1 and TP53 in U2OS spheroids, which – in the case of VEGF and RB1 – is favourable in the context of using U2OS spheroids in the *in vitro* model of osteosarcoma.

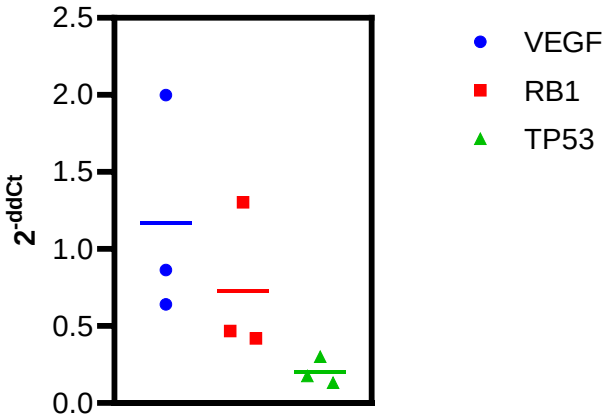

Figure 1-4 – Normalized gene expression in U2OS cell spheroids in relation to U2OS cell monolayer. GAPDH was used as a housekeeping gene. The data is presented as 2^{-ddCt} for each sample and their means.

The spheroids formed from mesenchymal stem cells hBMSCs or the combination of U2OS and hBMSCs (later on referred to as "MSC:U2OS"), on the contrary, were found to be stable and compact. In contrast to U2OS-only (monoculture) spheroids, their area decreased with time of incubation not due to disaggregation, but due to the spheroids becoming more and more dense (Figure 1-5). The idea of co-culturing osteosarcoma cells with MSCs stems not only from the need to obtain stable easy-to-use cell spheroids. Lately, with the focus shifting from cancer cells to their microenvironment, there has appeared evidence that interactions of cancer cells with MSCs are crucial for tumour development. In this regard, Freeman and co-authors investigated co-culture spheroids composed of osteosarcoma cells and MSCs in different ratios mimicking early-stage and late-stage osteosarcoma to understand the interplay between osteosarcoma and MSCs (Freeman et al., 2022). Thus, co-culturing U2OS cells with hBMSCs in direct contact is interesting from the point of technical optimization and from the point of introducing to the *in vitro* system a vital player in the bone cancer microenvironment.

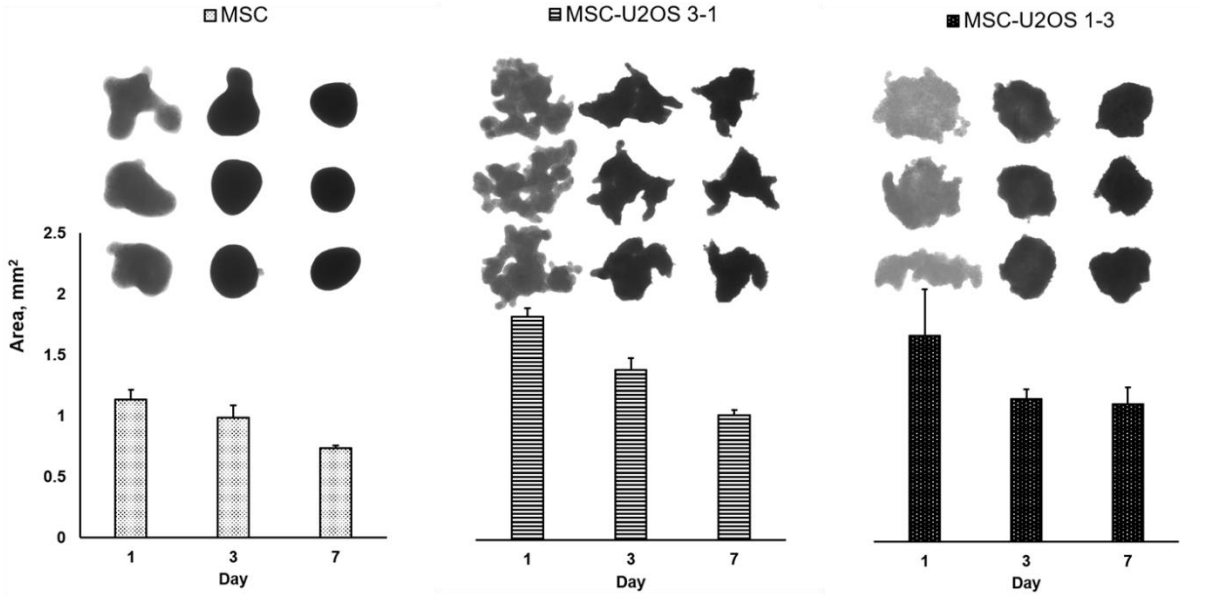

Figure 1-5 – Monitoring of cell spheroids formed on an agarose-coated plate. The images were obtained with a bright-field microscope and analysed using ImageJ software to calculate the area.

1.4.2. Spheroid morphological analysis

Morphological analysis of the spheroids was done by SEM. The morphology of the U2OS, hBMSCs and co-culture spheroids of different ratios is shown in Figure 1-6. As can be observed, U2OS spheroids are loose and neither form tight connections between cells nor produce sufficient ECM in comparison to co-culture spheroids and especially to hBMSCs spheroids. On the magnified areas, it can be observed that the majority of cells in the monoculture U2OS spheroid possess spherical morphology, while the co-culture spheroids contain a large number of cells with flattened morphology, as well as cells exhibiting numerous filopodia, which is in agreement with the bright-field microscopy observations and is evidence of intense cell-cell contacts (Dorst et al., 2014).

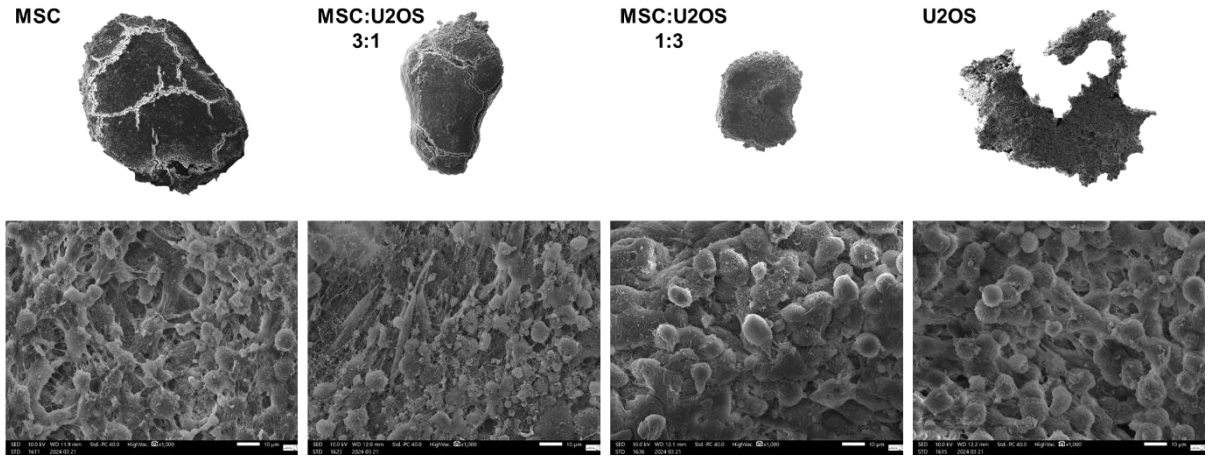

Figure 1-6 – SEM images of U2OS, hBMSCs and co-culture spheroids. Full spheroid images are presented in the upper row, and the lower row represents the magnified area. Scale bars 10 μm.

1.4.3. Spheroid mechanical characterization

Stiffness measurement is a well-known approach to differentiate between healthy tissues and malignant formations. Mechanical characterization of spheroids has been used to predict their invasiveness. Given the commonly used sizes of the spheroids, measuring their stiffness and elasticity can be tricky. AFM, nanoindentation, and micropipette aspiration techniques are the most famous ones. Cavitation rheology is yet another technique used to measure the elastic modulus of the spheroids (Blumlein et al., 2017). Jaiswal et al. developed so-called "microtweezers" able to measure the stiffness of healthy and malignant breast cell spheroids by transforming mechanical strain on the cantilevers to an electrical signal via piezo-actuator (Jaiswal et al., 2017).

In the present study, the mechanical stability of the spheroids was confirmed by nanoindentation analysis (Figure 1-7). The matrix scan revealed that the spheroids formed from hBMSCs only or from the 3:1 mixture of MSC:U2OS, respectively, are the stiffest (> 40 kPa) and do not vary significantly. The stiffness of co-culture spheroids with predominant U2OS cells was ~20 kPa, while U2OS spheroid, expectedly, was barely reaching 3 kPa. Intermediate stiffness of the cell spheroids composed of one part of hBMSCs cells and three parts of U2OS (MSC-U2OS 1-3) may pose this co-culture proportion as promising in terms of stability (not too soft) and invasiveness ability (not too stiff).

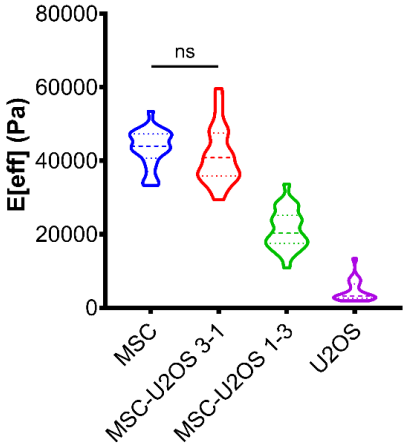

Figure 1-7 – Cell spheroid nanoindentation. The distribution of the values (in Pa) obtained from matrix scans of 4 biological replicates is shown for hBMSCs, U2OS and co-culture spheroids. The difference between all groups is significant ($p < 0.0001$) unless stated otherwise ("ns").

1.4.4. Spheroid metabolic activity and viability

Resazurin reduction (alamarBlue™) assay performed for the spheroids revealed similar metabolic activity patterns for monoculture (hBMSCs) and co-culture (MSC:U2OS) spheroids Figure 1-8. Overall, the co-culture spheroids were slightly more metabolically active – possibly, due to the presence of highly proliferative osteosarcoma cells. In general, the spheroids demonstrated a positive trend in metabolic activity dynamics, however, by the 7th day a decrease was observed in comparison to the 3rd-day point, which may be explained by the limitation of the medium volume coupled with static culture conditions and, subsequently, insufficient nutrient transport for the spheroids composed of a high number of cells.

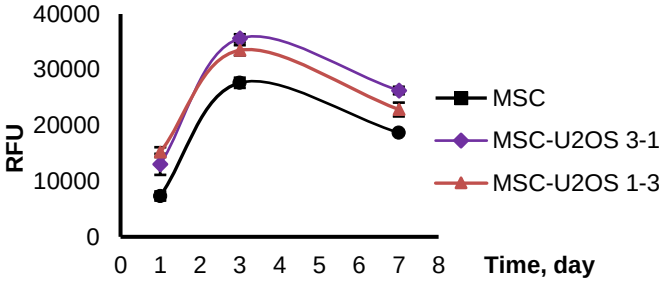

Figure 1-8 – Metabolic activity of the cell spheroids. The values are presented as means of RFU.

As for the live/dead assay of co-culture spheroids, the results are presented in Figure 1-9. The bars on the right to the fluorescent images represent the ratio between live and dead cells – with green colour indicating the live cell number being greater than the dead cell number, and red colour indicating the opposite.

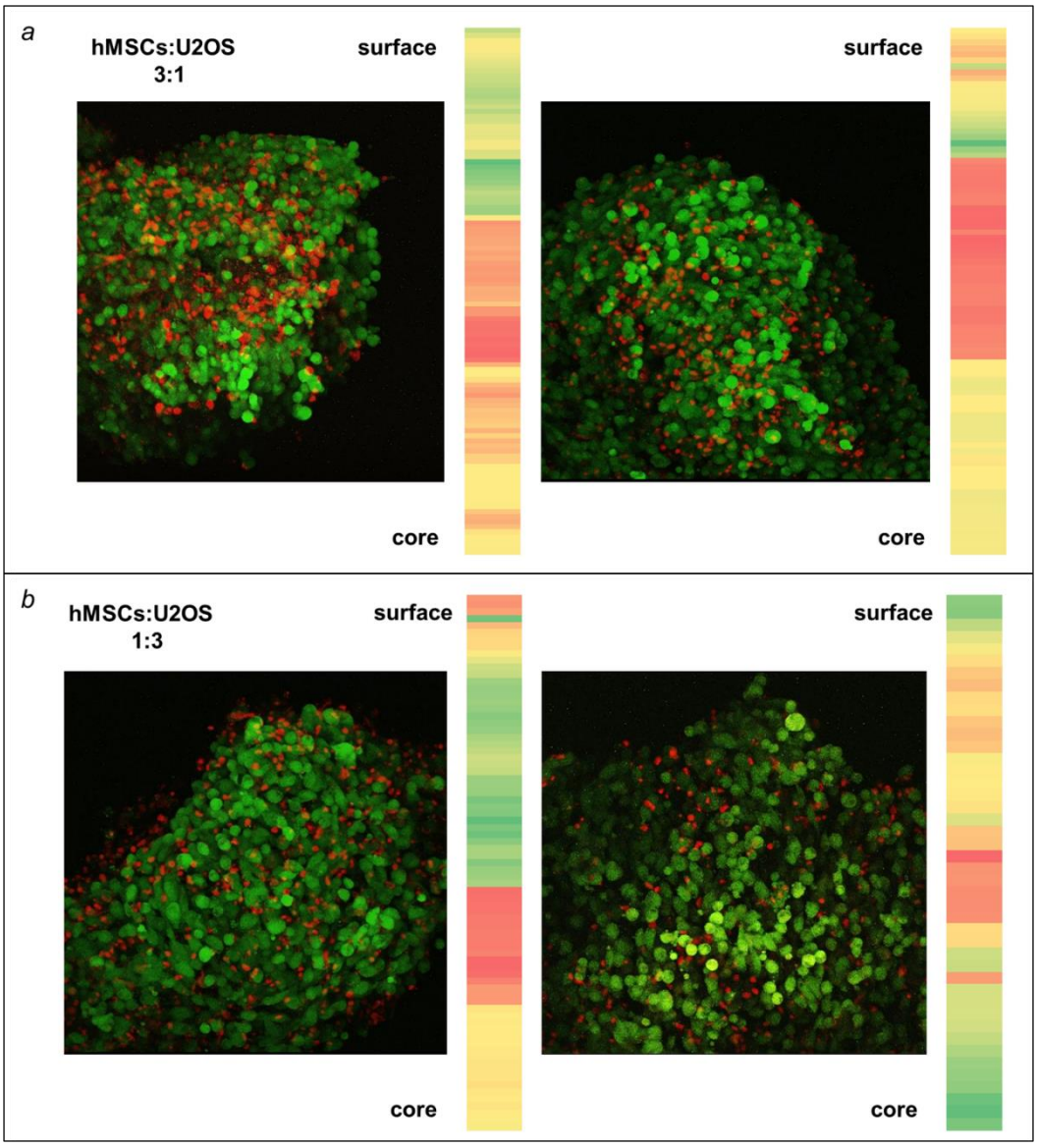

Figure 1-9 – Live/dead assay of co-culture U2OS-hBMSCs spheroids. Stacked images are presented. Heatmap bars reflect the live/dead ratio on each image taken (red colour reflects the predominance of dead cells, and green colour reflects the predominance of live cells.

Even though this method proved to be useful for the fast and precise batch quantitative analysis of a high number of raw live/dead images, the results revealed the limitations of the microscopy method due to the objective used – its inability to "reach" the cells residing in the core of the spheroid. Due to this reason, the images contained only information about the outer layer of the cells. Yet another technical limitation was caused by the fact that the objective of the microscope should have been immersed in the liquid with the spheroid, forcing the observer to use water or PBS rather than the culture medium. Since the cell spheroids were not fixed (the live/dead staining kit of choice cannot be preserved in the fixed specimens), the cells might have started to lose viability due to low temperature, lack of nutrients and disbalance of gases.

Nevertheless, the described method and the representation of the results may be found useful by the reader, thus, even such preliminary results of an unoptimized imaging technique have a right to be presented.

1.4.5. Spheroid migration assay

Figure 1-10 illustrates the principle of estimation of the area occupied by cells migrated from 3D-spheroid to 2D-monolayer. As can be observed, cells in the spheroids composed of hBMSCs only and a 3:1 ratio of MSC:U2OS did not demonstrate any migration potential – possibly, due to the extensive development of ECM. In contrast, the cell spheroids composed of a 1:3 ratio of MSC:U2OS demonstrated a fast migration from the spheroid to the culture plastic giving a hint on the migration – and, eventually, invasion – potential of such type of co-culture spheroids. Coupled with the nanoindentation analysis of the presented types of the spheroids, this result indicates that the spheroids with a 1:3 ratio of hBMSCs and U2OS cells, respectively, may serve best for the following applications from the perspective of the maintenance of invasion ability, as well as ease of handling.

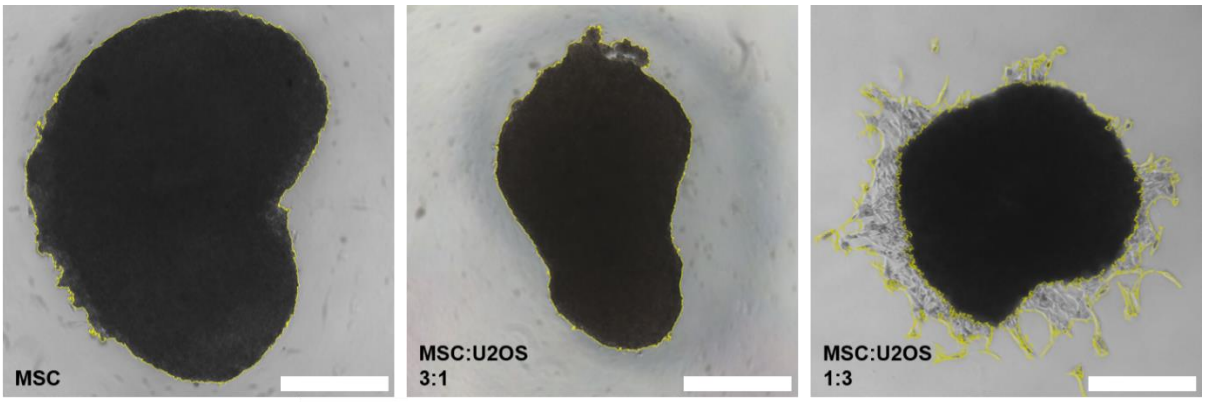

Figure 1-10 – Cell spheroid migration analysis using ImageJ software. The yellow line indicates the area of cells migrated from the 3D spheroid to the 2D monolayer. Scale bar 500 μm.

1.5. Conclusions

This Chapter illustrated the technical and functional features of spheroids as fundamental blocks of 3D *in vitro* models. In this Chapter, osteosarcoma (U2OS) spheroids appeared to be challenging to generate: the obtained cell aggregates were loose and difficult to

handle independently of their size and time of incubation. Even though the results of gene expression analysis demonstrated that the markers of osteosarcoma are expressed differentially in the loose osteosarcoma spheroid in comparison to the monolayer, it was then decided to enhance the mechanical stability of the spheroids while maintaining their invasion potential. Considering the osteosarcoma microenvironment *in vivo*, optimization of the spheroid generation was approached via co-culturing U2OS cells with human bone-marrow-derived MSCs (hBMSCs), as the latter are inevitable participants of bone tumour development. Taking advantage of hBMSCs which are known to produce abundant amounts of ECM, it became possible to obtain stable cell spheroids characterized by dense cell-cell contacts and high stiffness demonstrated throughout SEM and nanoindentation analyses. Furthermore, of two ratios of co-cultures tested, the one containing one part of hBMSCs and three parts of U2OS proved to be the right combination in terms of spheroid invasion ability shown in the migration assay. Finally, the method of batch analysis of z-stack images for quantitative analysis of live/dead assay was demonstrated on the example of the obtained spheroids. Overall, the results presented in Chapter 1 serve as evidence of the possibility of obtaining physiologically relevant mechanically stable cell spheroids of controllable size and preserved migration potential via co-culturing osteosarcoma cells and MSCs in an optimized ratio.

1.6. References

Assi, T., Watson, S., Samra, B., Rassy, E., Le Cesne, A., Italiano, A., & Mir, O. (2021). Targeting the VEGF Pathway in Osteosarcoma. *Cells 2021, Vol. 10, Page 1240*, *10*(5), 1240. https://doi.org/10.3390/CELLS10051240

Baek, N., Seo, O. W., Kim, M., Hulme, J., & An, S. S. A. (2016). Monitoring the effects of doxorubicin on 3D-spheroid tumor cells in real-time. *OncoTargets and Therapy*, *9*, 7207–7218. https://doi.org/10.2147/OTT.S112566

Baek, N., Seo, O. W., Lee, J., Hulme, J., & An, S. S. A. (2016). Real-time monitoring of cisplatin cytotoxicity on three-dimensional spheroid tumor cells. *Drug Design, Development and Therapy*, *10*, 2155–2165. https://doi.org/10.2147/DDDT.S108004

Bajpai, J., Sharma, M., Sreenivas, V., Kumar, R., Gamnagatti, S., Khan, S. A., Rastogi, S., Malhotra, A., & Bakhshi, S. (2009). VEGF expression as a prognostic marker in osteosarcoma. *Pediatric Blood & Cancer*, *53*(6), 1035–1039. https://doi.org/10.1002/PBC.22178

Blumlein, A., Williams, N., & McManus, J. J. (2017). The mechanical properties of individual cell spheroids. *Scientific Reports*, *7*(1), 7346. https://doi.org/10.1038/s41598-017-07813-5

Brancato, V., Oliveira, J. M., Correlo, V. M., Reis, R. L., & Kundu, S. C. (2020). Could 3D models of cancer enhance drug screening? *Biomaterials*, *232*, 119744. https://doi.org/10.1016/j.biomaterials.2019.119744

Brookes, M. J., Chan, C. D., Baljer, B., Wimalagunaratna, S., Crowley, T. P., Ragbir, M., Irwin, A., Gamie, Z., Beckingsale, T., Ghosh, K. M., & Rankin, K. S. (2021). Surgical advances in osteosarcoma. In *Cancers* (Vol. 13, Issue 3, pp. 1–26). MDPI AG. https://doi.org/10.3390/cancers13030388

Buenrostro, D., Mulcrone, P. L., Owens, P., & Sterling, J. A. (2016). The Bone Microenvironment: a Fertile Soil for Tumor Growth. In *Current Osteoporosis Reports* (Vol. 14, Issue 4, pp. 151–158). Current Medicine Group LLC 1. https://doi.org/10.1007/s11914-016-0315-2

Buijs, J. T., & van der Pluijm, G. (2009). Osteotropic cancers: From primary tumor to bone. *Cancer Letters*, *273*(2), 177–193. https://doi.org/10.1016/j.canlet.2008.05.044

Chow, T., Wutami, I., Lucarelli, E., Choong, P. F., Duchi, S., & Di Bella, C. (2021). Creating *In Vitro* Three-Dimensional Tumor Models: A Guide for the Biofabrication of a Primary Osteosarcoma Model. *Tissue Engineering Part B: Reviews*, *27*(5), 514–529. https://doi.org/10.1089/ten.teb.2020.0254

Cortini, M., Baldini, N., & Avnet, S. (2019). New advances in the study of bone tumors: A lesson from the 3D environment. In *Frontiers in Physiology* (Vol. 10, Issue JUN). Frontiers Media S.A. https://doi.org/10.3389/fphys.2019.00814

D'Acunto, M., Trombi, L., D'Alessandro, D., & Danti, S. (2019). Raman spectroscopy of osteosarcoma cells. *Physical Biology*, *16*(1). https://doi.org/10.1088/1478-3975/aaefbf

De Luca, A., Raimondi, L., Salamanna, F., Carina, V., Costa, V., Bellavia, D., Alessandro, R., Fini, M., & Giavaresi, G. (2018). Relevance of 3d culture systems to study osteosarcoma environment. *Journal of Experimental and Clinical Cancer Research*, *37*(1), 1–15. https://doi.org/10.1186/s13046-017-0663-5

Dorst, N., Oberringer, M., Grässer, U., Pohlemann, T., & Metzger, W. (2014). Analysis of cellular composition of co-culture spheroids. Annals of Anatomy - Anatomischer Anzeiger, 196(5), 303–311. https://doi.org/10.1016/j.aanat.2014.05.038

Fidler, I. J. (2003). The pathogenesis of cancer metastasis: the "seed and soil" hypothesis revisited. *Nature Reviews Cancer*, *3*(6), 453–458. https://doi.org/10.1038/nrc1098

Forsyth, R., & Hogendoorn, P. C. W. (2022). Epidemiology of primary bone tumors and economical aspects of bone metastases. In *Bone Cancer* (pp. 17–23). Elsevier. https://doi.org/10.1016/B978-0-12-821666-8.00038-4

Freeman, F. E., Burdis, R., Mahon, O. R., Kelly, D. J., & Artzi, N. (2022). A Spheroid Model of Early and Late-Stage Osteosarcoma Mimicking the Divergent Relationship between Tumor Elimination and Bone Regeneration. *Advanced Healthcare Materials*, *11*(7). https://doi.org/10.1002/adhm.202101296

Gauthaman, K., Yee, F. C., Cheyyatraivendran, S., Biswas, A., Choolani, M., & Bongso, A. (2012). Human umbilical cord wharton's jelly stem cell (hWJSC) extracts inhibit cancer cell growth in vitro. *Journal of Cellular Biochemistry*, *113*(6), 2027–2039. https://doi.org/10.1002/JCB.24073

Han, Y., Yang, J., Fang, J., Zhou, Y., Candi, E., Wang, J., Hua, D., Shao, C., & Shi, Y. (2022). The secretion profile of mesenchymal stem cells and potential applications in treating human diseases. *Signal Transduction and Targeted Therapy 2022 7:1*, *7*(1), 1–19. https://doi.org/10.1038/s41392-022-00932-0

Harris, M. A., & Hawkins, C. J. (2022). Recent and Ongoing Research into Metastatic Osteosarcoma Treatments. *International Journal of Molecular Sciences*, *23*(7), 3817. https://doi.org/10.3390/ijms23073817

Hegyi, M., Semsei, A. F., Jakab, Z., Antal, I., Kiss, J., Szendroi, M., Csoka, M., & Kovacs, G. (2011). Good prognosis of localized osteosarcoma in young patients treated with limb-salvage surgery and chemotherapy. *Pediatric Blood and Cancer*, *57*(3), 415–422. https://doi.org/10.1002/pbc.23172

Hoarau-Véchot, J., Rafii, A., Touboul, C., & Pasquier, J. (2018). Halfway between 2D and animal models: Are 3D cultures the ideal tool to study cancer-microenvironment interactions? In *International Journal of Molecular Sciences* (Vol. 19, Issue 1). MDPI AG. https://doi.org/10.3390/ijms19010181

Jafari, F., Javdansirat, S., Sanaie, S., Naseri, A., Shamekh, A., Rostamzadeh, D., & Dolati, S. (2020). Osteosarcoma: A comprehensive review of management and treatment strategies. In *Annals of Diagnostic Pathology* (Vol. 49, p. 151654). W.B. Saunders. https://doi.org/10.1016/j.anndiagpath.2020.151654

Jaiswal, D., Cowley, N., Bian, Z., Zheng, G., Claffey, K. P., & Hoshino, K. (2017). Stiffness analysis of 3D spheroids using microtweezers. *PLOS ONE*, *12*(11), e0188346. https://doi.org/10.1371/journal.pone.0188346

James, S., Fox, J., Afsari, F., Lee, J., Clough, S., Knight, C., Ashmore, J., Ashton, P., Preham, O., Hoogduijn, M., Ponzoni, R. D. A. R., Hancock, Y., Coles, M., & Genever, P. (2015). Multiparameter Analysis of Human Bone Marrow Stromal Cells Identifies Distinct Immunomodulatory and Differentiation-Competent Subtypes. *Stem Cell Reports*, *4*(6), 1004–1015. https://doi.org/10.1016/j.stemcr.2015.05.005

Jubelin, C., Muñoz-Garcia, J., Griscom, L., Cochonneau, D., Ollivier, E., Heymann, M. F., Vallette, F. M., Oliver, L., & Heymann, D. (2022). Three-dimensional in vitro culture models in oncology research. *Cell & Bioscience 2022 12:1*, *12*(1), 1–28. https://doi.org/10.1186/S13578-022-00887-3

Lindsey, B. A., Markel, J. E., & Kleinerman, E. S. (2017). Osteosarcoma Overview. *Rheumatology and Therapy*, *4*(1), 25–43. https://doi.org/10.1007/s40744-016-0050-2

Marazzi, F., Orlandi, A., Manfrida, S., Masiello, V., di Leone, A., Massaccesi, M., Moschella, F., Franceschini, G., Bria, E., Gambacorta, M. A., Masetti, R., Tortora, G., & Valentini, V. (2020). Diagnosis and treatment of bone metastases in breast cancer: Radiotherapy, local approach and systemic therapy in a guide for clinicians. In *Cancers* (Vol. 12, Issue 9, pp. 1–20). MDPI AG. https://doi.org/10.3390/cancers12092390

Menshikh, K. (2024). *ImageJ_Dummy_scripts* (1.0.0). GitHub. https://github.com/lastjunglist/ImageJ_Dummy_scripts

Mohseny, A. B., MacHado, I., Cai, Y., Schaefer, K. L., Serra, M., Hogendoorn, P. C. W., Llombart-Bosch, A., & Cleton-Jansen, A. M. (2011). Functional characterization of osteosarcoma cell lines provides representative models to study the human disease. *Laboratory Investigation*, *91*(8), 1195–1205. https://doi.org/10.1038/labinvest.2011.72

Monteiro, C. F., Custódio, C. A., & Mano, J. F. (2019). Three-Dimensional Osteosarcoma Models for Advancing Drug Discovery and Development. In *Advanced Therapeutics* (Vol. 2, Issue 3). Blackwell Publishing Ltd. https://doi.org/10.1002/adtp.201800108

Munoz-Garcia, J., Jubelin, C., Loussouarn, A., Goumard, M., Griscom, L., Renodon-Cornière, A., Heymann, M. F., & Heymann, D. (2021). In vitro three-dimensional cell cultures for bone sarcomas. In *Journal of Bone Oncology* (Vol. 30). Elsevier GmbH. https://doi.org/10.1016/j.jbo.2021.100379

Panczyszyn, E., Saverio, V., Monzani, R., Gagliardi, M., Petrovic, J., Stojkovska, J., Collavin, L., & Corazzari, M. (2024). FSP1 is a predictive biomarker of osteosarcoma cells' susceptibility to ferroptotic cell death and a potential therapeutic target. *Cell Death Discovery*, *10*(1), 87. https://doi.org/10.1038/s41420-024-01854-2

Papaccio, F., Paino, F., Regad, T., Papaccio, G., Desiderio, V., & Tirino, V. (2017). Concise Review: Cancer Cells, Cancer Stem Cells, and Mesenchymal Stem Cells: Influence in Cancer Development. *Stem Cells Translational Medicine*, *6*(12), 2115–2125. https://doi.org/10.1002/SCTM.17-0138

Pautke, C., Schieker, M., Tischer, T., Kolk, A., Neth, P., Mutschler, W., & Milz, S. (2004). Characterization of osteosarcoma cell lines MG-63, Saos-2 and U-2 OS in comparison to human osteoblasts. *Anticancer Research*, *24*(6), 3743–3748.

Pinto, B., Henriques, A. C., Silva, P. M. A., & Bousbaa, H. (2020). Three-dimensional spheroids as in vitro preclinical models for cancer research. *Pharmaceutics*, *12*(12), 1–38. https://doi.org/10.3390/pharmaceutics12121186

Ren, W., & Gu, G. (2017). Prognostic implications of RB1 tumour suppressor gene alterations in the clinical outcome of human osteosarcoma: a meta-analysis. *European Journal of Cancer Care*, *26*(1), e12401. https://doi.org/10.1111/ECC.12401

Roodman, G. D., & Silbermann, R. (2015). Mechanisms of osteolytic and osteoblastic skeletal lesions. *BoneKEy Reports*, *4*, 753. https://doi.org/10.1038/BONEKEY.2015.122

Tippett, V. L., Tattersall, L., Ab Latif, N. B., Shah, K. M., Lawson, M. A., & Gartland, A. (2023). The strategy and clinical relevance of in vitro models of MAP resistance in osteosarcoma: a systematic review. *Oncogene*, *42*(4), 259–277. https://doi.org/10.1038/s41388-022-02529-x

Tu, B., Peng, Z. X., Fan, Q. M., Du, L., Yan, W., & Tang, T. T. (2014). Osteosarcoma cells promote the production of pro-tumor cytokines in mesenchymal stem cells by inhibiting their osteogenic differentiation through the TGF-β/Smad2/3 pathway. *Experimental Cell Research*, *320*(1), 164–173. https://doi.org/10.1016/J.YEXCR.2013.10.013

Yang, C., Tian, Y., Zhao, F., Chen, Z., Su, P., Li, Y., & Qian, A. (2020). Bone microenvironment and osteosarcoma metastasis. In *International Journal of Molecular Sciences* (Vol. 21, Issue 19, pp. 1–17). MDPI AG. https://doi.org/10.3390/ijms21196985

Yu, X. W., Wu, T. Y., Yi, X., Ren, W. P., Zhou, Z. Bin, Sun, Y. Q., & Zhang, C. Q. (2014). Prognostic significance of VEGF expression in osteosarcoma: A meta-analysis. *Tumor Biology*, *35*(1), 155–160. https://doi.org/10.1007/S13277-013-1019-1/METRICS

Zamborsky, R., Kokavec, M., Harsanyi, S., & Danisovic, L. (2019). Identification of Prognostic and Predictive Osteosarcoma Biomarkers. *Medical Sciences 2019, Vol. 7, Page 28*, *7*(2), 28. https://doi.org/10.3390/MEDSCI7020028

Zhao, X., Wu, Q., Gong, X., Liu, J., & Ma, Y. (2021). Osteosarcoma: a review of current and future therapeutic approaches. In *BioMedical Engineering Online* (Vol. 20, Issue 1). BioMed Central Ltd. https://doi.org/10.1186/s12938-021-00860-0

Zheng, Y., Wang, G., Chen, R., Hua, Y., & Cai, Z. (2018). Mesenchymal stem cells in the osteosarcoma microenvironment: Their biological properties, influence on tumor growth, and therapeutic implications. *Stem Cell Research and Therapy*, *9*(1), 1–9. https://doi.org/10.1186/S13287-018-0780-X/FIGURES/2

Zschenker, O., Streichert, T., Hehlgans, S., & Cordes, N. (2012). Genome-Wide Gene Expression Analysis in Cancer Cells Reveals 3D Growth to Affect ECM and Processes Associated with Cell Adhesion but Not DNA Repair. *PLoS ONE*, *7*(4), e34279. https://doi.org/10.1371/journal.pone.0034279

2. Osteosarcoma environment *in vitro*: soft scaffold-based approach

2.1. Introduction

2.1.1. Key features of bone tumour and its microenvironment

As was discussed in the sections above, the challenging task of recreating bone cancer microenvironment *in vitro* may be approached in a step-by-step way, moving from a simple model to a more complex one by introducing new characteristics to a model with a reference to what is already known *in vivo*. Per this approach, the following sections are dedicated to known features of bone tumour microenvironment *in vivo*, how these features are implemented *in vitro* and which "building blocks" are being used.

Tumour unit

In vivo, avascular tumour masses are characterized by heterogeneity in a cancer cell population. This happens due to the fact that there is a gradient of oxygen and nutrients, thus, cells in the tumour mass can be roughly divided into 3 groups: outer highly proliferative layer, middle layer composed of quiescent cells, and necrotic core, where the cells lack exposure to oxygen and nutrients (Pinto et al., 2020). As was described in the above chapter, the basic approach to 3D *in vitro* modelling known as spheroid culture is able to meet these requirements and develop the above-mentioned layers – in the case when cell spheroids (cell aggregates) are compact but large enough (~500 um) (Jubelin et al., 2022). There are numerous approaches to developing cell spheroids, such as commercial or custom-made low-attachment multiwell plates, hanging drop method and others. However, while providing abundant cell-cell interactions and all dimensions for proliferation, spheroids of some cell types do not always provide sufficient cell-ECM interactions and require either to be immersed in the matrix or to be co-cultured with other cell types such as cancer-associated fibroblasts or tissue-specific stem cells. These multi-component models are frequently called organoids (Jubelin et al., 2022; Pinto et al., 2020). In the case of osteosarcoma and bone metastases, the matrix for supporting spheroids should resemble the bone tissue microenvironment, expectedly.

The common niche for osteosarcoma development and bone metastases is bone marrow

Osteosarcoma cells are believed to emerge from mesenchymal stem cells or progenitor cells hindered in their differentiation into osteoblasts (Gorlick & Khanna, 2010). The majority of osteosarcoma cases, approximately 80%, originate in the red bone marrow, predominantly located in the cavities formed by the trabecular bone's spongy architecture (Gorlick & Khanna, 2010). Primary cancers of bone tissue and bone metastases have different origins and molecular signalling during their development. However, the trends of modern research are such that the approaches used to create 3D *in vitro* models of these pathologies are quite similar. This is because, ultimately, both primary tumours and bone metastases develop and maintain their existence in the bone tissue environment possessing the same key features. The bone tumour microenvironment is rich in a wide variety of cell types: bone cells (osteoblasts, osteoclasts, and osteocytes), cancer-associated fibroblasts, mesenchymal stem cells, and immune cells

(macrophages, myeloid-derived suppressor cells, natural killer cells) all of which orchestrate together shaping the tumour fate and development (Buenrostro et al., 2016). In addition to that, bone matrix microstructure and rigidity, bone vasculature and the various inner and outer mechanical stimuli affect the bone tumour and are described in detail below.

Matrix stiffness, microstructure and mineralisation

For cortical and trabecular bone, tissue density is roughly 2.0 g/cm^3, and it varies relatively little in the adult skeleton. Human trabecular bone typically has a modulus of 10–3,000 MPa, but its strength – which is strongly and linearly connected with modulus – is typically two orders of magnitude lower, in the range of 0.1–30 MPa. Numerous tensile experiments, scanning acoustic microscopy, nanoindentation, and ultrasonic measurements all suggest that the elastic modulus of trabecular tissue is in the range of 10–20 GPa (Morgan et al., 2018). It was shown for intact tissues and then confirmed by *in vitro* studies that A-type proteins of the nuclear lamina – crucial participants of cytoskeleton-chromatin interactions – are expressed significantly more actively in stiffer tissues than in softer ones, thereby driving osteogenic differentiation of mesenchymal stem cells (Ivanovska et al., 2015). A softer environment normally drives the downregulation of YAP nuclear translocation, but recent studies show that if this soft environment possesses viscoelasticity, cells are able to spread and adhere to it as to the stiff substrate. The key factor is stress relaxation, which applies to substrates of lower stiffness, but elastic (Chaudhuri et al., 2015). A study by K. Charoen et al. compared osteosarcoma and adenocarcinoma spheroids embedded in a collagen matrix of varying elasticity (from 10 to 200 kPa). The successful growth and development of spheroids directly depended on the mechanobiological characteristics of the matrix: for example, spheroids from osteosarcoma cells "preferred" a more rigid gel, in contrast to spheroids from adenocarcinoma cells, which reached their maximum size in relatively soft variations of the collagen matrix (Charoen et al., 2014).

Tumour stroma stiffness increases during tumour development, but this is not the case with osteosarcoma, which does not show an increase in tumour stroma stiffness when compared to healthy bone (Thai et al., 2021). In tissues that are prone to stiffening, the process leading to the development of cancer starts with the stiffening of the environment surrounding the tumour. Cells produce forces on the stiffening extracellular matrix, which increases tension in their cytoskeleton, forms focal adhesions, and promotes the growth of the tumour (Domura et al., 2017). Thus, ECM stiffness is a key parameter for study in models of the disease (Thai et al., 2021). Not only stiffness may be altered during the development of cancerous tissue but also its microstructural organization. In cancerous diseases, the changes in ECM are a frequently observed phenomenon. In a humanized rat model designed by implanting orthotopically human MSCs-seeded scaffold and following injection of human osteosarcoma cells, the developed tumour tissue was characterized by a different orientation of collagen fibrils in comparison to native bone rat and healthy ECM produced by MSCs prior to osteosarcoma cells injection. Collagen fibrils in the ECM of orthotopic osteosarcoma tissue did not have laminar alignment, and in general were shorter and in lower density than in the healthy ECM (Lahr et al., 2022).

Bone tissue has a unique matrix composition consisting of 70% minerals and 30% collagen matrix (González Díaz et al., 2019). The inorganic component of bone mainly consists

of hydroxyapatite (HAp) crystals, but recently it has been debated, that the form of the bone mineral component is rather hydrated amorphous calcium phosphate, which, however, should be further studied (Roohani et al., 2021). However, the same properties of bone have a beneficial effect on tumour development. Studies of metastatic breast cancer showed that HAp provokes mitogenesis and the secretion of enzymes responsible for matrix remodelling. In a highly mineralized matrix, secretion of pro-osteoclastic factors by tumour cells is also observed. Finally, a high calcium level has long been proposed to activate pathways that promote the survival and metastatic capacity of tumour cells (Zhang et al., 2019). The ECM of bone tissue is rich in type I collagen, osteopontin and bone sialoprotein. Increased expression of these factors has been also observed in metastases.

Hypoxic and acidic environment

The bone marrow is known to be a highly hypoxic environment, with pO_2 of 1-7%. As a result, the overexpression of hypoxia-induced factor 1 alfa (HIF1A) was observed in two-thirds of bone metastases. Hypoxia is known to modulate multiple steps of bone metastasis, including premetastatic niches, dormancy, and osteolytic vicious cycles (Zhang et al., 2019). The acidic environment of bone may be further exemplified by abnormal metabolic activities of metastatic cancer cells. An acidic milieu increases bone resorptive activity, possibly contributing to the osteolytic vicious cycle.

Salamanna and co-authors made an attempt to model bone metastasis *in vitro* and used bone tissue derived from patients and cells of breast or prostate cancer (Salamanna et al., 2016). Such selection of cells moved their studies to a sex-related investigation. The models were cultured in dynamic conditions with normal and hypoxic levels of oxygen. First, they demonstrated the specificity of colonization of breast and prostate cancer cells depending on sex. Second, by 4D micro-CT, they showed that in hypoxic conditions bone colonization with cancer cells and its following resorption was increased in comparison to normoxic.

The behaviour of primary bone cancer cells is also altered in hypoxic conditions: one study investigated the gene expression profiles of osteosarcoma MG-63 cells and observed overexpression of α-chains of fibronectin and collagen receptors α5 and α2 in hypoxia. The altered profiles confirmed the microscopy observation: osteosarcoma cell spheroids formed from MG-63 cells were characterized by a stronger attachment to the culture vessel surface in hypoxia in comparison to normoxic conditions (Indovina et al., 2006).

Vasculature

Bone is a highly vascularized tissue. Similar to primary bone tumours, the vasculature is known to play an important role in metastasis. In contrast to the suppressive cues of mature vessels, the sprouting neovasculature promotes the progression of metastatic outgrowth by secreting TGF- β1 and periostin (Sowder & Johnson, 2019). Teixeira et al. succeeded in designing a vascularized *in vitro* model of breast cancer to study tumour-stroma interactions. They used freeze-dried pre-vascularized alginate modified with arginyl glycyl aspartic acid (RGD) sequences and co-seeded with fibroblasts. In this case, RGD-peptide makes the matrix more cell-friendly, while fibroblasts provide angiogenic factors (Teixeira et al., 2021).

Mechanical stimuli

Bone tissue is continuously exposed to mechanical forces *in vivo*, and such forces are vital for bone development and homeostasis, yet their role in bone cancer is largely unknown (Figure 2-1). Mechanical loading causes deformations in bones, but in the order two times less than the one which could be felt by cells *in vitro*, suggesting that local forces are more important than overall ones (X. Chen et al., 2021; Micalet et al., 2021; Stylianopoulos et al., 2012). Whole-tissue level mechanical loading, however, is crucial, for it creates pressure gradients which induce fluid (~25% of bone tissue by volume) movement in bone (Chary & Jain, 1989; Nia et al., 2018). Fluid movement is necessary for the effective transport of solutes to cells and back and for inducing shear stress (Walker-Samuel et al., 2018). Shear stress, in turn, may alter tumour cell proliferation rate and secretion profile, making this parameter a must-have in a 3D model to ensure adequate drug response results (Trachtenberg et al., 2018).

We summarized what is known about the abovementioned and other forces from the perspective of *in vitro* models and *in vivo* evidence in the review article entitled "Biomechanical Aspects in Bone Tumour Engineering" published in Tissue Engineering – Part B: Reviews (Menshikh et al., 2023). In this manuscript, we discuss both outer stimuli stemming from mechanical loading and "inner" stimuli, such as roughness and stiffness of the matrix, which are also able to influence the behaviour of the cells. Moreover, we describe the treatment strategies of osteosarcoma that act via mechanisms connected to the biomechanics of bone cancer. Finally, we try to understand, whether the gap *in vitro-in vivo* is bridged in terms of biomechanical stimuli by analysing existing advanced 3D *in vitro* models.

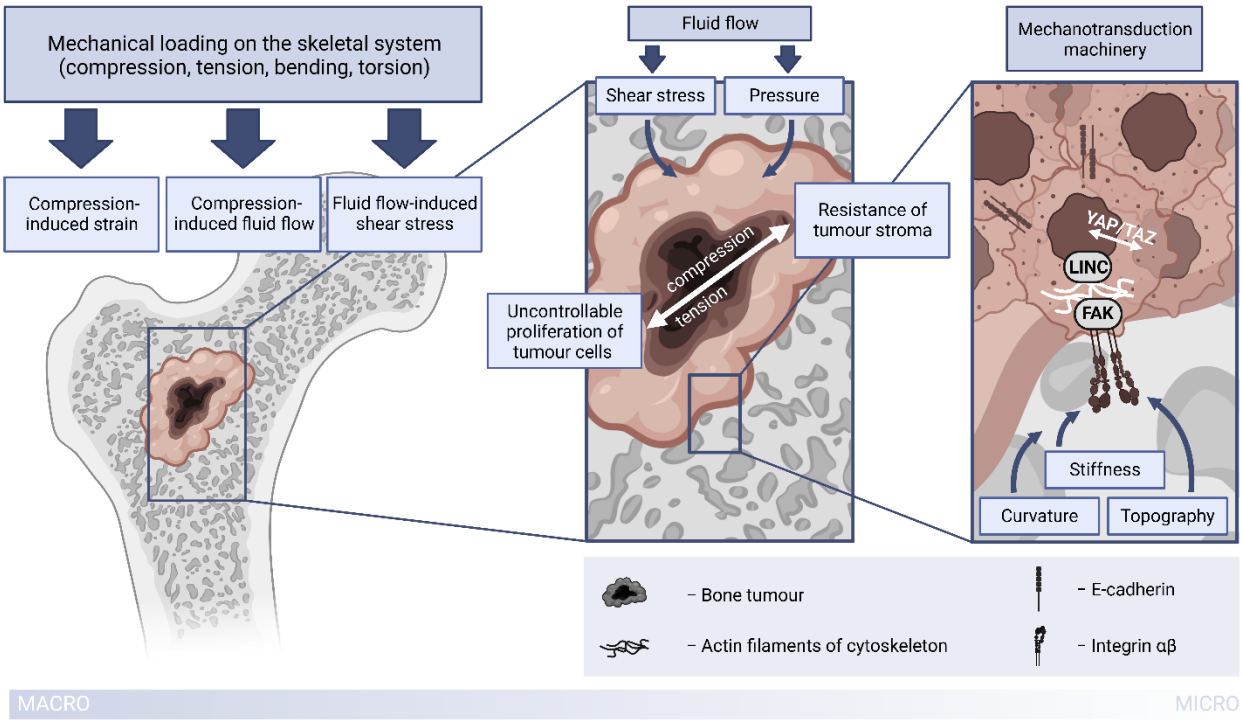

Figure 2-1 – Mechanical stimuli affecting bone tumours (Menshikh et al., 2023).

***

Considering all of the above, the task of mimicking bone tumour environment *in vitro* requires a complex approach, in which all key features would be addressed. Thanks to the recent achievements in the Biomaterials field, the solution could be using materials mimicking the physiological osteosarcoma environment from the biomechanical point of view. In this scenario, tumorigenic cells embedded in such a matrix should resemble the osteosarcoma morphology and biochemical environment. Apart from the requirement to resemble the environment, fundamental requirements are to be met: cytocompatibility, structural and mechanical relevance, ease of handling, and resistance to external stimuli. Various scaffolds like hydrogels, mineral-based scaffolds, electrospun fibres, and 3D-printed scaffolds are used, and some of the approaches will be discussed in the section below.

2.1.2. Modern approaches to 3D *in vitro* modelling of bone cancer

At the moment, numerous 3D *in vitro* models of various types of cancer have been designed and implemented. However, some success has been achieved mainly for soft tissue cancers, while models of primary cancer and bone metastases are full of shortcomings.

Xenografts as scaffolds for engineering bone microenvironment

Decellularized bovine bone is frequently used as a matrix for cells in tumour modelling. Though the achievement of fully safe material not triggering the immune response is a complex process, decellularized bone possesses unique morphological characteristics similar to those of trabecular bone tissue in humans. Sakolish et al. used such scaffolds to build a model of Ewing sarcoma. In their case, they "humanized" the material by setting up an osteogenic process via seeding hBMSCs, and after that arranged osteosarcoma spheroids within these scaffolds. Worth noting that all the *in vitro* experiments were conducted in two different laboratories bringing similar results which indicates that scaffolds are able to support reproducibility and, consequently, make the tumour model robust and replicable (Sakolish et al., 2020).

Hydrogels' usage in osteosarcoma tumour engineering

Scaffold-based tumour engineering is more reasonable than that without any matrix simulations. Various hydrogel-based models have been described in the context of bone cancer, although the question remains whether their mechanical characteristics are enough: native bone is much stiffer than the hydrogels used to imitate the matrix (10-15 MPa versus 1-10 kPa). In addition, the pH-dependency makes collagen-based hydrogels unsuitable for the study of the effects of tumour acidosis, a feature that is crucial for the development of bone cancer (Cortini et al., 2019). However, there are a number of studies utilizing a hydrogel-based approach for bone tumour modelling. Monteiro et al. conducted comparative research analysing single-cell units and spheroids embedded in ECM-mimicking hydrogel. The evident difference in matrix invasion and drug response pointed at the spheroid-in-gel system as a more trustworthy one (M. Monteiro et al., 2020). In their next paper, authors used not only osteosarcoma spheroids but also tri-culture with mesenchymal cells and osteoblasts highlighting the importance of considering tumour cell-microenvironment crosstalk in the onset of engineered 3D model as a drug test-system (C. F. Monteiro et al., 2021).

Bone-on-a-chip

An interesting study was focused on modelling a bone microenvironment via organ-on-a-chip technology. Taking trabecular bone architecture as a reference, Galván-Chacón et al. used two-photon polymerisation technology to produce a porous scaffold. Then, it was modified by hydroxyapatite-simulating CaPs, and seeded with hBMSCs inside a chip. Throughout 21 d of cultivation, it was noted that cells not only were showing remarkable viability and ability to produce collagenous ECM but also to mineralize it (Galván-Chacón et al., 2021). All this characterizes this approach as promising and can be used consequently for constructing microenvironments for bone cancer modelling.

2.1.3. Alginate-based 3D *in vitro* models

Alginates are naturally occurring polysaccharides found in large quantities in widespread brown algae. The industry typically uses sodium salt of alginic acid, which is obtained in several stages: alkaline extraction from algae, precipitation with calcium chloride, and conversion to alginic acid using hydrochloric acid for subsequent purification. Owing to their qualities including gelling capacity, low toxicity, easiness of chemical modification and great affordability, alginate hydrogels are the most extensively tested materials for bone tissue engineering (BTE) and bioprinting. The US Food and Drug Administration (FDA) has determined that alginate polysaccharide is safe for use in humans. Alginates are suitable for cell loading and, above other materials employed as solid scaffolds, have the benefit of being injectable due to their intrinsic ionic crosslinking (Hernández-González et al., 2020). High molecular weight alginate is thought to serve better for hard tissue engineering, while low molecular weight alginate shows better biodegradability (Venkatesan et al., 2015).

Both alginate hydrogels' printability and proneness to crosslinking open a wide variety of opportunities in terms of stiffness and micro- and macrostructure of the resulting material. By choosing between various crosslinking agents such as calcium chloride and magnesium sulfate, their concentrations, and the moment of crosslinking – before, after or even during the bioprinting, – it is possible to gain the bioink suitable for precise, geometrically accurate printing (Gonzalez-Fernandez et al., 2021). By varying yet another parameter - the amount ratio of the alginate hydrogel to the crosslinking agent – stiffness can be controlled, and even stiffness gradients throughout the volume of the material can be obtained. When cell-laden, such hydrogel may guide cell differentiation by its stiffness gradient (Freeman & Kelly, 2017).

Frequently, micro- and nanoparticles (NPs) of various natures are incorporated into the alginate scaffolds to give them additional bioactivity, enhance mechanical properties or modify the material's microstructure depending on the final application. For instance, in a study by Zvicer et al. on the functional characterization of alginate scaffolds containing silver NPs, it was shown that alginate with a higher guluronate/mannuronate (G/M) ratio possessed higher compressive strength than the one with a lower guluronate content (~64 kPa against ~44 kPa). The authors hypothesized that the stabilization of silver NPs might happen similarly to the binding of calcium cations, which are known to form stronger bonds with G units than with M units, thus, the addition of NPs to the alginate scaffold with high G/M ratio is beneficial for the enhancing the mechanical properties of such scaffolds (Zvicer et al., 2019).

Sarker et al. developed freeze-dried scaffolds from oxidized alginate hydrogel reinforced with a 45S5 bioactive glass (BG) in order to control the degradability and enhance the mechanical strength of the scaffolds. It was noticed that BG45S5 facilitates the gelation, enhances the crosslinking degree of the gels and promotes apatite formation. The compressive stress and compressive modulus of scaffolds with BG increase from 326 ± 49 kPa to 908 ± 17 kPa and from 65 ± 13 kPa to 417 ± 33 kPa compared to oxidized alginate hydrogel matrix alone (Sarker et al., 2016).

2.2. Aim

The aim of this Chapter is to evaluate the potential of freeze-dried scaffolds composed of alginate and bioactive glass to serve as a bone-like environment for the 3D *in vitro* model of osteosarcoma. First, by varying the parameters of scaffold production, I obtain several types of scaffolds and characterize them in the context of similarity to trabecular bone microstructure. Then, the scaffolds are analysed from the point of their rehydration and porosity after rehydration. These characterization steps serve as a bottleneck for narrowing down the diversity of the scaffolds since sufficient porosity is essential for further application in perfusion bioreactors. This is followed by cytocompatibility evaluation – with murine and human osteosarcoma spheroids, as well as with MSCs and endothelial cells. Finally, the chosen scaffold type is tested in the perfusion bioreactor "3D Perfuse" developed in the Innovation Center of the Faculty of Technology and Metallurgy, Belgrade, Serbia, where my secondment took place and where I carried out part of the work described in the present Chapter.

2.3. Materials and Methods

2.3.1. Materials

Low-glucose, as well as high-glucose Dulbecco's modified Eagle's medium (DMEM), fetal bovine serum (FBS), trypsin EDTA 1X, ethanol (EtOH, BioUltra, ≥ 99.8%, molecular biology grade, CAS: 64-17-5), phosphate-buffered saline (PBS, ready-to-use tablets, Ref. N. P4417-100TAB), resazurin sodium salt (Ref. N. R7017-5G, CAS: 62758-13-8), alginic acid sodium salt (medium viscosity Cat. No. A2033-250G), paraformaldehyde (Reagent grade, crystalline, Ref. N. P6148-1KG, CAS: 30525-89-4) and collagen (PureCol® EZ Gel, 5 mg/mL) were purchased from Sigma-Aldrich, USA. Penicillin-streptomycin (PS) and fluorescent live/dead assay (LIVE/DEAD, L3224) were purchased from Invitrogen, USA. Calcium chloride (1M aq. soln., CAS: 10043-52-4) was purchased from Thermo Scientific Chemicals. Multiwell plates (Ref. N. 30024) were purchased from SPL Life Sciences, Korea. Agarose (Certified Molecular Biology Agarose, Cat. No. 1613100) was purchased from Bio-Rad Laboratories, USA. Cell lines used for the research have the following specifications: human bone marrow-derived stem cells (hBMSCs, hTERT-BMSC clone Y201, isolated from bone marrow and immortalized through hTERT lentiviral vectors (James et al., 2015)) were kindly provided by Prof. P. Genever, University of York; human umbilical vein cell line (EA.hy926, CRL2922), human osteosarcoma cell line (U2OS, HTB96) and murine osteosarcoma cell line (K7M2-wt, CRL2836) were purchased in American Type Culture Collection, Manassas, VA, USA.

2.3.2. Alginate-bioactive glass scaffold production

The scaffolds were composed of medium-viscosity alginate and bioactive glass particles (BG, 77% SiO_2, 9% P_2O_5, 14% CaO (wt. %), Ø <100 nm and Ø ~ 500 nm) kindly provided by the Polytechnical University of Turin. The components (alginate dissolved in distilled water (3 wt. % and 4 wt. %) and 2 wt. % BG particles) were mixed in syringes, the mixture was poured into a 48-well plate in a volume of 500 µL in each well and polymerized for 24 h between paper discs soaked in 270 mM $CaCl_2$ solution. The solidified samples were transferred to test tubes to be soaked in 270 mM $CaCl_2$ for another 48 hours. The samples were transferred back to the multiwell plate and instantly frozen at -20 ^{0}C overnight, at -80 ^{0}C for 1 h, and freeze-dried at 0.200 hPa and -50 ^{0}C for 72 h. The scheme of the scaffold production is presented in Figure 2-2. Prior to *in vitro* cell studies, the freeze-dried scaffolds were cut gently from top and bottom to open pores, soaked in 1 mL of 70% ethanol, washed with distilled water, dried under UV exposure for 30 min from both sides and pre-soaked in 1 mL of culture medium for 4 h. The optimal proportions of alginate and BG were chosen based on the analysis with scanning electron microscopy (SEM), supplemented with element mapping.

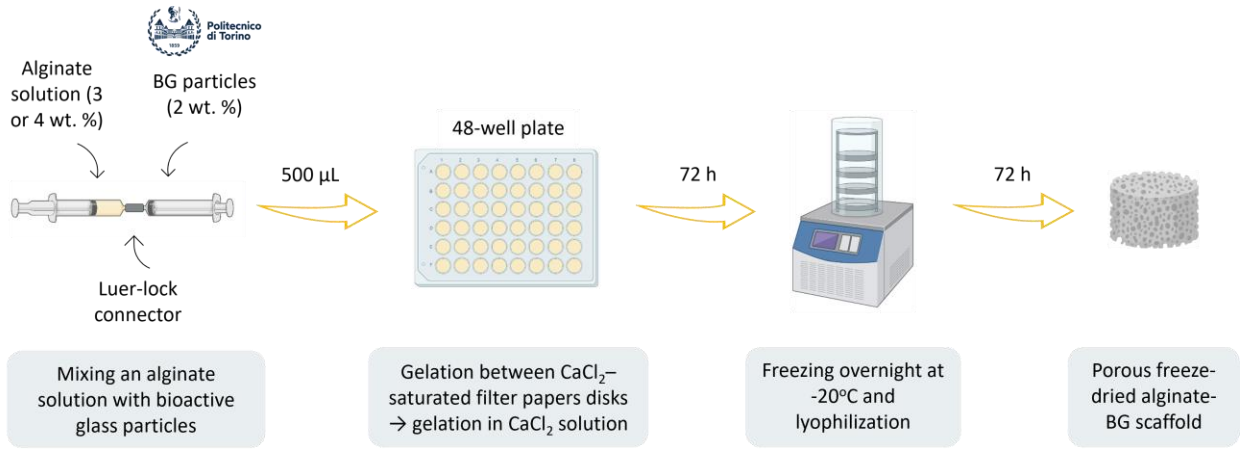

Figure 2-2 – Alginate-bioactive glass scaffold production. Created with Biorender.com.

2.3.3. Alginate-bioactive glass scaffold characterization

To assess morphological properties such as pore size and pore distribution, as well as an elemental profile of the scaffolds, they were analysed by SEM with an energy-dispersive X-ray spectrometer. For this, the freeze-dried alg-BG scaffolds were mounted on the sample holder and covered with a thin layer of gold with a sputter coater (DII-29019SCTR Smart Coater, JEOL, Japan), and then images were collected by SEM (JSM-IT500, JEOL, Japan) at different magnifications and element mapping was done.

2.3.4. Rehydration and porosity of alginate-bioactive glass scaffolds

To analyse the scaffolds' proneness to rehydration, the samples were soaked in complete culture medium and measured at the time points of 1, 2, 4, 24 and 48 h in terms of weight, height, and diameter. To estimate the scaffolds' microstructural characteristics in a dry state (after freeze-drying) and in a rehydrated state (after soaking in medium), a cryosectioning method was used. Morphology of the cross-sections was observed by light microscopy, and

the images were processed in ImageJ software (ImageJ 1.53t, Wayne Rasband et al., NIH, USA).

2.3.5. Rheological characterization of alginate-bioactive glass scaffolds

To describe and assess the deformation and flow behaviour of the scaffolds, an oscillatory rheometer was used (Modular Compact Rheometer MCR 302, Anton Paar, Germany). Briefly, freeze-dried scaffolds were sanded off from both sides to open the pores and to equalize the height, sterilized in 70 % ethanol for 2 h, washed with deionized H_2O and immersed in FBS-enriched cell culture medium at 37 °C. Rehydrated scaffolds were taken out at 2, 4, 6, 24, 48 and 168 h for analysis. For this, the sample was positioned on the plate of the rheometer (Plate Peltier Temperature Device) set to 37 °C and sandwiched by a measuring plate (Ø 10 mm). First, an amplitude sweep test was performed with the measuring plate oscillating at the constant frequency of 1 Hz from 0.01% to 100% shear strain. Then, the linear viscoelastic region was determined, and a frequency sweep (from 100 to 0.01 Hz) test was performed at the constant strain of 1%.

2.3.6. Cell culture and cell seeding procedure

For the investigation of scaffold cytocompatibility, several cell lines were used. Immortalized human bone marrow-derived stem cells (hBMSCs) were cultivated in low-glucose DMEM supplemented with 15 % FBS and 1 % PS. Human osteosarcoma cells (U2OS) and human endothelial umbilical vein cells (EA.hy926) were cultivated in high-glucose DMEM supplemented with 10 % FBS and 1 % PS. All cell lines were cultivated at 37 ºC in the humidified atmosphere containing 5 % CO_2. Before experiments, cells were cultivated until 80-90% confluence, detached by trypsin-EDTA, harvested, and used for experiments.

In the case of cell spheroid-based studies, cells were seeded at agarose-coated multiwell plates to form aggregates. In brief, agarose was dissolved in dH_2O, the 1,5% solution was poured into the wells of a 48-well plate in a volume of 150 µL in sterile conditions, and the plate was maintained open under UV exposure for 2 h. The cells were seeded in each well of the agarose-coated plate and cultured in 500 µL of complete medium in standard conditions. The formation of the spheroids was monitored by light microscopy, and half of the medium volume was changed every 2-3 days.

The tested pre-rehydrated scaffolds were seeded by cells in two different ways. In the case of the cell suspension method, the cells were routinely harvested, suspended in collagen and seeded on top of the scaffolds. In the case of the spheroid-based method, cell spheroids were arranged in collagen one by one within the scaffolds' pores. After 3 hours of collagen gelation at 37 ºC, the cell-seeded scaffolds were transferred to a clean multiwell plate and 1.5 mL of culture medium were added. The cell-seeded scaffolds were cultured in standard conditions with a regular medium replacement.

To trigger the formation of the tubule-like cell network in scaffolds seeded with EA.hy926, VEGF was added to the culture medium. The co-culture studies were performed with the use of endothelial single-cell suspension and osteosarcoma cell spheroids seeded on the scaffold simultaneously. The viability of hBMSCs, U2OS and EA.hy926 cells was monitored by resazurin reduction assay, light microscopy, and fluorescent microscopy with

live/dead staining. The cultured constructs at the end of incubation were fixed, dehydrated, and dried for scanning electron microscopy.

2.3.7. Perfusion bioreactor studies

For the investigation of scaffolds' cytocompatibility and performance in perfusion bioreactor, murine osteosarcoma cell line K7M2-wt was used. The cells were cultivated in high-glucose DMEM supplemented with 10% FBS, 1% L-Glutamine, and 1% PS-Amphotericin B at 37ºC in the humidified atmosphere containing 5% CO_2.

K7M2-wt cells were seeded in the tested pre-rehydrated scaffolds in the form of cell suspension (15×10^6 cells per 1 cm^3 of scaffold volume) and in the form of spheroids similar to the above-described method. The cell-seeded scaffolds were placed in a low-attachment 12-well plate for cell suspension to prevent cells from adhering to the bottom of the plate, and 2.5 mL of culture medium was added after 3 h of collagen gelation.

After 1 day of cultivation in standard (static) conditions, cell-seeded scaffolds were loaded into the chambers of perfusion bioreactors ("3D Perfuse", Innovation Center of the Faculty of Technology and Metallurgy, Belgrade, Serbia). Three perfusion bioreactors were connected to the recirculation loop filled with 15 mL of culture medium (Figure 2-3).

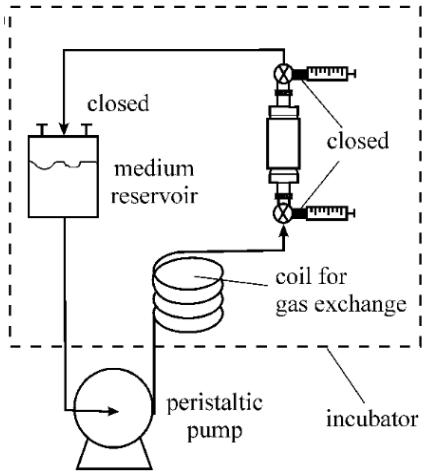

Figure 2-3 – Scheme of a perfusion bioreactor system inside an incubator. Adapted from Stojkovska et al. (2020).

Continual flow through the samples at the constant flow rate of 0.18 mL/min was established by a multichannel peristaltic pump (LabN1 Peristaltic Pump, Shenchen). This flow rate corresponds to the superficial fluid velocity of ~40 μm/s. The control in this study was presented by the cell-seeded scaffolds cultivated under static conditions. 40% of medium was exchanged on the 3rd and 6th days of cultivation in both static and dynamic conditions.

To assess the viability of the cells seeded on the scaffolds, a resazurin reduction assay was used. For this, cell-seeded scaffolds either from flasks or from the chambers of the bioreactors were placed into the wells of 24-well plate and cultivated for 4 hours in 2 mL of 40 mM resazurin salt solution in complete medium. After this, the medium was transferred to cuvettes and the absorption was read on the spectrophotometer at the wavelengths of 570 nm (lower wavelength, LW) and 600 nm (higher wavelength, HW). To calculate the percentage of

the reduced resazurin (that can be correlated with the relative percentage of metabolically active cells), the following formula suggested by the manufacturer was used:

$$A_R(LW) = (A_{LW} - A_{HW}) * R_0 * 100 A_R(LW) = (A_{LW} - A_{HW}) * R_0 * 100,$$

where A_R is percentage of reduced resazurin, A_{LW} – observed absorbance at lower (570 nm) wavelength, A_{HW} – observed absorbance at higher (600 nm) wavelength, and R_0 is a correction factor calculated as

$$R_0 = A_{0(LW)}/A_{0(HW)} R_0 = A_{0(LW)}/A_{0(HW)},$$

where $A_{0(LW)}$ and $A_{0(HW)}$ are absorbances of oxidized form at lower (570 nm, LW) and higher (600 nm, HW) wavelengths, respectively. After the performance of the viability assay, the scaffolds were fixed in the paraformaldehyde for the following histological analysis or in the 2.5% glutaraldehyde solution and processed by dehydration in increasing concentrations of ethanol for field emission scanning electron microscopy (FE-SEM) analysis. For histological analysis, the samples were cut via the cryosectioning method as described before and stained by Hematoxylin & Eosin staining according to the manufacturer's recommendations (cat. N. 461316941; 032319385 Carl Roth). FE-SEM was performed using a MIRA 3 XMU instrument (TESCAN, Brno, Czech Republic) after deposition of an atomic gold layer.

2.3.8. Statistical analysis

Each group of samples was represented by three replicates. Results are shown as mean value ± standard deviation, where applicable. Comparison between groups within experimental time points was performed in Prism (v8, GraphPad Software, USA) using one-way ANOVA with Tukey correction for multiple comparisons, preceded by normal distribution Shapiro–Wilk's test and homoscedasticity Levene's median test. For each comparison performed, the difference was determined as significant for $p < 0.05$.

2.4. Results and Discussion

2.4.1. Freeze-dried alginate-bioactive glass scaffold characterization

Each parameter of scaffold preparation is of great importance and influences the outcome. As was discussed previously, the content of guluronic and mannuronic units in the alginate results in stronger or weaker gelation. In addition, gelation depends on the chelator agent (for instance, calcium or magnesium cations), its concentration and even the volume and daily exchange of the gelation solution. Next, two other parameters to consider are the speed and the temperature of freezing. Instant freezing at -80 ºC may result in decreased porosity, while gradual freezing in an isopropanol-filled container or at -20 ºC is usually optimal. Referring to the microstructure of trabecular bone, the desired parameters of the material would be 80% porosity and interconnected pores with diameters of 300 µm and larger (Haugen et al., 2019; Morgan et al., 2018). The time of freeze-drying depends not only on the volume of the scaffolds but also on the presence of the inorganic part: the more inorganic phase is present, the longer the lyophilisation. Moreover, the pressure after the lyophilisation should be gradually balanced to maintain the microstructure of the scaffolds. Finally, the dried scaffolds

might need post-processing – sandpaper or cutting from both sides to open the pores clogged during the gelation process and rehydration prior to following application, for instance, before cell seeding (Marsich et al., 2013; Ocando et al., 2021; Sarker et al., 2016; Stojkovska et al., 2021).

Throughout the set-up of the method of scaffold production, referring to the evidence in the literature and eventually considering the data from SEM and elemental analysis, the optimal parameters were established: the polymerization period of 72 hours with a regular change of polymerizing solution ($CaCl_2$), freezing at -20ºC overnight and freeze-drying for 72 hours (0.200 hPa, -50 ºC). Three compositions of scaffolds were chosen: 4% alginate-BG500, 4% alginate-BG100 and 3% alginate-BG100, all with 2 wt. % of the mineral phase represented by bioactive glass powder. The chosen scaffolds' microarchitecture was comparable to that of the trabecular bone tissue in terms of porosity and spatial arrangement (Figure 2-4, c, d, e). The bioactive glass particles were shown to be evenly distributed with the maintenance of the initial morphology (Figure 2-5).

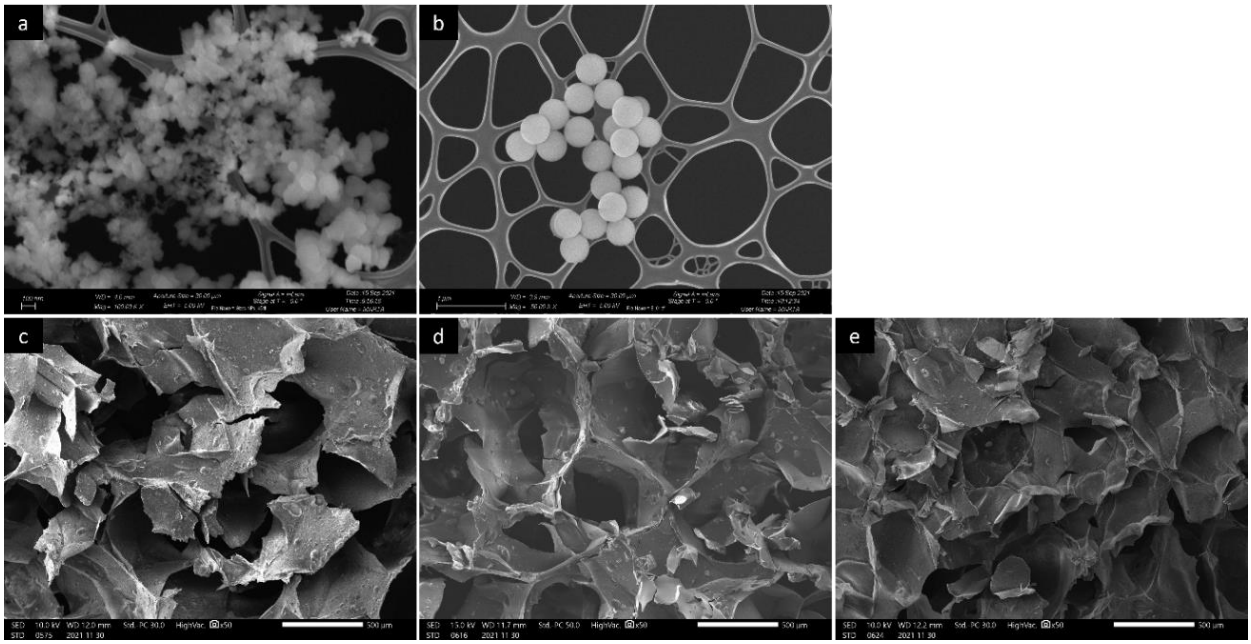

Figure 2-4 – Scanning electron microscopy images of BG particles with the composition of 77% SiO2, 9% P2O5, 14% CaO (wt.%) and cross-section of freeze-dried alginate-bioactive glass scaffolds. Images a and b represent BG with diameters of <100 μm and ~500 μm (BG100 and BG500, scale bar 100 nm and 1 μm, respectively), and images c, d and e represent scaffolds with the contents of 4% alginate-BG500, 4% alginate-BG100 and 3% alginate-BG100, respectively, scale bar 500 μm.

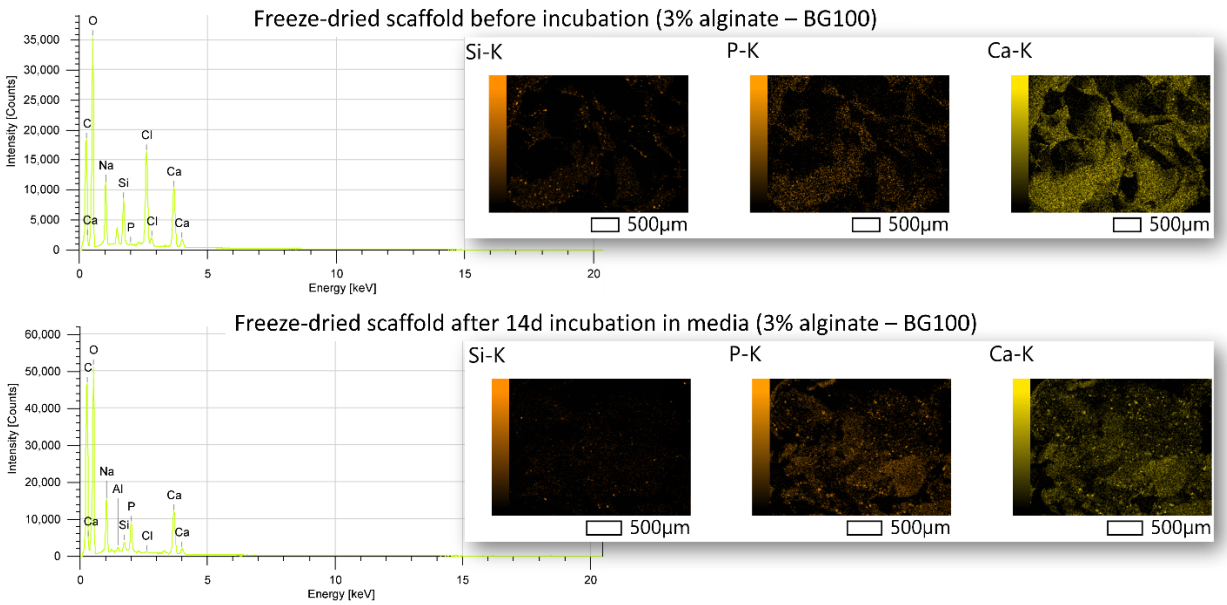

Figure 2-5 – Energy-dispersive X-ray spectroscopy of the freeze-dried scaffolds with the composition of 3 wt.% alginate and bioactive glass with the particle diameter of < 100 µm before and after incubation in culture medium for 2 weeks in standard conditions of 37ºC, 5% CO_2 and humidified atmosphere. Pronounced peaks of calcium, phosphorous and silica are observed at both time points. Element mapping demonstrates an even spread of the aforementioned elements.

2.4.2. Preliminary cytocompatibility assay and co-culture

The viability of the hBMSCs and EA.hy926 seeded on the scaffolds in the form of suspension was estimated by resazurin reduction assay and Calcein AM staining followed by fluorescent microscopy (Figure 2-6). In particular, hBMSCs seeded in the form of suspension were found to spontaneously form spheroid-like aggregates in the pores of the scaffolds within 1 week of cultivation (Figure 2-6, *a*). Metabolic activity of both hBMSCs and EA.hy926 was higher on the scaffolds composed of 3% alginate and 2% BG100 compared to cells cultured in other compositions (Figure 2-6, *b*). Overall metabolic activity decreased for both cell lines by the 2nd week of the experiment – probably, due to insufficient nutrients and gas transport in the circumstances of voluminous scaffolds and static culturing conditions. In addition, the scaffolds were tested for their suitability to host endothelial cells and potential vascularization. For this, the scaffold was pre-soaked in the medium containing VEGF. VEGF enhances endothelial cell proliferation and triggers the formation of vessel-like structures. Optimal concentrations for culturing on transwell inserts covered with Matrigel were determined by Bai and co-authors: one application of VEGF in a concentration of 50 ng/mL was enough to boost the proliferation of endothelial cells and their invasion through the membrane towards the bottom (Bai et al., 2014). Chen et al. used the combination of VEGF to increase the osteogenicity of their 3D-printed hydroxyapatite composite scaffolds. They immersed dried scaffolds in 1 µg/mL VEGF PBS solution at 37 °C and used the residue amount of growth factor in the solution to calculate the amount loaded on the scaffold (S. Chen et al., 2020). Ding et al. loaded chitosan-alginate nanoparticles with VEGF using a solution of 100 ng/ml (Ding et al., 2020). Wang et al. increased osteo- and angiogenicity of silk fibroin-hydroxyapatite

particles via continuous dropping of VEGF solution (0.1 μg/μL) in 3 : 4 ratio, v/w for 12 h at 4 °C (Q. Wang et al., 2017).

At the 1-week point of incubation, no difference is observed in comparison to EA.hy926-seeded scaffolds not containing any stimulation (Figure 2-6, *c*, left and middle). Remarkably, when EA.hy926 are seeded on the alg-BG scaffolds together with the U2OS spheroids, the network formation between the spheroid masses is observed (Figure 2-6, b). However, due to the non-specificity of the staining (Calcein AM indicates all live cells), it is hard to say which cell type has a bigger impact on network formation.

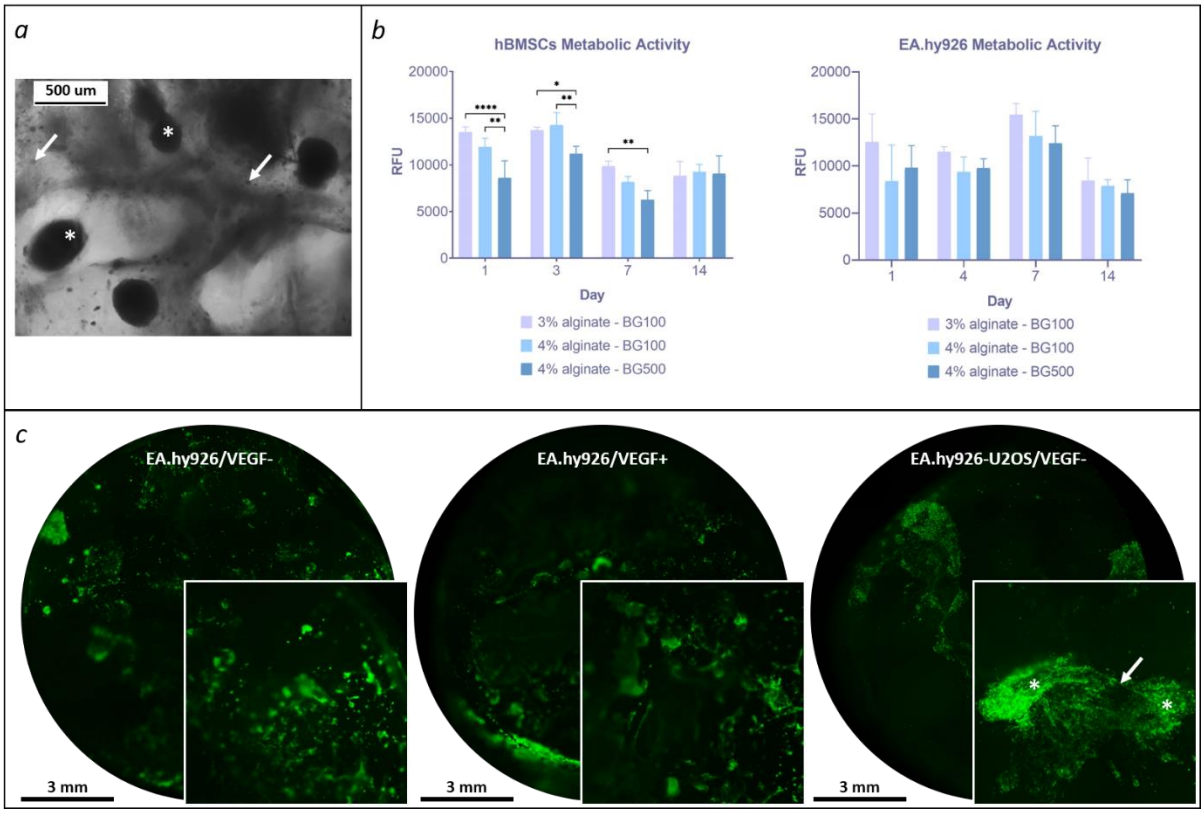

Figure 2-6 – Preliminary cytocompatibility analysis of alginate-bioactive glass scaffolds. (a) The spontaneous formation of hBMSCs cell spheroids (marked with stars) within the pores of the alg–BG scaffold after 1 week of cultivation; bright-field microscopy, scale bar 500 μm. (b) Metabolic activity of hBMSCs and EA.hy926 seeded cultured on the scaffolds; the values are presented as mean ± SD of relative fluorescent units (RFU). * - significant differences between groups of samples, $p < 0.05$. (c) EA.hy926 cells seeded on the 3% alg-2% BG100 scaffolds with or without VEGF and/or U2OS spheroids; Calcein AM staining, fluorescent microscopy, scale bar 3 mm.

2.4.3. Rehydration and porosity assessment

Based on the handling impressions, preliminary observation of mechanical stability and homogeneity of the resulting scaffolds, only one composition was chosen for the following analyses and applications – 3% alginate-2% BG100, later referred to as “alg-BG”. Considering the application of the scaffolds – that is, in brief, to be seeded with cells and placed under constant fluid flow, – it was necessary to assess the overall porosity of the scaffolds before and after rehydration. The scaffolds absorbed most of the liquid in the first 4 hours of soaking in medium (Figure 2-7), thus, this period of rehydration was chosen as an optimal one prior to the

seeding procedure. The scaffolds were swollen enough to prevent cells from experiencing tensile forces, and still not fully rehydrated to be able to entrap the cells within the pores.

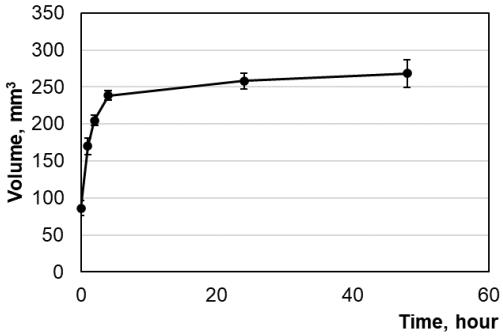

Figure 2-7 – The increase of the scaffolds' volume throughout the rehydration test made by soaking the freeze-dried samples in culture medium. The values are presented as the average ± standard deviation of three replicates.

Second, to understand whether the scaffold would enable the fluid flow, porosity was assessed. It decreased by only ~6% with rehydration, and the majority of the pores were represented by large pores from 300 µm up to 2 mm (Figure 2-8).

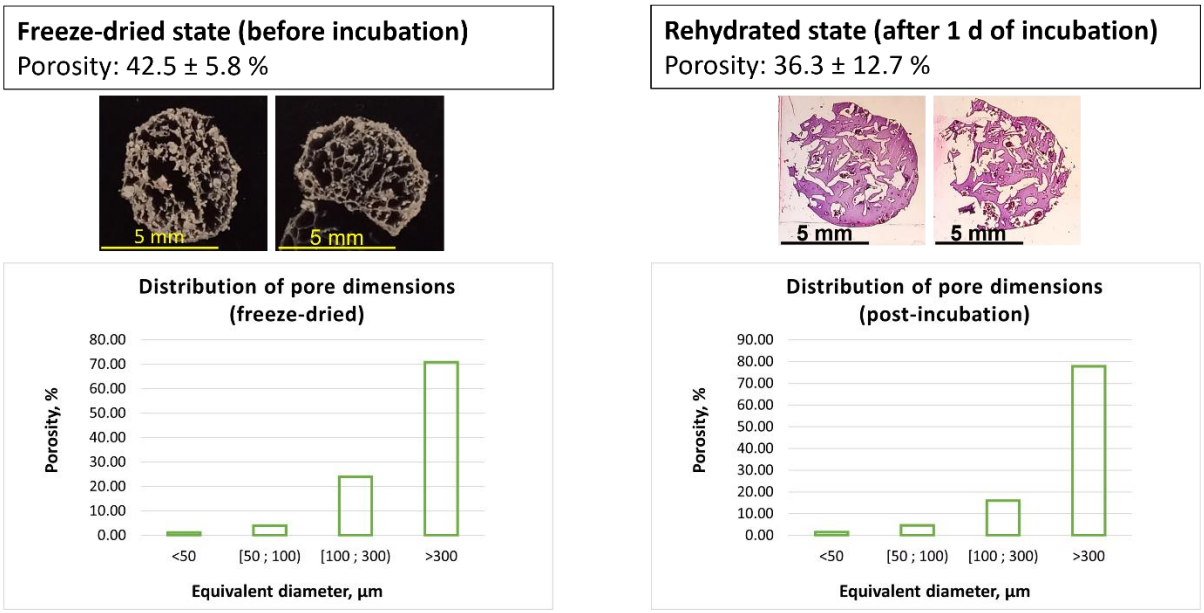

Figure 2-8 – Alg-BG scaffolds porosity assessment. Upper-row images: cross-section of the dry scaffold (left) and after rehydration in culture medium (right). The swelling of the scaffolds after rehydration and incubation in medium for a total of 24 hours led to a decrease in porosity by 6.2%. The majority of pores were represented by large pores (from 300 µm to 2 mm) in samples both in the dry and rehydrated state.

2.4.4. Rheological characterization of alginate-bioactive glass scaffolds

To characterize the viscoelastic behaviour of the alg-BG scaffolds depending on the various periods of incubation in medium, an oscillation frequency sweep test was performed. First, to determine the linear viscoelastic region of the alg-BG scaffolds, the amplitude stress sweep test was conducted within the oscillation strain range of 0.01–1000% in log mode at a

constant frequency of 1.0 Hz (Figure 2-9). The shear strain of 1% was chosen as a constant parameter of the following oscillation frequency sweep.

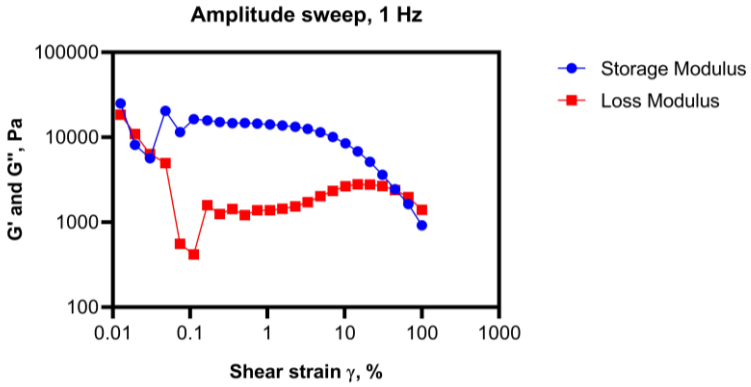

Figure 2-9 – Amplitude stress sweep test of a rehydrated alg-BG scaffold obtained in log mode at a constant frequency of 1.0 Hz.

The storage modulus G′ and loss modulus G″ were measured during angular frequency acceleration from 0.01 to 100 rad/s (Figure 2-10).

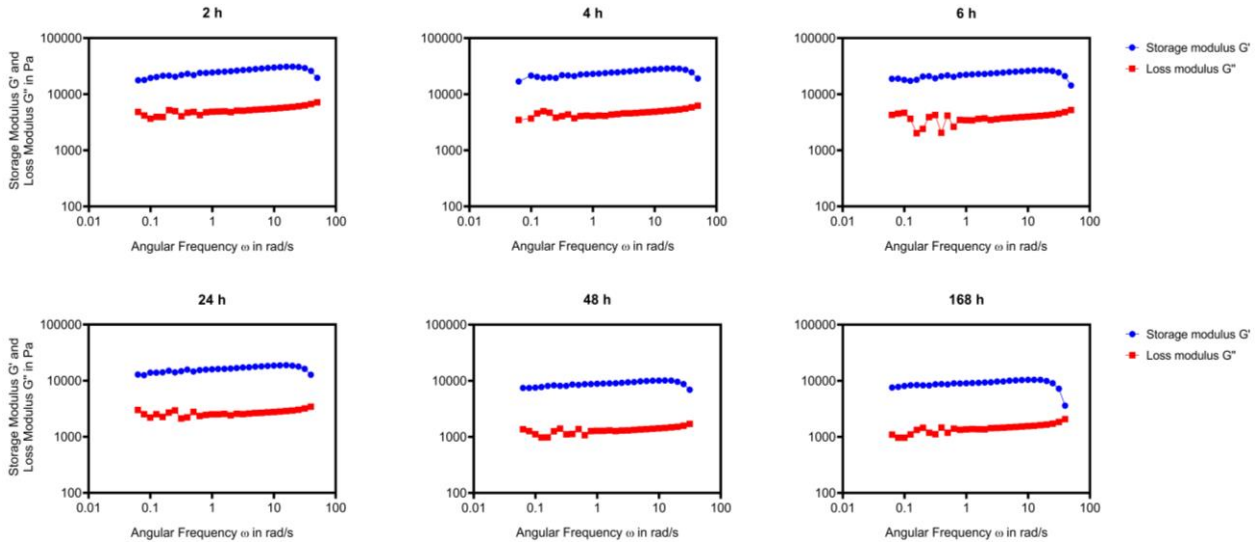

Figure 2-10 – Frequency sweep test of a rehydrated alg-BG scaffold obtained in log mode at a constant strain of 1%.

Literature observation showed that in the majority of recent cases, rheological studies of alginate-based materials are focused mainly on 3D-printing applications and thus are investigating the properties of non-cross-linked or partially cross-linked inks. As a result, referential storage modulus values were found to be in the order of 1000 Pa – ten times lower than the observed >10000 Pa in fully cross-linked alg-BG hydrogels.

Nonetheless, the complete cross-linking of alg-BG scaffolds used in this study did not guarantee the stability of the hydrogels in the culture medium. With incubation time, storage modulus decreased, which was highly evident since the 24-hour point of incubation (Figure 2-10, lower row). After 48 h of incubation, storage modulus did not exceed 10000 Pa, and after

168 hrs (7 d) there was a pronounced approximation of storage and loss moduli curves pointing to the transition from the elastic state of material to the viscous – or, in another words, degradation of the scaffold. The latter might be explained by the presence of bioactive glass: Bertuola et al. based on complex viscosity parameters of their alginate-hyaluronic acid gels with the addition of bioactive glass suggested that BG could disrupt the microstructure of the hydrogel. This suggestion, however, has been made for the compositions containing up to 8% of BG, and not for lower (2 and 4%) content (Bertuola et al., 2021). Sarker et al., on the contrary, observed increased cross-linking kinetics caused by the presence of BG particles in alginate-gelatin gels (Sarker et al., 2016).

2.4.5. Perfusion bioreactor studies

Cell spheroid formation and cell seeding efficiency

Murine osteosarcoma K7M2-wt cells demonstrated a good ability to form stable cell aggregates within 1 week (Figure 2-11). The seeding number of 1×10^5 proved to be the most suitable in terms of the morphology of the spheroid and the easiness of handling.

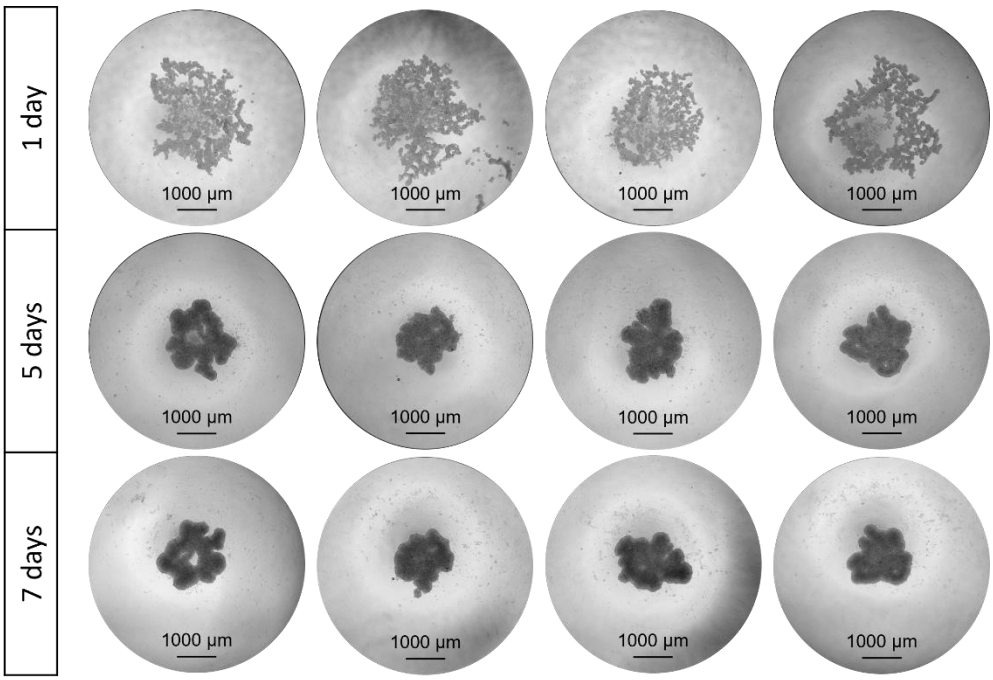

Figure 2-11 – K7M2-wt cell spheroids formation. The morphology changes from disaggregated cell clusters on the 1st day to compact cell aggregates on the 7th day of cultivation on an agarose-coated plate. Light microscopy. Scale bar 1000 µm.

For each experiment performed with scaffolds, cell seeding efficiency was evaluated by counting the cells remaining in the wells of a multiwell plate, where the cell-seeded scaffolds were cultivated for 1 day prior to loading into the bioreactor chambers. In the case of experiments with cell suspension, scaffolds were seeded with 98,8 ± 0,9% efficiency. In the case of spheroid-based cell seeding, the loss of $^1/_3$ was observed only in one of three initial samples.

Cell metabolic activity assays

The tested alg-BG scaffolds proved to be suitable to retain both cell suspension and cell spheroids for up to 1 day of cultivation in static conditions. However, after cultivation in the bioreactor chambers, a remarkable loss of cells was observed due to scaffold degradation (Figure 2-12). Evaluation of the scaffolds after 1 day of culture in static conditions and after 1 week of culture in a bioreactor showed a decrease in mass for ~17%, while the samples cultured in static conditions, on the contrary, gained around 9% of weight after 1 week. This degradation correlates with the data obtained during the rheological studies, where the loss of elastic modulus was observed after 24 h of incubation in medium. It should be underlined, that the observation has been carried out in static conditions, so, the degradation in the perfusion bioreactor with constant fluid flow is not fully unexpected. Nevertheless, the metabolic activity of the cells increased throughout the experiment, and in the case of spheroids, it was significantly higher in the perfusion bioreactor systems compared to the initial culture, as well as slightly higher compared to the static culture, indicating the beneficial impact of continuous medium flow on the cells in the investigated *in vitro* model due to providing efficient mass transport and adequate shear stresses.

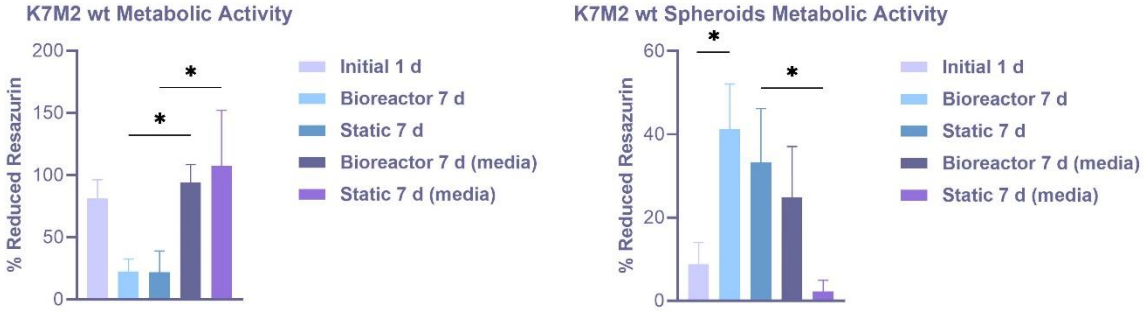

Figure 2-12 – K7M2-wt cells (left) and cell spheroids (right) viability on the alg–BG scaffolds after 1 day of culture in static conditions (*Initial*) and 7 days culture in dynamic (*Bioreactor*) and static conditions. The metabolic activity of the cells out of the scaffolds is represented by *Bioreactor (media)* and *Static (media)*. Results are shown as mean value ± standard deviation.

Morphological analysis of the cell-seeded scaffolds

The cell-seeded scaffolds were characterized by means of FE-SEM and histological analysis. Seeding cell suspension on the alg–BG scaffolds revealed the spontaneous formation of spheroids within the pores of the scaffolds on the 1st day of the cultivation (Figure 2-13), and the tight integration within the scaffold whenever the retention of the spheroid takes place (Figure 2-14).

***

Overall, perfusion bioreactor studies demonstrated that the scaffolds pose a favourable microenvironment for murine osteosarcoma cell spheroids and support their initial structure as voluminous dense cell aggregates, but their mechanical stability is lacking. Moreover, the high cell seeding efficiency observed in two types of seeding methods – cell-suspension-based and spheroid-based – indicated that the optimization of neither of these methods is required. We

observed, however, that retention of the cells in the scaffold pores (even in the case of cell suspension when a spontaneous spheroid formation was shown) and insufficient integration into the scaffold structure coupled with the scaffold degradation led to the washing out of the cells from the scaffolds in the bioreactor cultures. One of the possible ways of enhancing cell integration into the scaffold structure is modifying alginate with the RGD sequence mentioned earlier. RGD-peptide modification was shown to enhance the attachment, proliferation, migration and differentiation of various types of cells in the alginate scaffolds (Andersen, Auk-Emblem, and Dornish, 2015). In the context of the present study, it might be beneficial for better cell spheroid integration into the scaffold microstructure and, consequently, better retention of the spheroids in the scaffold cultured in bioreactor systems. On the other hand, from the morphological point of view, such modification might lead to excessive cell migration leading to the loss of the spheroid morphology. Regarding the possible optimization of the mechanical stability of the freeze-dried alg-BG scaffold *per se*, it is important to maintain the balance between chemical modification of the material and preservation of its cytocompatibility. For instance, in the study on alginate-encapsulated hepatocytes, the researchers encountered the loss of biomass due to degradation of the alginate beads while cultured in a bioreactor. They hypothesized that it might happen due to the presence of various molecules and ions in the culture medium (for instance, lactate as a possible calcium cation chelator or sodium and magnesium as possible anti-gelling cations). The authors used poly-L-lysine coating as a reinforcement agent for the maintenance of the alginate beads in the bioreactor. In comparison to introducing "stronger" chelators such as barium or strontium, this alternative may help to preserve the cytocompatibility of the scaffolds (Pasqua, 2021).

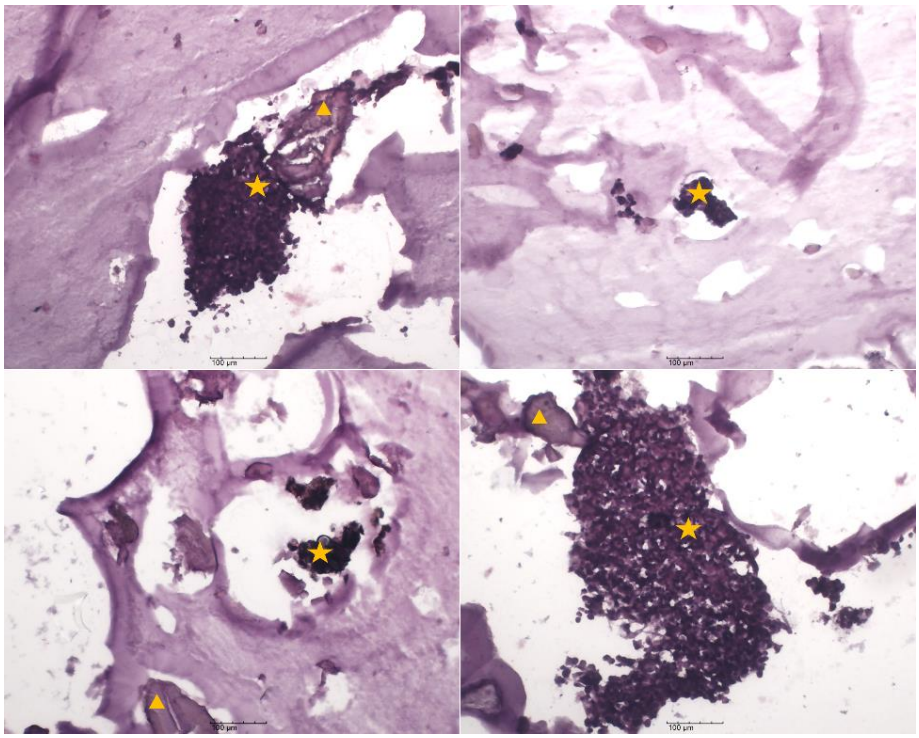

Figure 2-13 – The spontaneous formation of K7M2-wt cell aggregates (marked with stars) within the pores of the alg–BG scaffold after 1 d of cultivation in static conditions. Bioactive glass particles are marked with triangles. Haematoxylin & Eosin staining, scale bar 100 μm.

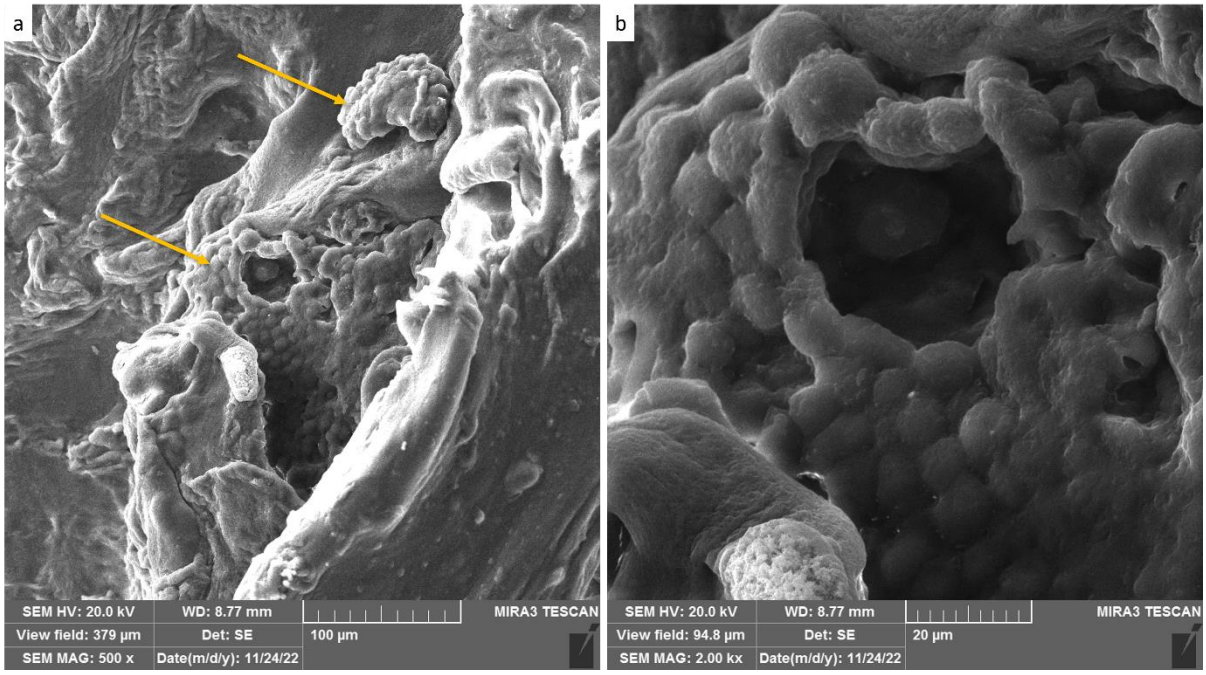

Figure 2-14 – FE-SEM images of K7M2-wt cell spheroids spontaneously formed within the pores of alg–BG scaffolds, retained and integrated within the structure for the 7 days of cultivation in the bioreactor. The cell spheroids are marked with yellow arrows (*a*). The region with cells is magnified in the image *b*.

2.5. Conclusions

In this part of the work, I optimized the method of freeze-dried alginate-bioactive glass scaffold production with controllable pore size, evaluated them in terms of material characteristics and cytocompatibility, and assessed the performance of the chosen type of scaffold in the perfusion bioreactor system. While being structurally similar to trabecular bone, compatible with key cell lines representatives of bone cancer microenvironment (osteosarcoma U2OS, bone-marrow-derived mesenchymal stem cells hBMSCs and endothelial EA.hy926) and possessing sufficient porosity for the following perfusion bioreactor studies, the alg-BG scaffolds did not prove to be mechanically stable. This was shown in the results of the rheological measurements in the rehydration study, and later during the study focused on dynamic culture. In this latter part of the study, the viability and morphology of the murine osteosarcoma K7M2-wt cells pointed to the suitability of the scaffolds for serving as an engineered microenvironment for osteosarcoma cell spheroids – limited to culture in static conditions. In terms of dynamic conditions, alg-BG scaffolds supported both the retention of the spheroids and spontaneous formation of cell aggregates; but their degradation led to the consequent loss of cells in the prefusion system. Thus, insufficient mechanical properties limit the use of the obtained alg-BG scaffolds in the present study, owing to its primary aim.

Part of the experiments displayed in this chapter were done in collaboration with PREMUROSA ESR Ivana Banicevic under the supervision of Prof. Bojana Obradovic during the secondment to the TMF of the University of Belgrade (Belgrade, Serbia).

2.6. References

Andersen, T., Auk-Emblem, P., & Dornish, M. (2015). 3D Cell Culture in Alginate Hydrogels. Microarrays, 4(2), 133–161. https://doi.org/10.3390/microarrays4020133

Bai, Y., Leng, Y., Yin, G., Pu, X., Huang, Z., Liao, X., Chen, X., & Yao, Y. (2014). Effects of combinations of BMP-2 with FGF-2 and/or VEGF on HUVECs angiogenesis in vitro and CAM angiogenesis in vivo. *Cell and Tissue Research*, *356*(1), 109–121. https://doi.org/10.1007/s00441-013-1781-9

Buenrostro, D., Mulcrone, P. L., Owens, P., & Sterling, J. A. (2016). The Bone Microenvironment: a Fertile Soil for Tumor Growth. In Current Osteoporosis Reports (Vol. 14, Issue 4, pp. 151–158). Current Medicine Group LLC 1. https://doi.org/10.1007/s11914-016-0315-2

Charoen, K. M., Fallica, B., Colson, Y. L., Zaman, M. H., & Grinstaff, M. W. (2014). Embedded multicellular spheroids as a biomimetic 3D cancer model for evaluating drug and drug-device combinations. *Biomaterials*, *35*(7), 2264–2271. https://doi.org/10.1016/j.biomaterials.2013.11.038

Chary, S. R., & Jain, R. K. (1989). Direct measurement of interstitial convection and diffusion of albumin in normal and neoplastic tissues by fluorescence photobleaching. In *Proc. Nati. Acad. Sci. USA* (Vol. 86).

Chaudhuri, O., Gu, L., Darnell, M., Klumpers, D., Bencherif, S. A., Weaver, J. C., Huebsch, N., & Mooney, D. J. (2015). Substrate stress relaxation regulates cell spreading. *Nature Communications 2015 6:1*, *6*(1), 1–7. https://doi.org/10.1038/ncomms7365

Chen, S., Shi, Y., Zhang, X., & Ma, J. (2020). Evaluation of BMP-2 and VEGF loaded 3D printed hydroxyapatite composite scaffolds with enhanced osteogenic capacity in vitro and in vivo. *Materials Science and Engineering: C*, *112*, 110893. https://doi.org/10.1016/j.msec.2020.110893

Chen, X., Hughes, R., Mullin, N., Hawkins, R. J., Holen, I., Brown, N. J., & Hobbs, J. K. (2021). Atomic force microscopy reveals the mechanical properties of breast cancer bone metastases. *Nanoscale*, *13*(43), 18237–18246. https://doi.org/10.1039/d1nr03900h

Cortini, M., Baldini, N., & Avnet, S. (2019). New advances in the study of bone tumors: A lesson from the 3D environment. In *Frontiers in Physiology* (Vol. 10, Issue JUN). Frontiers Media S.A. https://doi.org/10.3389/fphys.2019.00814

Ding, Y., Zhao, A., Liu, T., Wang, Y., Gao, Y., Li, J., & Yang, P. (2020). An Injectable Nanocomposite Hydrogel for Potential Application of Vascularization and Tissue Repair. *Annals of Biomedical Engineering*, *48*(5), 1511–1523. https://doi.org/10.1007/s10439-020-02471-7

Domura, R., Sasaki, R., Okamoto, M., Hirano, M., Kohda, K., Napiwocki, B., & Turng, L.-S. (2017). Comprehensive study on cellular morphologies, proliferation, motility, and epithelial–mesenchymal transition of breast cancer cells incubated on electrospun polymeric fiber substrates. *Journal of Materials Chemistry B*, *5*(14), 2588–2600. https://doi.org/10.1039/C7TB00207F

Freeman, F. E., & Kelly, D. J. (2017). Tuning alginate bioink stiffness and composition for controlled growth factor delivery and to spatially direct MSC Fate within bioprinted tissues. *Scientific Reports*, *7*(1), 1–12. https://doi.org/10.1038/s41598-017-17286-1

Galván-Chacón, V. P., Zampouka, A., Hesse, B., Bohner, M., Habibovic, P., & Barata, D. (2021). Bone-on-a-Chip: A Microscale 3D Biomimetic Model to Study Bone Regeneration. *Advanced Engineering Materials*, 2101467. https://doi.org/10.1002/ADEM.202101467

González Díaz, E. C., Sinha, S., Avedian, R. S., & Yang, F. (2019). Tissue-engineered 3D models for elucidating primary and metastatic bone cancer progression. In *Acta Biomaterialia* (Vol. 99, pp. 18–32). Acta Materialia Inc. https://doi.org/10.1016/j.actbio.2019.08.020

Gonzalez-Fernandez, T., Tenorio, A. J., Campbell, K. T., Silva, E. A., & Leach, J. K. (2021). Alginate-Based Bioinks for 3D Bioprinting and Fabrication of Anatomically Accurate Bone Grafts. *Tissue Engineering Part A*, *27*(17–18), 1168–1181. https://doi.org/10.1089/ten.tea.2020.0305

Gorlick, R., & Khanna, C. (2010). Osteosarcoma. In *Journal of Bone and Mineral Research* (Vol. 25, Issue 4, pp. 683–691). https://doi.org/10.1002/jbmr.77

Haugen, H. J., Lyngstadaas, S. P., Rossi, F., & Perale, G. (2019). Bone grafts: which is the ideal biomaterial? *Journal of Clinical Periodontology*, *46*(S21), 92–102. https://doi.org/10.1111/jcpe.13058

Hernández-González, A. C., Téllez-Jurado, L., & Rodríguez-Lorenzo, L. M. (2020). Alginate hydrogels for bone tissue engineering, from injectables to bioprinting: A review. *Carbohydrate Polymers*, *229*(May 2019), 115514. https://doi.org/10.1016/j.carbpol.2019.115514

Indovina, P., Ferrante, A., Rainaldi, G., & Santini, M. T. (2006). Hypoxia and Ionizing Radiation: Changes in Adhesive Properties and Cell Adhesion Molecule Expression in MG-63 Three-Dimensional Tumor Spheroids. *Cell Communication & Adhesion*, *13*(3), 185–198. https://doi.org/10.1080/15419060600734153

Ivanovska, I. L., Shin, J. W., Swift, J., & Discher, D. E. (2015). Stem cell mechanobiology: Diverse lessons from bone marrow. In *Trends in Cell Biology* (Vol. 25, Issue 9, pp. 523–532). Elsevier Ltd. https://doi.org/10.1016/j.tcb.2015.04.003

James, S., Fox, J., Afsari, F., Lee, J., Clough, S., Knight, C., Ashmore, J., Ashton, P., Preham, O., Hoogduijn, M., Ponzoni, R. D. A. R., Hancock, Y., Coles, M., & Genever, P. (2015). Multiparameter Analysis of Human Bone Marrow Stromal Cells Identifies Distinct Immunomodulatory and Differentiation-Competent Subtypes. *Stem Cell Reports*, *4*(6), 1004–1015. https://doi.org/10.1016/j.stemcr.2015.05.005

Jubelin, C., Muñoz-Garcia, J., Griscom, L., Cochonneau, D., Ollivier, E., Heymann, M. F., Vallette, F. M., Oliver, L., & Heymann, D. (2022). Three-dimensional in vitro culture models in oncology research. *Cell & Bioscience 2022 12:1*, *12*(1), 1–28. https://doi.org/10.1186/S13578-022-00887-3

Lahr, C. A., Landgraf, M., Wagner, F., Cipitria, A., Moreno-Jiménez, I., Bas, O., Schmutz, B., Meinert, C., Cavalcanti, A. D. S., Mashimo, T., Miyasaka, Y., Holzapfel, B. M., Shafiee, A., McGovern, J. A., & Hutmacher, D. W. (2022). A humanised rat model of osteosarcoma reveals ultrastructural differences between bone and mineralised tumour tissue. *Bone*, *158*, 116018. https://doi.org/10.1016/j.bone.2021.116018

Marsich, E., Bellomo, F., Turco, G., Travan, A., Donati, I., & Paoletti, S. (2013). Nano-composite scaffolds for bone tissue engineering containing silver nanoparticles: preparation, characterization and biological properties. *Journal of Materials Science: Materials in Medicine*, *24*(7), 1799–1807. https://doi.org/10.1007/s10856-013-4923-4

Menshikh, K., Banicevic, I., Obradovic, B., & Rimondini, L. (2023). Biomechanical Aspects in Bone Tumor Engineering. *Tissue Engineering Part B: Reviews*. https://doi.org/10.1089/ten.teb.2023.0106

Micalet, A., Moeendarbary, E., & Cheema, U. (2021). 3D in Vitro Models for Investigating the Role of Stiffness in Cancer Invasion. *ACS Biomaterials Science and Engineering*. https://doi.org/10.1021/acsbiomaterials.0c01530

Monteiro, C. F., Custódio, C. A., & Mano, J. F. (2021). Bioengineering a humanized 3D tri-culture osteosarcoma model to assess tumor invasiveness and therapy response. *Acta Biomaterialia*, *134*, 204–214. https://doi.org/10.1016/j.actbio.2021.07.034

Monteiro, M. v., Gaspar, V. M., Ferreira, L. P., & Mano, J. F. (2020). Hydrogel 3D: In vitro tumor models for screening cell aggregation mediated drug response. *Biomaterials Science*, *8*(7), 1855–1864. https://doi.org/10.1039/c9bm02075f

Morgan, E. F., Unnikrisnan, G. U., & Hussein, A. I. (2018). Bone Mechanical Properties in Healthy and Diseased States. *Annual Review of Biomedical Engineering*, *20*, 119. https://doi.org/10.1146/ANNUREV-BIOENG-062117-121139

Nia, H. T., Datta, M., Seano, G., Huang, P., Munn, L. L., & Jain, R. K. (2018). Quantifying solid stress and elastic energy from excised or in situ tumors. *Nature Protocols*, *13*(5), 1091–1105. https://doi.org/10.1038/nprot.2018.020

Ocando, C., Dinescu, S., Samoila, I., Daniela Ghitulica, C., Cucuruz, A., Costache, M., & Averous, L. (2021). Fabrication and properties of alginate-hydroxyapatite biocomposites as efficient biomaterials for bone regeneration. *European Polymer Journal*, *151*(April), 110444. https://doi.org/10.1016/j.eurpolymj.2021.110444

Pasqua, M., Pereira, U., de Lartigue, C., Nicolas, J., Vigneron, P., Dermigny, Q., & Legallais, C. (2021). Preclinical characterization of alginate-poly-L-lysine encapsulated HepaRG for extracorporeal liver supply. Biotechnology and Bioengineering, 118(1), 453–464. https://doi.org/10.1002/bit.27583

Pinto, B., Henriques, A. C., Silva, P. M. A., & Bousbaa, H. (2020). Three-dimensional spheroids as in vitro preclinical models for cancer research. *Pharmaceutics*, *12*(12), 1–38. https://doi.org/10.3390/pharmaceutics12121186

Roohani, I., Cheong, S., & Wang, A. (2021). How to build a bone? - Hydroxyapatite or Posner's clusters as bone minerals. *Open Ceramics*, *6*, 100092. https://doi.org/10.1016/j.oceram.2021.100092

Sakolish, C., House, J. S., Chramiec, A., Liu, Y., Chen, Z., Halligan, S. P., Vunjak-Novakovic, G., & Rusyn, I. (2020). Tissue-Engineered Bone Tumor as a Reproducible Human in Vitro Model for Studies of Anticancer Drugs. *Toxicological Sciences*, *173*(1), 65. https://doi.org/10.1093/TOXSCI/KFZ220

Salamanna, F., Borsari, V., Brogini, S., Giavaresi, G., Parrilli, A., Cepollaro, S., Cadossi, M., Martini, L., Antonio, M., & Fini, M. (2016). An in vitro 3D bone metastasis model by using a human bone tissue culture and human sex-related cancer cells. *Oncotarget*, *7*(47), 76966–76983. https://doi.org/10.18632/oncotarget.12763

Sarker, B., Li, W., Zheng, K., Detsch, R., & Boccaccini, A. R. (2016). Designing Porous Bone Tissue Engineering Scaffolds with Enhanced Mechanical Properties from Composite Hydrogels Composed of Modified Alginate, Gelatin, and Bioactive Glass. *ACS Biomaterials Science and Engineering*, *2*(12), 2240–2254. https://doi.org/10.1021/ACSBIOMATERIALS.6B00470

Sowder, M. E., & Johnson, R. W. (2019). Bone as a Preferential Site for Metastasis. *JBMR Plus*, *3*(3), 1–10. https://doi.org/10.1002/jbm4.10126

Stojkovska, J., Zvicer, J., Andrejevic, M., Janackovic, D., Obradovic, B., & Veljovic, D. N. (2021). Novel composite scaffolds based on alginate and Mg-doped calcium phosphate fillers: Enhanced hydroxyapatite formation under biomimetic conditions. *Journal of Biomedical Materials Research. Part B, Applied Biomaterials*, *109*(12), 2079–2090. https://doi.org/10.1002/JBM.B.34856

Stojkovska, J., Zvicer, J., Milivojevic, M., Petrovic, I., Stevanovic, M., & Obradovic, B. (2020). Validation of a novel perfusion bioreactor system in cancer research. *Hemijska Industrija*, *74*(3), 187–196. https://doi.org/10.2298/HEMIND200329015S

Stylianopoulos, T., Martin, J. D., Chauhan, V. P., Jain, S. R., Diop-Frimpong, B., Bardeesy, N., Smith, B. L., Ferrone, C. R., Hornicek, F. J., Boucher, Y., Munn, L. L., & Jain, R. K. (2012). Causes, consequences, and remedies for growth-induced solid stress in murine and human tumors. *Proceedings of the National Academy of Sciences of the United States of America*, *109*(38), 15101–15108. https://doi.org/10.1073/pnas.1213353109

Teixeira, F. C., Chaves, S., Torres, A. L., Barrias, C. C., & Bidarra, S. J. (2021). Engineering a Vascularized 3D Hybrid System to Model Tumor-Stroma Interactions in Breast Cancer. *Frontiers in Bioengineering and Biotechnology*, *9*. https://doi.org/10.3389/FBIOE.2021.647031/FULL

Thai, V. L., Griffin, K. H., Thorpe, S. W., Randall, R. L., & Leach, J. K. (2021). Tissue engineered platforms for studying primary and metastatic neoplasm behavior in bone. *Journal of Biomechanics*, *115*, 110189. https://doi.org/10.1016/j.jbiomech.2020.110189

Trachtenberg, J. E., Santoro, M., Williams, C., Piard, C. M., Smith, B. T., Placone, J. K., Menegaz, B. A., Molina, E. R., Lamhamedi-Cherradi, S. E., Ludwig, J. A., Sikavitsas, V. I., Fisher, J. P., & Mikos, A. G. (2018). Effects of Shear Stress Gradients on Ewing Sarcoma Cells Using 3D Printed Scaffolds and Flow Perfusion. *ACS Biomaterials Science and Engineering*, *4*(2), 347–356. https://doi.org/10.1021/acsbiomaterials.6b00641

Venkatesan, J., Bhatnagar, I., Manivasagan, P., Kang, K. H., & Kim, S. K. (2015). Alginate composites for bone tissue engineering: A review. *International Journal of Biological Macromolecules*, *72*, 269–281. https://doi.org/10.1016/J.IJBIOMAC.2014.07.008

Walker-Samuel, S., Roberts, T. A., Ramasawmy, R., Burrell, J. S., Johnson, S. P., Siow, B. M., Richardson, S., Gonçalves, M. R., Pendse, D., Robinson, S. P., Barbara Pedley, R., & Lythgoe, M. F. (2018). Investigating low-velocity fluid flow in tumors with convection-MRI. *Cancer Research*, *78*(7), 1859–1872. https://doi.org/10.1158/0008-5472.CAN-17-1546

Wang, Q., Zhang, Y., Li, B., & Chen, L. (2017). Controlled dual delivery of low doses of BMP-2 and VEGF in a silk fibroin–nanohydroxyapatite scaffold for vascularized bone regeneration. *Journal of Materials Chemistry B*, *5*(33), 6963–6972. https://doi.org/10.1039/C7TB00949F

Zhang, W., Bado, I., Wang, H., Lo, H. C., & Zhang, X. H. F. (2019). Bone Metastasis: Find Your Niche and Fit in. *Trends in Cancer*, *5*(2), 95–110. https://doi.org/10.1016/j.trecan.2018.12.004

Zvicer, J., Miskovic-Stankovic, V., & Obradovic, B. (2019). Functional bioreactor characterization to assess potentials of nanocomposites based on different alginate types and silver nanoparticles for use as cartilage tissue implants. *Journal of Biomedical Materials Research - Part A*, *107*(4), 755–768. https://doi.org/10.1002/jbm.a.36590

3. Osteosarcoma environment *in vitro*: hard scaffold-based approach

3.1. Introduction

3.1.1. Calcium phosphates in bone tissue engineering

Calcium phosphates are widely used in bone tissue engineering due to their biocompatibility, biodegradability, and structural similarity with the inorganic content of bone minerals. The fact that hydroxyapatite, a member of the calcium phosphates group, is the main inorganic component of bone serves as motivation for the use of calcium phosphates (Haugen et al., 2019). In bone tissue engineering, they are frequently used as implant coatings or as a paste – for instance, mixed with the patient's platelets (Surmenev et al., 2014; Vogel et al., 2006). The main limitation of calcium phosphate-based materials and other bioceramics is their brittleness (Haugen et al., 2019).

Due to its availability, osteoinductive, and osteoconductive properties, beta-tricalcium phosphate (β-TCP) – one of the most popular calcium phosphates in the field of biomaterials – is frequently used as a material for bone grafts (Bohner et al., 2020). 3D printing with β-TCP with the following sintering allows for a controlled hierarchical structure with the presence of micro- and macropores enabling enhanced cell attachment and proliferation (Paredes et al., 2024).

3.1.2. Recapitulating bone architecture

The curvature of the material in contact with cells is known to influence (to some extent) the cell behaviour. Convex or concave roughness which has a curvature radius comparable to the dimensions of a cell, can lead to cytoskeleton reorganization and cell stretching, bridging, spherical shape or detaching, followed by altered activation of molecular signalling (Baptista et al., 2019). The curvature of the bone tissue plays an important role in cell fate along with biological signalling. It was demonstrated *in vitro* that the curvature affects the process of mineralization (Vetsch et al., 2016).

An interesting work done by Rüdrich and co-authors connected the macro- and microscopic peculiarities of matrix curvature influence on cell behaviour. The authors seeded murine pre-osteoblastic cells on silica-doped hydroxyapatite scaffolds possessing different microporosity and containing macro-sized openings of various shapes and sizes. The observation of how cells colonized the openings pointed to the importance of initial cytoskeleton distribution which is directly related to microstructure (Rüdrich et al., 2019).

3D-printed calcium phosphate scaffolds, particularly β-TCP, offer attractive solutions with their availability, osteoinductive properties, and controlled hierarchical structure. Not the easiest material for printing, β-TCP still can be used to print scaffolds with microstructure and porosity positively modulating cell attachment, as well as osteogenic and angiogenic processes (Feng et al., 2023). Sintering techniques are one of the ways to enable control over the material’s microstructure. For instance, Wang and co-authors used various sintering temperatures for their 3D-printed β-TCP scaffolds and clearly demonstrated how this

parameter affects the microstructure of the material (Figure 3-1) (C. X. Wang et al., 2004). Additionally, they demonstrated that the hardness and stiffness of the scaffolds are influenced by the sintering – with increasing temperatures leading to decreasing Young's modulus.

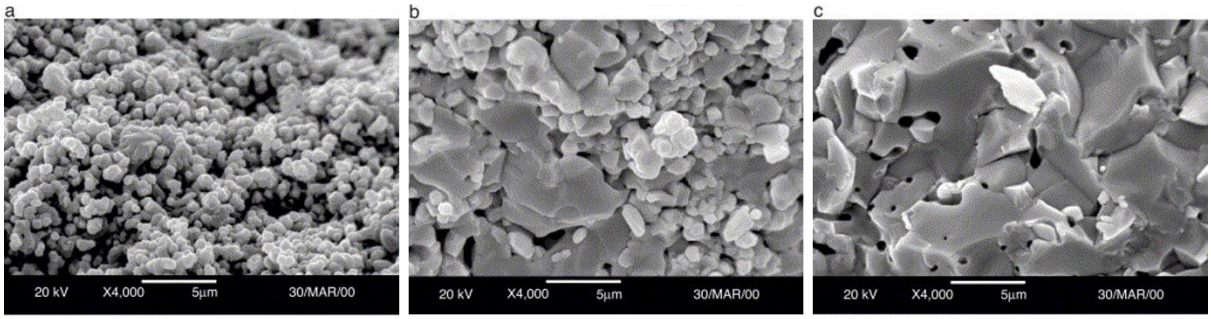

Figure 3-1 - SEM micrographs of TCP specimens sintered at different temperatures. (a) 1100 °C. (b) 1200 °C. (c) 1300 °C. Adapted from Wang et al., 2004.

3.2. Aim

In this Chapter, I am focusing on the "hard scaffold-based" approach – in contrast to the "soft scaffold-based" approach investigated in the previous Chapter 2. By utilizing the scaffolds produced from tricalcium phosphate by 3D printing, I aim to obtain a more reproducible and mechanically stable model. To demonstrate the applicability of the scaffolds for fulfilling the needs of the osteosarcoma model *in vitro*, I describe the material characterization presented by nanoindentation analysis and scanning electron microscopy. Then, I am moving to cytocompatibility evaluation of the scaffolds, testing them separately with all the participants of the future *in vitro* model – osteosarcoma spheroids, MSCs and endothelial cells. I extend the study to the tests with three different bioreactors and present a brief overview of transcriptomic data obtained throughout one of the bioreactor studies with primary MSCs.

3.3. Materials and Methods

3.3.1. Materials

Low-glucose, as well as high-glucose Dulbecco's modified Eagle's medium (DMEM), Minimum Essential Medium (MEM, GlutaMAX™ Supplement) α, fetal bovine serum (FBS), trypsin EDTA 1X, ethanol (EtOH, BioUltra, ≥ 99.8%, molecular biology grade, CAS: 64-17-5), dexamethasone (≥ 97%, CAS: 50-02-2), phosphate-buffered saline (PBS, ready-to-use tablets, Ref. N. P4417-100TAB), resazurin sodium salt (Ref. N. R7017-5G, CAS: 62758-13-8), alginic acid sodium salt (medium viscosity Cat. No. A2033), β-glycerophosphate disodium salt hydrate (BioUltra, ≥ 99% (titration), CAS: 154804-51-0), and L-ascorbic acid 2-phosphate sesquimagnesium salt hydrate (≥ 95%, CAS: 50-81-7), Tween® 20 Detergent (Molecular Biology Grade, CAS: 9005-64-5), paraformaldehyde (Reagent grade, crystalline, Ref. N. P6148-1KG, CAS: 30525-89-4) and hexamethyldisilazane (HMDS, reagent grade, ≥ 99%,

CAS: 999-97-3), and Pluronic® (F-127) were purchased from Sigma-Aldrich, USA. Human Basic Fibroblast Growth Factor (FGF2) was purchased from Cell Signaling Technology, USA., Sigma-Aldrich, USA) Penicillin-streptomycin (PS), Alexa Flour 594-conjugated phalloidin (Ref. N. A12381), and TRIzol™ were purchased from Invitrogen, USA. Transwell inserts (Thincert™, 0.4 µm porosity) were purchased from Greiner Bio-One, Austria. 24-well plates (Ref. N. 30024) purchased from SPL Life Sciences, Korea. 4′,6-Diamidino-2-phenylindole dihydrochloride (DAPI, Ref. N. 90229, CAS: 28718-90-3) was purchased from Millipore, USA. Alkaline Phosphatase Assay Kit (ALP, Colorimetric, ab83369) was bought from Abcam, UK. Coomasie reagent (Protein Assay Dye Reagent Concentrate, Ref. N. 5000006), agarose (Certified Molecular Biology Agarose, Cat. No. 1613100), iScript™ cDNA Synthesis Kit and master mix for quantitative real-time PCR (SsoAdvanced Universal SYBR Green Supermix) were purchased from Bio-Rad Laboratories, USA. β-TCP powder (Whitlockite) was purchased from Plasma Biotal Limited, UK. Primers for qPCR were designed using PrimerQuest™ Tool and synthesized by Integrated DNA Technologies (IDT, USA). Cell lines used for the research have the following specifications: human bone marrow-derived stem cells (hBMSCs, hTERT-BMSC clone Y201, isolated from bone marrow and immortalized through hTERT lentiviral vectors (James et al., 2015)) were kindly provided by Prof. P. Genever, University of York; human umbilical vein cell line (EA.hy926, CRL2922), human osteosarcoma cell line (U2OS, HTB96) and murine osteosarcoma cell line (K7M2-wt, CRL-2836™) were purchased in American Type Culture Collection, Manassas, VA, USA; primary human bone marrow-derived stem cells (pBMSCs) were purchased from RoosterBio, USA.

3.3.2. Scaffold production

The scaffolds were produced by mixing β-TCP powder with Pluronic®, 3D-printing the mix in the form of a cylinder with a grid-like structure, and subsequent sintering. For the ink preparation, Pluronic® and ultrapure water (30% w/w, from here referred to as pl30) were mixed with a magnetic stirrer at high rpm for around 6-8 hours to get a homogeneous phase, pl30 was kept on ice to preserve it from solidifying. Next, 86% vol (=68% weight) pl30 and 14% vol (=32% weight) β-TCP powder were vortexed at 2500 rpm for around 30 s and cooled down on the ice for around 30 s repeatedly until the ink was homogeneous. With a syringe, the mixture was transferred to the cartridge to be attached to the 3Dn Tabletop Printer (nScrypt Inc., Orlando, Florida, USA). The scaffolds were printed using a script in .txt format; the height of each of the scaffolds was 8 mm, and the diameter was 10 mm. The printed scaffolds were left overnight in a drying oven at 37 ºC degrees. The following day the scaffolds were sintered as follows:

1. RT → 500 °C: 8 h 20 min (1 °C/min)
2. 500 °C = const: 1 h
3. 500 °C → 1150 °C: 2 h 10 min (5 °C/min)
4. 1150 °C = const: 3 h
5. 1150 °C → 500 °C: 2 h 10 min (5 °C/min)
6. 500 °C → RT: free cooling

3.3.3. Mechanical and morphological characterization

To assess the morphological properties of 3D-printed β-tricalcium phosphate (β-TCP) scaffolds such as pore size and pore distribution, as well as an elemental profile of the scaffolds, they were analysed by SEM with an energy-dispersive X-ray (EDX) spectrometer (JSM-IT500, Jeol, Japan). Information about the 3D structure of the scaffolds was obtained with the help of micro-computed tomography (µCT, MicroXCT-400, Carl Zeiss X-ray Microscopy, Inc., USA) using 80 kV tube voltage, a 0.4× objective, and visualization via Avizo software (Thermo Fischer Scientific, USA) as described previously (Szczodra et al, 2024). To assess the mechanical properties of the material on a micro-scale, the scaffolds were indented by the probe (stiffness of 176.6 N/m and tip radius of 9.0 µm) with Piuma Nanoindenter (Optics11 Life, NL). Measurement was performed in demineralised water to minimize attraction forces between the material and the tip. The view of the measurement procedure is shown in Figure 3-2. Optimization of the obtained data was done by indentation model on the relevant range with the use of DataViewer Software (v2.5.7, Optics11 Life, NL).

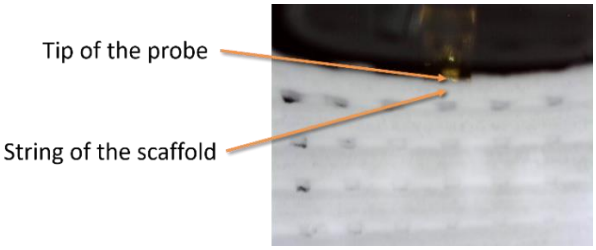

Figure 3-2 – Nanoindentation of β-TCP scaffold.

3.3.4. Fourier-transform infrared spectroscopy of β-TCP scaffolds

To confirm the presence of functional groups characteristic for β-TCP after scaffold production, Fourier-transform infrared spectroscopy was used (PerkinElmer Spectrum One FTIR Spectrophotometer (PerkinElmer, Waltham, MA)) and the analysis was performed via attenuated total reflection (ATR) method. For this, the scaffold was milled to powder, and a small amount of the powder was applied to ATR crystal which is a high-refractive-index prism. The spectra of the scaffold with Pluronic® F127 (before sintering) and without Pluronic® (after sintering) were acquired within the wavenumber range 4000-600 cm^{-1}, setting the resolution at 2 cm^{-1}, with each spectrum obtained by averaging 32 scans. The spectra were background-corrected and normalized to the band with the highest intensity. Band assignments and spectral decomposition were compared with the data found in the literature.

3.3.5. X-Ray diffraction analysis

To confirm that the β-TCP structure is maintained after sintering, an X-ray diffraction (XRD) analysis was conducted. The scaffolds were ground to fine powder, and measurements were performed in the 10–100° using 2θ diffraction angle range and cobalt tube (Kα = 1.789 Å) with Empyrean (Malvern Panalytical, UK).

3.3.6. Cytocompatibility evaluation

To estimate the cytocompatibility of β-TCP scaffolds, an *in vitro* assay via direct contact with cells was set up. Considering the future perspectives of scaffold usage – that is, in brief, employing them as a matrix for the osteosarcoma model, – two cell lines were chosen for the preliminary studies: human osteosarcoma and human bone marrow-derived mesenchymal stem cells.

Cell culture and spheroid formation

Human bone marrow-derived mesenchymal stem cells (hBMSCs) were cultivated in low-glucose DMEM supplemented with 15 % FBS and 1 % PS at 37 ºC in the humidified atmosphere containing 5 % CO_2. Human osteosarcoma cells (U2OS) were cultivated in high-glucose DMEM supplemented with 10 % FBS and 1% PS at 37 ºC in a humidified atmosphere containing 5 % CO_2. To obtain cell spheroids, firstly, a 48-well plate was coated with 1.5 % agarose solution in sterile conditions and let solidify and sterilize at room temperature under UV exposure for 2 h. Then, U2OS cells were seeded in single-cell suspension in the number of 50×10^3 cells per well of the agarose-coated multiwell plate. Cells were supplemented with culture media and incubated in standard conditions with media being changed every 2 or 3 days.

B-TCP scaffolds cytocompatibility assay

Prior to use in the cytocompatibility assay, β-TCP scaffolds were sterilized by heating at 140 ^{0}C for 3 h and quickly washed in sterile PBS. In the case of hBMSCs, cells were trypsinized, suspended in a 1:1 mixture of media and 5 mg/mL collagen and seeded on a β-TCP scaffold. In the case of U2OS, 1-week cell spheroids were used in the assay. The spheroids were gently transferred from the 48-well plate by pipetting, immersed in the collagen-media mixture and injected into each scaffold. After 3 h of collagen solidifying, the scaffolds were transferred to the clean wells of 24-well plate and 1.5 mL of the culture media was added. The culture media was changed every 2 or 3 days. On the 1st, 3rd and 7th days of the incubation period of cells on β-TCP scaffolds, cell metabolic activity and morphology were assessed by means of resazurin reduction assay and fluorescent microscopy with live/dead staining, respectively. At the end of the incubation period, the cell-seeded scaffolds were fixed in paraformaldehyde, dehydrated by exposing them to ethanol in increasing concentration and dried out by immersing them in HMDS overnight in the open air. After the gold-sputtering (DII-29019SCTR Smart Coater, Jeol, Japan), the samples were analysed by SEM.

3.3.7. Perfusion bioreactor study

To estimate the supremacy of β-TCP scaffolds in dynamic conditions, a perfusion bioreactor was employed. In the perspective of utilizing the scaffolds as vascularized units, they were seeded with endothelial cells.

Cell culture and cell seeding procedure

The human endothelial umbilical vein cells (EA.hy926) were cultivated in high-glucose DMEM supplemented with 10 % FBS and 1 % PS and maintained at 37 ºC in the humidified atmosphere containing 5 % CO_2. Before cell seeding, β-TCP scaffolds were sterilized by

heating at 140 ^{0}C for 3 h and quickly washed in sterile PBS. EA.hy926 were trypsinized, suspended in a 1:1 mixture of media and 5 mg/mL collagen as described before and seeded on β-TCP scaffolds. After 3 h of collagen solidifying, the scaffolds were transferred to the clean wells of 24-well plate and 1.5 mL of the culture media was added.

Set-up of the bioreactor

After 1 day of cultivation in standard (static) conditions, cell-seeded scaffolds were loaded into the chambers of perfusion bioreactors as described previously ("3D Perfuse", Innovation Center of the Faculty of Technology and Metallurgy, Belgrade, Serbia). On the 7th day (one day in static culture and 6 days in perfusion bioreactor) of the incubation period of cells on β-TCP scaffolds, bioreactor systems were disassembled, and the scaffolds were taken for examination. Cell metabolic activity and morphology were assessed through resazurin reduction assay, fluorescent microscopy and SEM as described above.

3.3.8. Co-culture study

To evaluate possible inputs of cell-cell crosstalk in the investigated *in vitro* model in static and dynamic conditions, co-culture was set up using osteosarcoma U2OS and endothelial EA.hy926 cells in Quasi Vivo® (QV900, Kirkstall, Ltd, UK) system. For this, mixed U2OS-EA.hy926 cell suspension (3.5×10^4 of U2OS and 3.5×10^4 EA.hy926 per one well) was seeded on the agarose-coated plate. Then, the 5-day mature spheroids were seeded in 50 µL of collagen on the β-TCP scaffolds as described before, and the scaffolds were cultured in 3 mL of culture media for 3 days. The scaffolds were divided into 3 groups for the analysis and following cultivation as shown in the scheme in Figure 3-3.

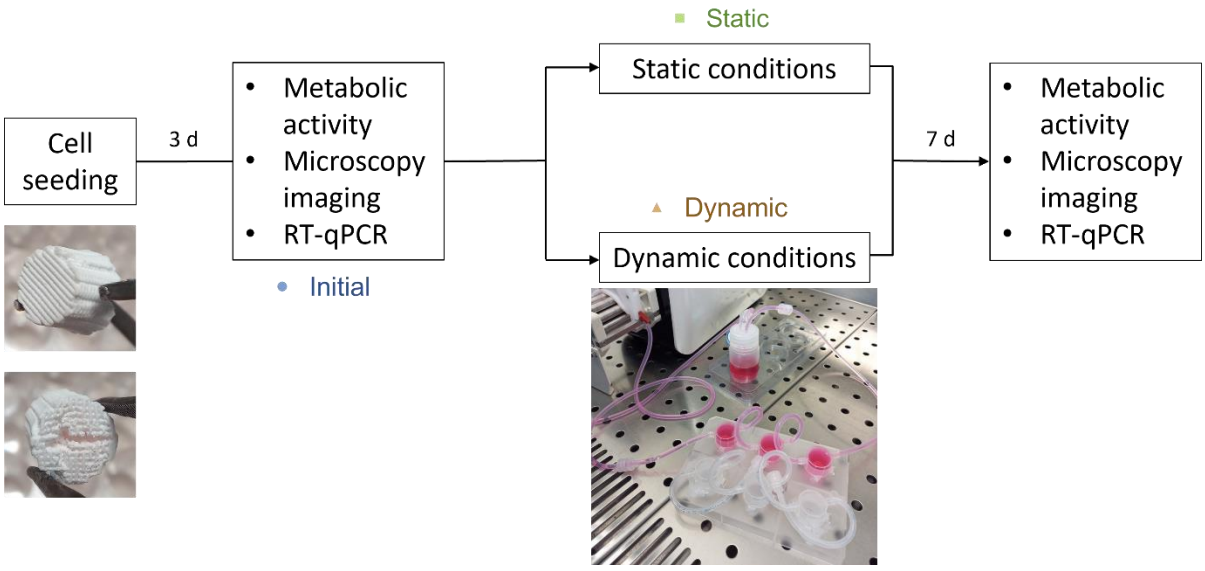

Figure 3-3 – Scheme of co-culture experiment and sample group labelling. *Initial* – cell-seeded scaffolds cultured in standard conditions for 3 days. *Static conditions* – cell-seeded scaffolds cultured in standard conditions for 6 days; *dynamic conditions* – scaffolds in bioreactor culture.

In the case of bioreactor culture ("Dynamic"), the scaffolds were placed in the chambers of the Quasi Vivo® system, and the chambers were sequentially connected to the pump and media reservoir as shown in Figure 3-4 and placed in the incubator. The peristaltic pump

parameters were set with respect to media superficial velocity of 40 μm/s. The flow rate was calculated using the cross-sectional area of the chamber. In the case of static culture ("Static"), the scaffolds were placed in the T-75 flasks and immersed in a medium.

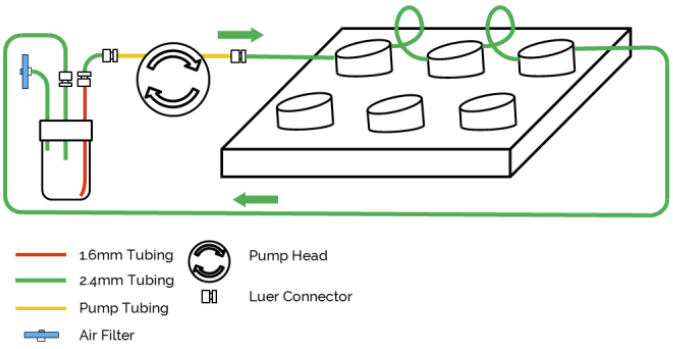

Figure 3-4 – Scheme of QV900 bioreactor system used for culturing cell-seeded scaffolds ("Dynamic" group).

The samples of three groups (Initial, Static and Dynamic) were analysed employing metabolic activity (resazurin reduction) assay, fluorescent microscopy, and RT-qPCR. For the latter, the samples were ground to powder, and the RNeasy Plus Mini Kit (Qiagen, Hilden, Germany) was used to extract RNA. The expression of VEGF and RB1 genes was analysed on the synthesized cDNA with a mix for quantitative real-time PCR. GAPDH was used as a housekeeping gene. The sequences of forward and reverse primers are listed in Table 3-1.

Table 3-1 – Gene primer sequences.

Gene	Forward primer	Reverse primer
GAPDH	5'- GTA TGA CAA CAG CCT CAA GAT -3'	5'- GTC CTT CCA CGA TAC CAA AG -3'
RB1	5'- AGC CTA TCT CCG GCT AAA TA -3'	5'- GTC CAA ATG CCT GTC TCT C -3'
VEGF	5'- ACC AGA GGA AAG TGG TGT -3'	5'- CAT GAG CTC CAC AGT CAA G -3'

3.3.9. Nanokicking study

Primary human bone marrow-derived stem cells (pBMSCs, RoosterBio, USA) were cultivated in Minimum Essential Medium (MEM, GlutaMAX™ Supplement) α supplemented with 10 %FBS, 1 % PS, and 10 ng/mL FGF2, and maintained at 37 ºC in the humidified atmosphere containing 5 % CO_2. Prior to cell seeding, β-TCP scaffolds were sterilized by heating at 140 ^{0}C for 3 h, quickly washed in sterile PBS and immersed overnight in an FBS-enriched culture medium. PBMSCs were trypsinized, suspended in a 1:1 mixture of media and 5 mg/mL collagen and seeded on β-TCP scaffolds in the number of 3×10^5 cells per scaffold. After 3 h of collagen solidifying, the scaffolds were transferred to a 24-well plate, and 1.5 mL of the culture media was added.

Set-up of the nanovibrational bioreactor

After 3 days of cultivation in standard conditions, cell-seeded scaffolds were divided into two groups and placed into two 24-well plates. One plate was maintained in standard (static) conditions, and the other plate was attached by the magnets onto the platform of the nanovibrational bioreactor providing oscillation of around 30 nm (Figure 3-5). Underneath the

top plate, piezo-active ceramics are located and are being expanded by external voltage set to 1 Vpp and 1 kHz realizing this way a reverse piezo effect (Pemberton et al., 2015).

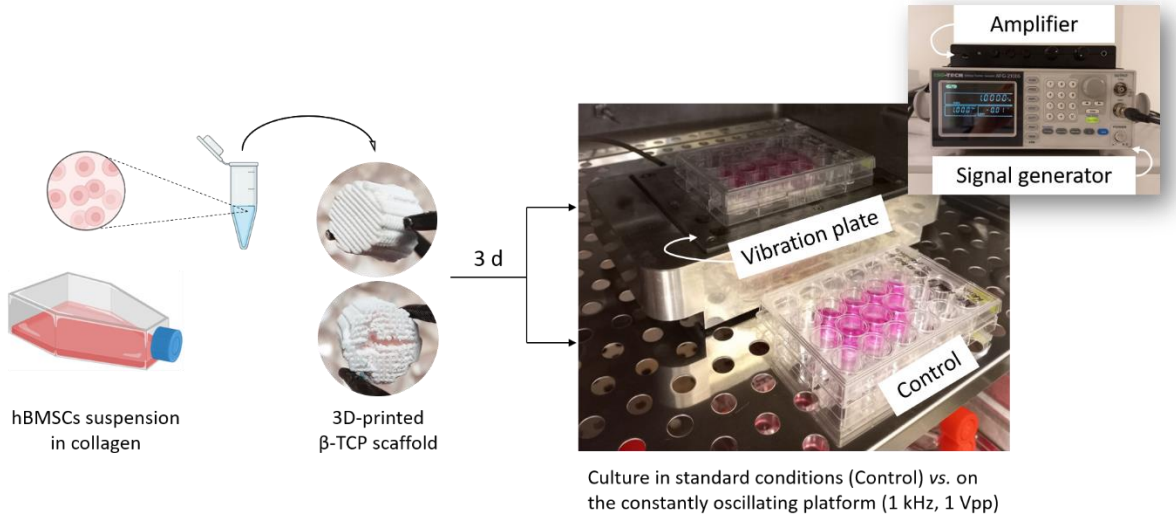

Figure 3-5 – Scheme of nanovibrational bioreactor set-up.

Cell metabolic activity and morphology, while cultured on the scaffolds in two conditions, were assessed by means of resazurin reduction assay and fluorescent microscopy with Calcein AM/Ethidium homodimer-1 staining following the manufacturer's instruction. Along with that, total protein and total RNA were extracted from the cell-seeded scaffolds for gene expression analysis and ALP activity assay. For total RNA extraction, the cell-seeded scaffolds were disrupted by thorough vortexing in 2-mL tubes with tungsten carbide beads in lysis buffer, and then the standard protocol of RNeasy Plus Mini Kit was followed. Total protein was recovered from flow-through by acetone precipitation method.

mRNA-Seq and differential gene expression analysis

The concentration and integrity of the extracted RNA were analysed on the spectrophotometer (NanoDrop 2000, Thermo Scientific, USA) and BioAnalyzer (Agilent RNA 6000 Nano, Agilent Technologies, USA), respectively. The mRNA sequencing was performed by Novogene (Cambridge, UK) using the NovaSeq 6000 platform (Illumina, United States), generating paired-end 150 bp reads. The reads were aligned to the Homo Sapiens (GRCh38/hg38) reference genome.

3.4.0. Statistical analysis

Each group of samples was represented by three replicates. Results are shown as mean value ± standard deviation, where applicable. Comparison between groups within experimental time points was performed in Prism (v8, GraphPad Software, USA) using one-way ANOVA with Tukey correction for multiple comparisons, preceded by normal distribution Shapiro–Wilk's test and homoscedasticity Levene's median test. For each comparison performed, the difference was determined as significant for $p < 0.05$.

3.4. Results and Discussion

3.4.1. Material characterization

Micro-CT, SEM and EDX

An overview of the scaffold structure is presented in Figure 3-6. On the macroscale, the scaffolds were characterized by lattice strings with an average width of 372.83 ± 40.44 µm and spaces of 170.95 ± 32.92 µm between neighbouring strings. On the microscale, the material was composed of granules with diameters varying between 6.03 and 31.13 µm and with inter- and intragranular porosity. The average diameter of the granules remained stable with time of immersing in media (15.67 ± 7.2 µm, 15.99 ± 6.07 µm, and 16.83 ± 5.67 µm for intact scaffold, scaffold incubated in media for 3 days and 7 days, respectively).

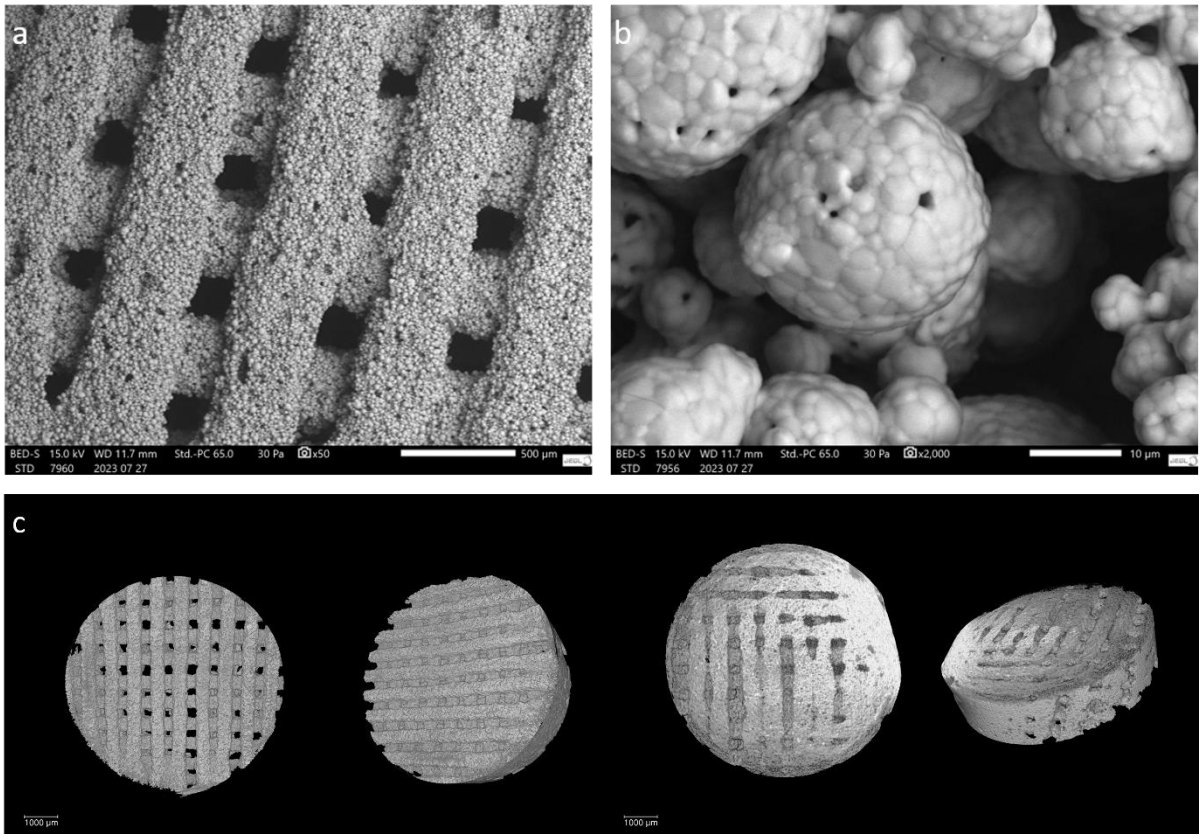

Figure 3-6 – Macro- and microstructure of the 3D-printed β-TCP scaffolds defined by SEM (*a* and *b*) and µCT (*c*). Scale bars 500 µm (*a*), 10 µm (*b*) and 1000 µm (*c*).

The distribution of elements and their maintenance throughout different incubation periods (3 days and 7 days in media) are shown in Figure 3-7, 3-8 and 3-9. Overall, by demonstrating the diversity of porosity of the scaffolds, the presence of macro- and microstructures forming convex and concave roughness of the surface, and even the distribution of the key elements over them, it was forecasted that such features would be beneficial for the following cell culture studies by means of facilitating cell attachment, spread and integration into the scaffold structure. As was demonstrated in the preceding Chapter on the alginate scaffolds, the lack of cell integration and robust attachment to the scaffold structure

may consequently lead to the washing out of the cells during the culture in a perfusion bioreactor culture.

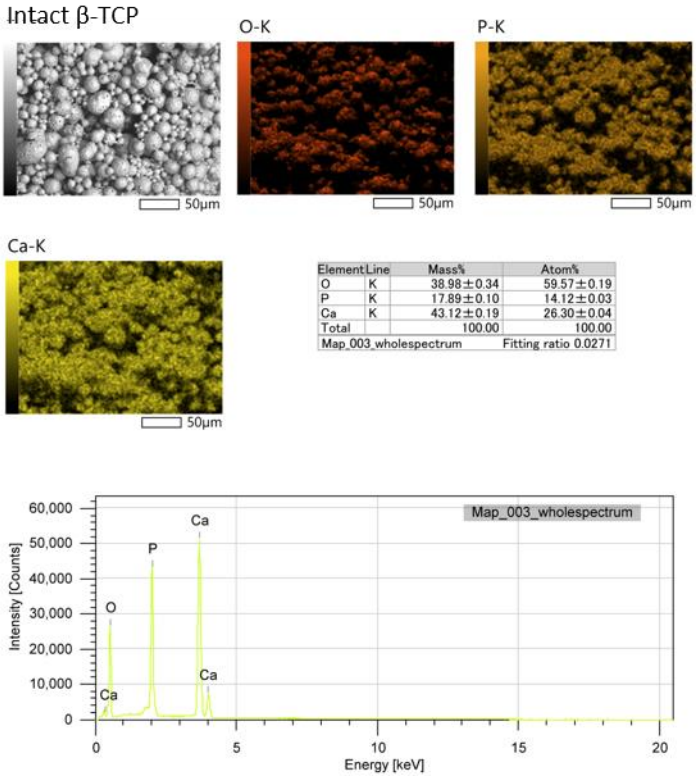

Figure 3-7 – EDX analysis of the intact β-TCP scaffold.

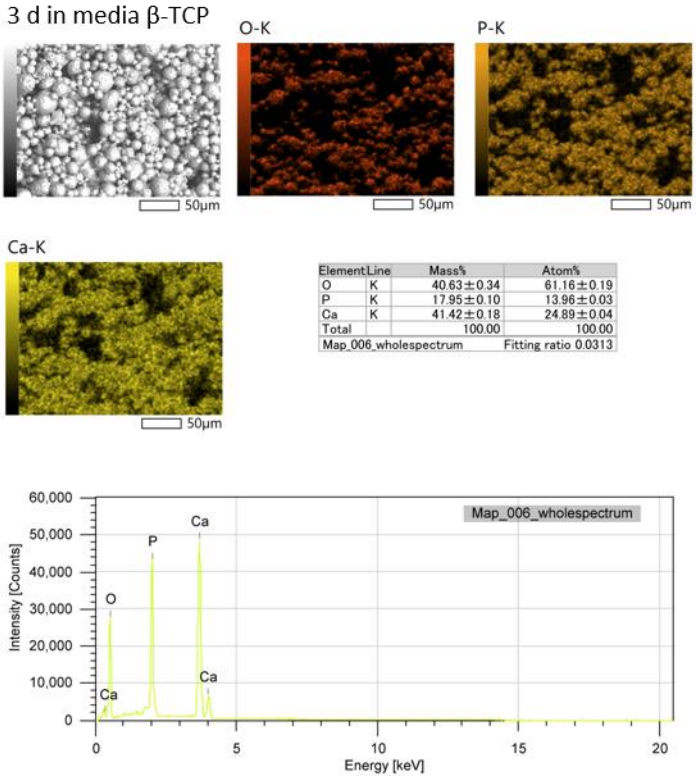

Figure 3-8 – EDX analysis of the β-TCP scaffold incubated in media for 3 days.

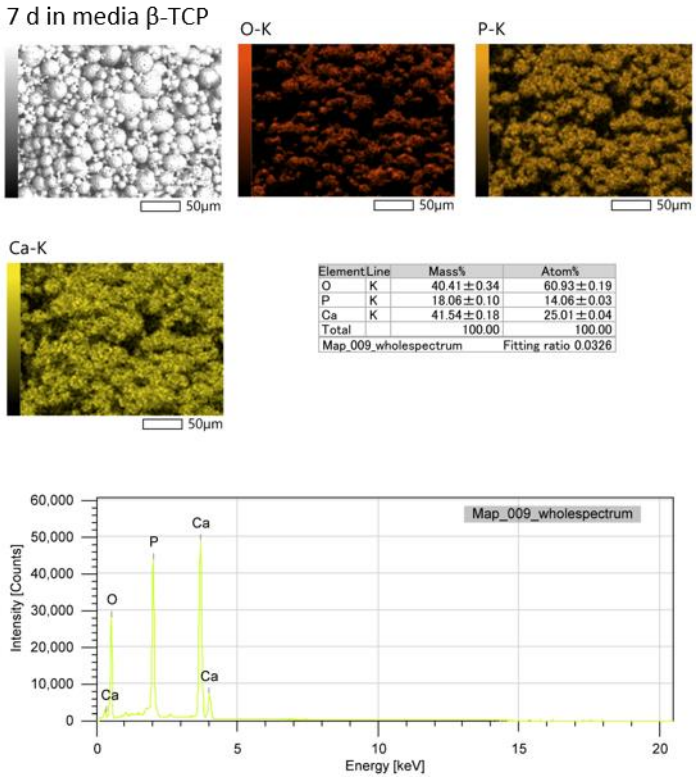

Figure 3-9 – EDX analysis of the β-TCP scaffold incubated in media for 7 days.

Nanoindentation

Due to the high intragranular porosity and circular cross-section of the strings of the scaffolds and peculiarities of the nanoindentation process, there was a wide range of effective Young's modulus values determined. The distribution of values obtained by indenting a 10 × 10 µm matrix of the string is shown in Figure 3-10, *a*. The values were divided into three distinct groups: the majority of the indented points resulted in the average E (eff) = 66.46 ± 29.26 MPa, and two other smaller groups reached the average of 274.75 ± 114.27 MPa and 1412.5 ± 509.75 MPa. The topography of the string indented along a single axis is presented in panel *b* of Figure 3-10. Two examples of measurement outcomes are shown in panel *c* of the same figure.

It is worth underlining, that along with the microstructural properties of the scaffold, its stiffness plays an important role in the fate of the cell. In the examples from the literature presented earlier, the molecular signalling of the cells, their migration and differentiation may be altered by the stiffness of the surrounding matrix thanks to mechanotransduction mechanisms transforming mechanical stimuli into biochemical cues. In the context of bone cancer, the scaffold serving as a microenvironment for the bioengineered tumour unit is expected to exhibit high stiffness – at least, higher than that of a tumour unit itself. Now, considering the previous results of the nanoindentation of the cell spheroids, it can be concluded, that the β-TCP scaffold will appear stiffer than any of the chosen cell spheroid ratios (Young's modulus of 3:1 MSC:U2OS spheroids was around 40 kPa, of 1:3 MSC:U2OS spheroids – 20 kPa, and U2OS – 3 kPa at maximum). Even though it was difficult to define the β-TCP scaffold stiffness by the nanoindentation method due to the scaffold's highly porous

structure, the values lie in the range of MPa, thus making the scaffolds an order of magnitude stiffer than the cell spheroids.

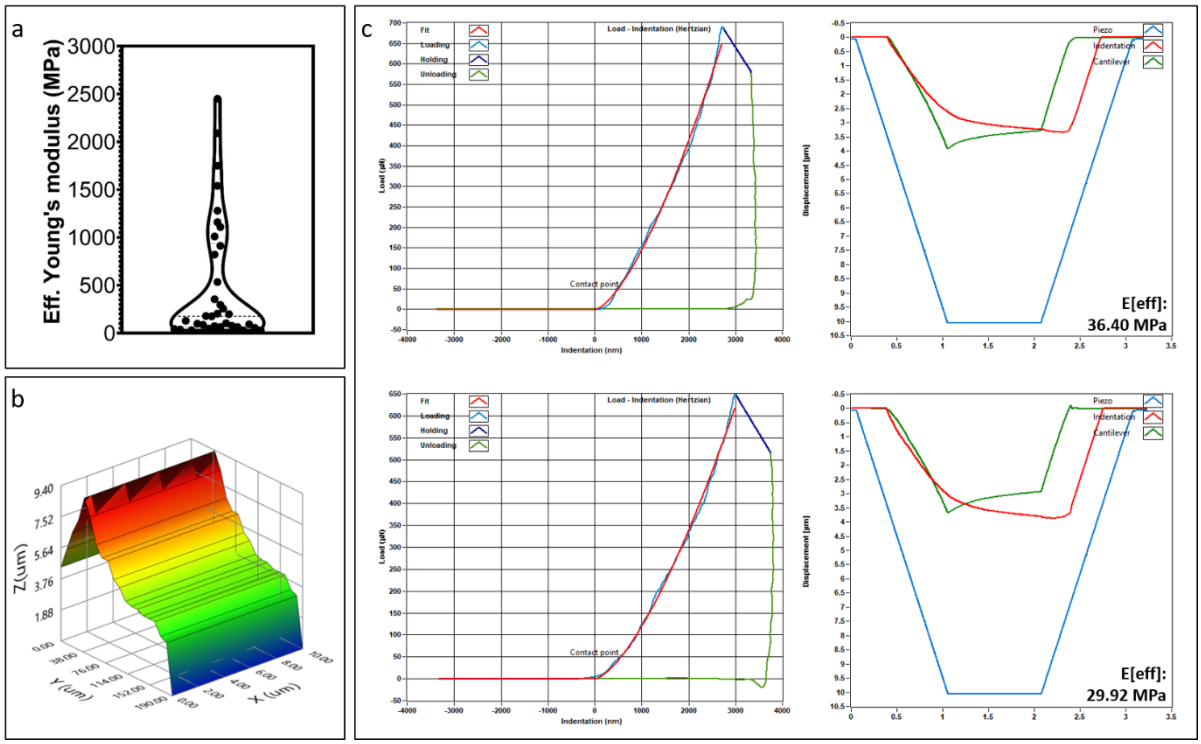

Figure 3-10 – Nanoindentation of the β-TCP scaffold: distribution of E(eff) values obtained on one string (a), the topography of the indented area (b), and an example of measurement outcome (c).

Fourier-transform infrared spectroscopy and X-ray powder diffraction analysis

FTIR-ATR spectroscopy was used to assess the changes in the surface chemical structure of the scaffolds before and after sintering Figure 3-11. The scaffolds in both states exhibited three main peaks: 997 and 924 cm^{-1} corresponding to HPO_4^{2-}, and 722 cm^{-1} corresponding to OH^-. There was also one peak characteristic only for β-TCP after sintering (1213 cm^{-1} – PO_4^{3-}). The rest of the peaks were attributed to Pluronic® F127 (Branca et al., 2018; Gibson et al., 2000; Kwon et al., 2003).

XRD analysis was done to evaluate the maintenance of the β-TCP after sintering. The results are presented in Figure 3-12. The signal from the sintered scaffold was found to match the theoretical β-TCP pattern (Kostov-Kytin et al., 2018; TAVARES et al., 2013).

Together, the results of the FTIR and XRD analyses allow us to conclude that chemical features of the biomaterial are preserved throughout the production of the scaffolds; moreover, it means that the prediction of the performance of the β-TCP scaffolds *in vitro* – at least, in the indirect contact with cells, – can be made based on the abundant literature on the properties of the bulk β-TCP. However, the next step could be the analysis of the scaffold surface chemistry and ion release after a prolonged period of incubation in a culture medium.

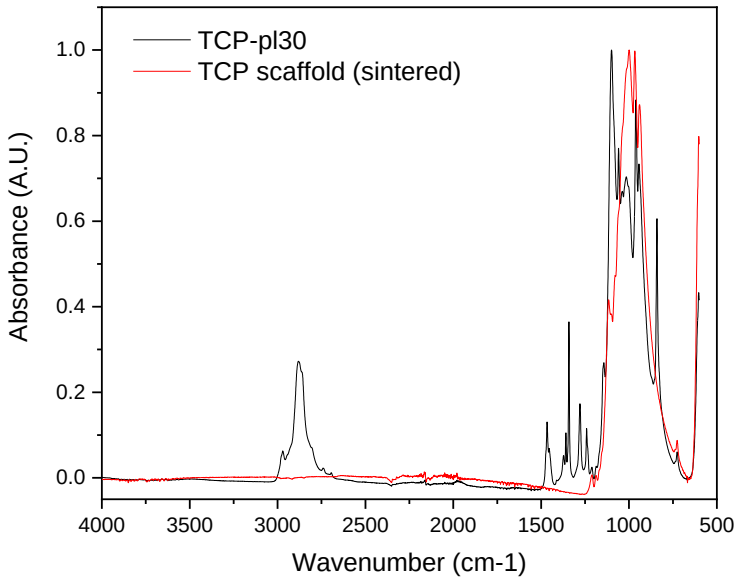

Figure 3-11 – FTIR-ATR spectroscopy of β-TCP scaffolds before (black line) and after (red line) sintering.

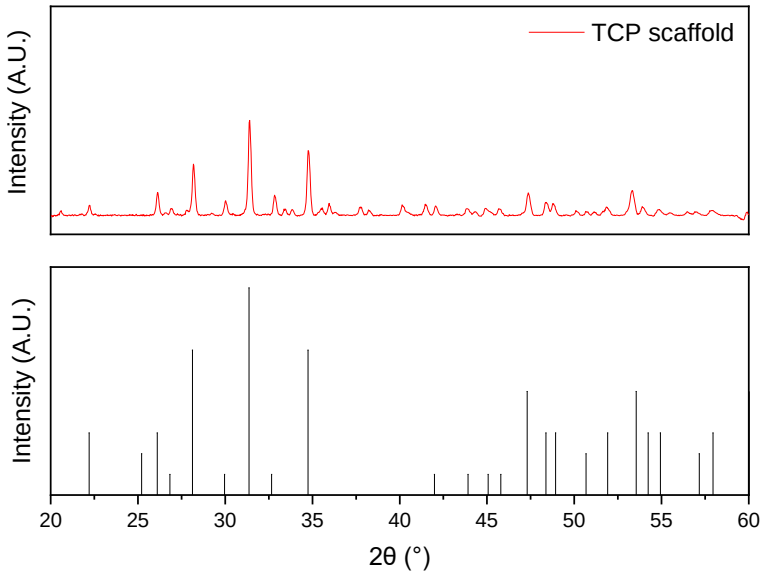

Figure 3-12 – XRD analysis of β-TCP scaffolds after sintering.

3.4.2. Cytocompatibility evaluation

Cell viability assessment showed different trends in the metabolic activity of hBMSCs cells and U2OS spheroids cultivated on printed β-TCP scaffolds (Figure 3-13). Due to a higher total cell count, on the first day of cultivation hBMSCs demonstrated higher relative fluorescent unit (RFU) values than U2OS cell spheroids. The difference was maintained on the 3rd day. However, the viability of hBMSCs after 1 week decreased significantly compared to the previous time points and equalized to that of U2OS. Osteosarcoma cell spheroids, in contrast, showed significantly higher metabolic activity on the 7th day compared to the 1st day of the test. The decrease in metabolic activity of hBMSCs on the scaffolds may be related to the inefficient mass transport in the conditions of standard culture with a limited culture medium volume.

Taking into account that the number of hBMSCs cells seeded in suspension exceeded drastically the number of U2OS cells used for spheroid generation, it is quite expected to observe cells becoming less metabolically active with time. In the case of spheroids, on the contrary, the surrounding scaffold could serve as a support for further growth and proliferation, and, again, due to the comparably lower number of cells, the volume of the culture medium seems to be sufficient. Coming back to the first Chapter, where we could observe the decrease in metabolic activity of the spheroids by day 7 of cultivation, it should be noted, that the spheroids are prepared in the 48-well plate; thus, when transferred to more spacious wells of a 24-well plate containing larger volumes of culture medium, the spheroids are expected to become more active in terms of their growth and proliferation.

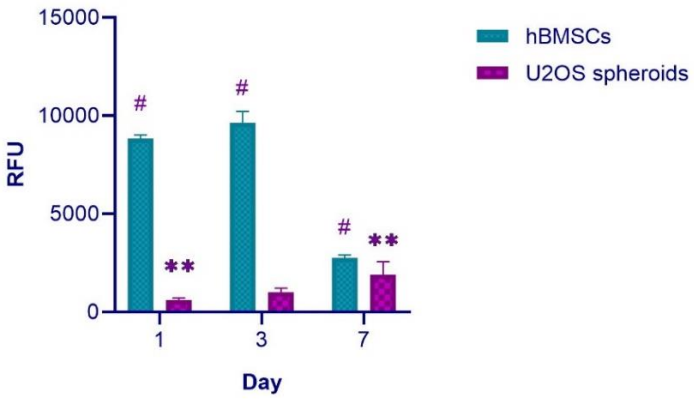

Figure 3-13 – Viability of U2OS cell spheroids and hBMSCs cultivated on the printed TCP scaffolds. The values are presented as mean ± SD of relative fluorescent units (RFU), n = 3. Multiple comparisons performed via two-way ANOVA with Tukey's correction, ** - significant differences between groups of samples, $p < 0.01$, # - $p < 0.0001$.

The live/dead staining performed on the 7th day of the culture of hBMSCs on β-TCP scaffolds showed the even spread of the cells throughout the sample volume (Figure 3-14, *a*). Cells mostly covered the surfaces of the scaffold and possessed an elongated shape. U2OS cell spheroids at the same time point were arranged in the centre of the scaffold, partly covering the scaffold's surface, as well as being supported by the collagen or extracellular matrix (Figure 3-14, *b*). Such distribution of cells is important in the context of the engineered model of osteosarcoma: the use of β-TCP scaffold is dictated by a need for a bone-mimicking environment. Having hBMSCs attached, elongated and homogeneously spread within the scaffold is a positive outcome, and, as we will see in the following sections, a prolonged period of culture may result in the intensive synthesis of ECM, closer approximating a bone-like environment. Next, when speaking about the tumour unit (which is represented by the cell spheroid in the developed model), we are seeking the maintenance of the cell spheroid within the scaffold along with its integration into the surrounding environment. In the figure below, it can be observed that after 7 days in culture cells remain aggregated but at the same time attached to the scaffold surface.

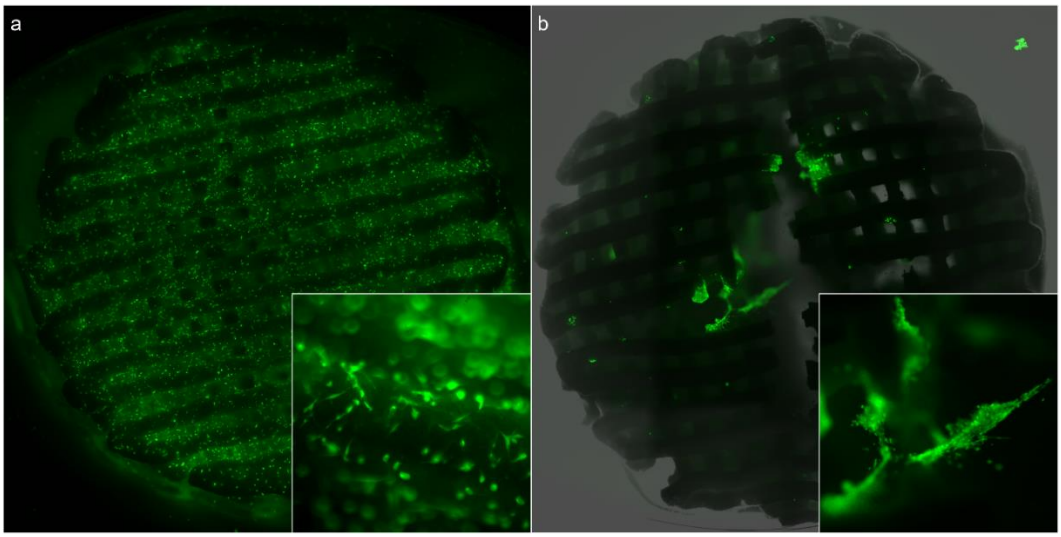

Figure 3-14 – Fluorescent microscopy images of hBMSCs (a) and U2OS cell spheroids (b) seeded on 3D-printed β-TCP scaffolds. Calcein AM staining.

SEM imaging of β-TCP scaffolds seeded with hBMSCs and cultivated for 7 days showed the residues of collagen matrix stretched between the elements of the scaffold (Figure 3-15, *a*). It was also possible to see single cells on top of the matrix's surface, however, due to the structure of β-TCP scaffolds it was difficult to distinguish between the calcium phosphate clusters and cell bodies (Figure 3-15, *b*). In the case of U2OS cell spheroids, it was impossible to observe the spheroids because of their position in the depth of the scaffold volume (Figure 3-16, *a*). However, in both *in vitro* models, there was a remarkable difference in the structure of the collagen matrix compared to the scaffolds cultivated without cells: the collagen stayed intact and did not undergo any degradation in the absence of the cells (Figure 3-16, *b*). This difference supports the evidence of cell viability: their activity led to the degradation of the collagen introduced as a supporting matrix for seeding the cells on the scaffolds. As we will see later, after the extended culture periods, the cells are able to synthesize their own ECM when cultured on the 3D-printed β-TCP scaffolds.

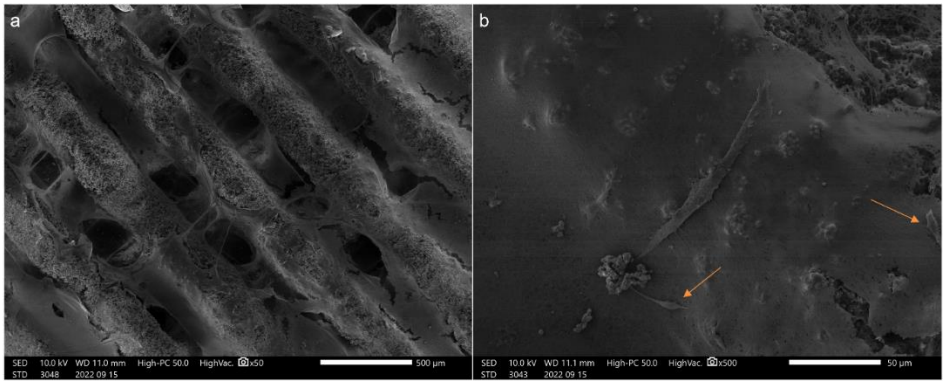

Figure 3-15 – Scanning electron microscopy images of the 3D-printed β-TCP scaffolds seeded with hBMSCs in collagen and cultivated for one week. The residues of the collagen matrix stretched between the scaffold's elements can be observed (a) as well as several single cells (b, arrows). Bar scales 500 μm and 50 μm, respectively.

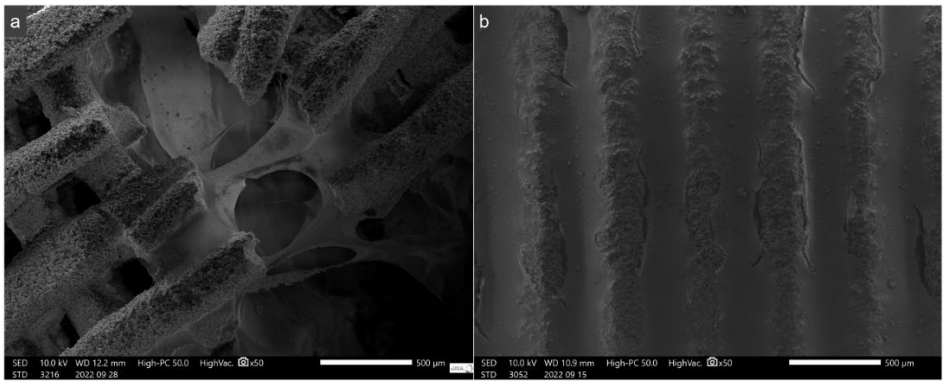

Figure 3-16 – Scanning electron microscopy images of the 3D-printed ß-TCP scaffolds seeded with U2OS cell spheroids in collagen and cultivated for one week (*a*) and the scaffold with collagen without cells cultivated in the same conditions (*b)*. Bar scales 500 µm.

3.4.3. Perfusion bioreactor study

The viability of EA.hy926 after 1 week of cultivation on β-TCP scaffolds decreased significantly compared to the initial values, independently of conditions – static flask or perfused chambers of the bioreactor (Figure 3-17). Within the latest time point, the metabolic activity of the cells cultivated in bioreactors was slightly higher than that of those cultivated in a flask. If for static cultures – that stayed in the flask with a relatively large volume of the medium and yet without constant fluid flow, – a decrease in metabolic activity might be expected (I am referring to the above results of the cytocompatibility assay with hBMSCs), for bioreactor studies that are thought to be provided not only with sufficient amounts of nutrients but also their efficient circulation, the drop in metabolic activity was not completely understood. Behind this outcome, at least two reasons could stand: first, the scaffolds might be not fully compatible specifically with endothelial cells; second, and more likely, since a similar effect had been observed for hBMSCs, the β-TCP scaffolds might require an additional step of preparation for *in vitro* biological assays. The tendency of porous calcium phosphate materials to intensively adsorb proteins from the surrounding environment is widely known. Thus, supplementary incubation of the scaffolds in the serum-rich medium prior to cell seeding may prevent the lack of nutrients which cells might face due to protein adsorption.

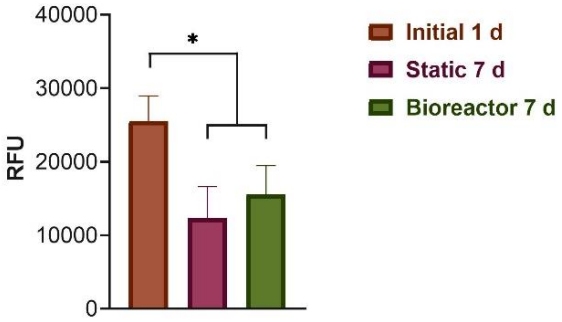

Figure 3-17 – Metabolic activity of EA.hy926 cells cultivated on the printed β-TCP scaffolds for 1 day in static conditions ('Initial 1 d') and 7 days in static ('Static 7 d') and perfusion ('Bioreactor 7 d'). The values are presented as mean ± SD of relative fluorescent units (RFU), n = 3. Multiple comparisons were performed via two-way ANOVA with Tukey's correction, * - significant differences between groups of samples, $p < 0.05$.

The live/dead staining performed on the 7th day of a culture of EA.hy926 on the β-TCP scaffolds showed the difference in how the cells penetrated the 3D structure of the scaffold (Figure 3-18). In the case of incubation in static conditions – in flasks – cells evenly covered the surfaces of the scaffold, possessed an elongated shape and both lined the material and the fibres of collagen or cell-produced ECM, which were found stretched within the gaps of the scaffold (Figure 3-18, *a, c*). In the case of incubation in perfusion conditions – in chambers of a bioreactor – the cells were found concentrated in groups, mostly in the centre of the scaffold, where the gaps were the largest (Figure 3-18, *b, d*). This may point to the washing out of the endothelial cells from the scaffold in perfusion conditions (bioreactor cultures) – possibly, due to insufficient attachment of the cells to the scaffold's surface. The solution to this obstacle may be a prolongation of the initial scaffold culturing period: instead of only 1 day of the culturing in standard (static) conditions before placing the scaffolds into the chambers of the perfusion bioreactor, the cell-seeded scaffolds can be cultured, for instance, for three days to let the cells better "adapt" to the new environment – proliferate more, occupy a wider area of the scaffold surface, and produce more ECM.

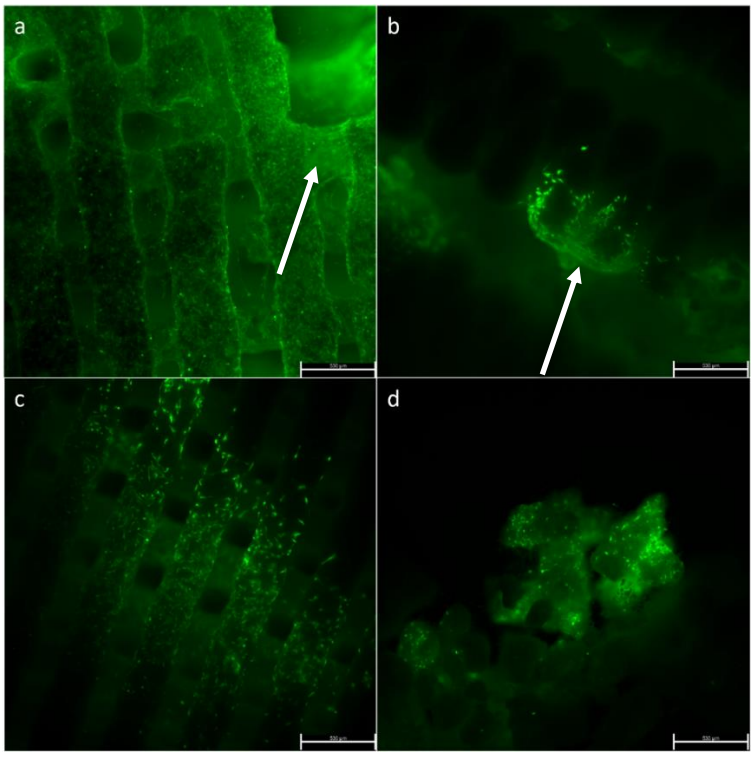

Figure 3-18 – Fluorescent microscopy images of EA.hy926 seeded on 3D-printed β-TCP scaffolds and cultivated in static conditions (a, c) and dynamic (bioreactor) (b, d) conditions. Cells and remaining collagen (or newly synthesized extracellular matrix) stretched between the structures of the scaffold are indicated with arrows. Calcein AM staining. Scale bar 530 um.

Scanning electron microscopy revealed no morphological difference between the samples incubated in static and dynamic conditions. The β-TCP scaffold with EA.hy926 cells cultivated in static conditions is shown in Figure 3-19, *a*. It was possible to see the residues of

the collagen matrix as well as single cells on top of the matrix's surface and embedded in it (Figure 3-19, *c*, *d*).

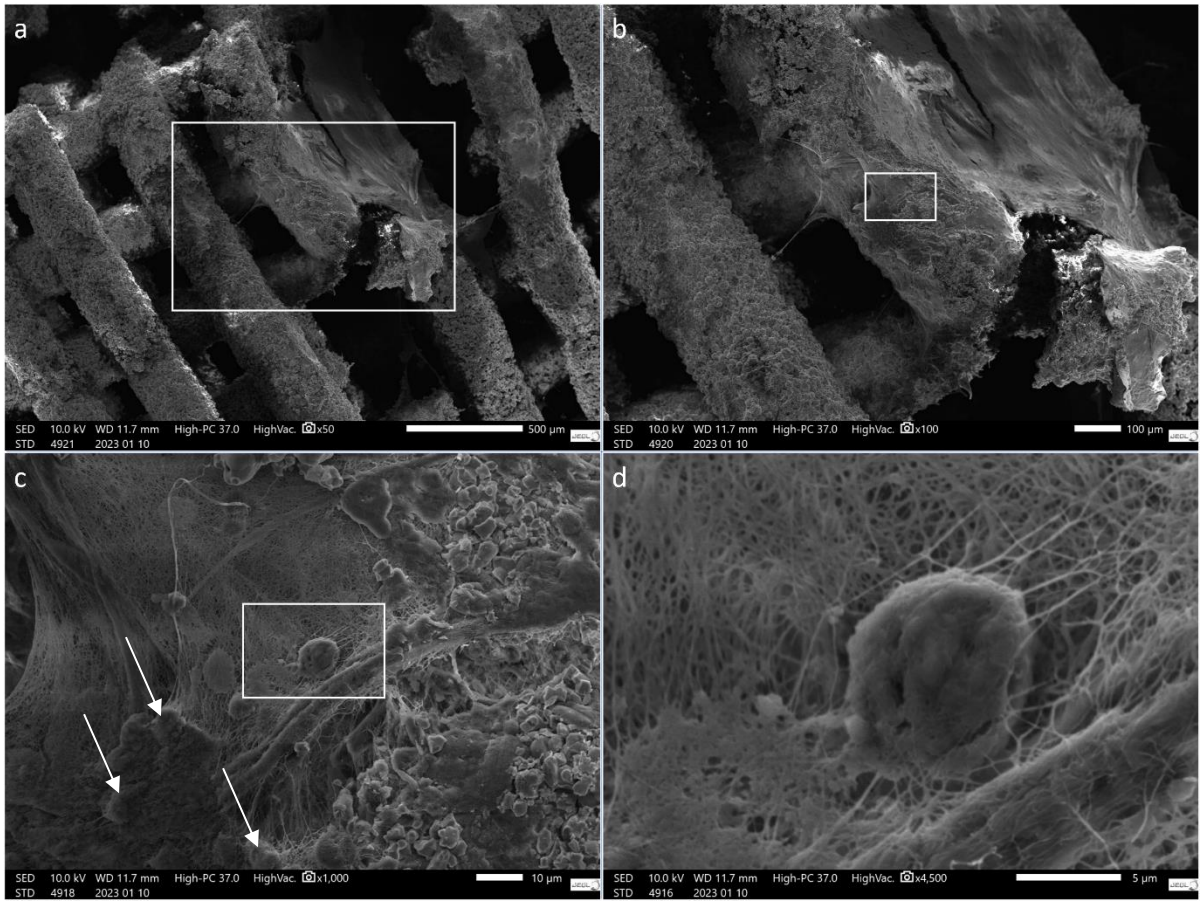

Figure 3-19 – Scanning electron microscopy images of the 3D-printed TCP scaffolds seeded with EA.hy926 cells in collagen and cultivated for one week in static conditions. Regions observed in higher magnification (×100, ×1000, ×4500 for b, c, and d, respectively) are indicated with rectangles, and cells are indicated with arrows.

3.4.4. Co-culture study

Co-culture cell spheroid viability

Resazurin reduction assay demonstrated an increase in cell metabolic activity in co-culture U2OS-EA.hy926 cell spheroids cultivated on the scaffolds in static (flask) and dynamic (Quasi Vivo® system) conditions. Due to possible spheroid displacement during the procedure of transferring the cell-seeded scaffolds from plates to flasks or Quasi Vivo chambers, there was a high variation in the obtained RFU values. However, a significant difference in metabolic activity was shown between the group of scaffolds cultivated for 7 days in dynamic conditions, and the initial 3-day scaffolds (Figure 3-20). Interestingly, even without taking the additional step of incubating the scaffolds in a serum-rich medium and prolonging the culture in standard (static) conditions for up to 3 days before transferring the scaffolds into the chambers of the bioreactor, we observe the increase in metabolic activity, not seen for hBMSCs and endothelial cells before. We saw, however, that the increase of the activity is observed in the U2OS

spheroids on the β-TCP scaffolds, thus, the explanation could be the following: either the majority of the activity in the co-culture is provided by osteosarcoma spheroid, or co-culturing endothelial and osteosarcoma cells is beneficial for either of the cell types, or both. As will be explained in Chapter 4, co-culturing different cell types is coupled with numerous challenges, one of which is the inability to distinguish the state of each cell type co-cultured, including metabolic activity, by straightforward methods. For instance, in the present case, we are able to make conclusions on the metabolic activity of the overall *in vitro* model only.

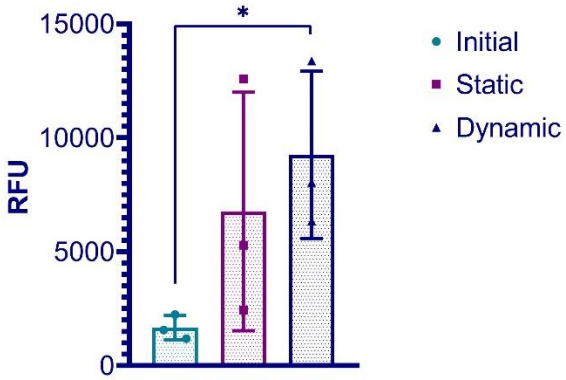

Figure 3-20 – Co-culture cell spheroid metabolic activity on the β-TCP scaffolds cultivated in static (Initial – 3 days in the well-plate, Static – 3 days in the well-plate and 7 more days in a flask) and dynamic (Dynamic - 3 days in the well-plate and 7 more days in the Quasi Vivo® system) conditions. Multiple comparisons were performed via two-way ANOVA with Tukey's correction, * - significant differences between groups of samples, $p < 0.05$.

Gene expression analysis

To evaluate the potential input of dynamic conditions to the tumour-like behaviour of the studied co-culture model, the expression levels of two genes were analysed. Vascular endothelial growth factor (VEGF) overexpression and retinoblastoma 1 (RB1) downregulation or absence are widely known markers of tumour progression and invasiveness. The expression of these genes was analysed in the cell-seeded scaffolds after cultivation in static (flasks) or dynamic (perfusion Quasi Vivo® system) conditions and related to the expression in the 3-day (initial) cell-seeded scaffolds. VEGF was upregulated in both *Static* and *Dynamic* groups of samples with no significant difference between them, while in the case of RB1, the expression was detectable only in the *Static* group and slightly upregulated in relation to the *Initial* (Figure 3-21). Overall, these results may point to at least two intermediate conclusions. First, the pronounced upregulation of VEGF in the co-cultures on the scaffolds at the 7-day point in comparison to the 1-day point may indicate a positive interplay between the co-cultured cell types, where U2OS spheroids might express VEGF to attract endothelial cells and eventually boost endothelial cell growth. Second, the expression level of RB1 in the bioreactor cultures was not detectable, which may mean that the osteosarcoma spheroid possibly exhibited more "aggressive" behaviour when cultured in the bioreactor, positioning the latter as a more physiologically relevant culture system. Again, it is worth underlining, that one of the challenges of the analysis of co-cultures is distinguishing between the effects observed for the different cell types. In the context of gene expression analysis, it might be complemented with

immunofluorescence microscopy with the use of a VEGF antibody – not only to confirm the expression of the VEGF gene but also to analyse its pattern.

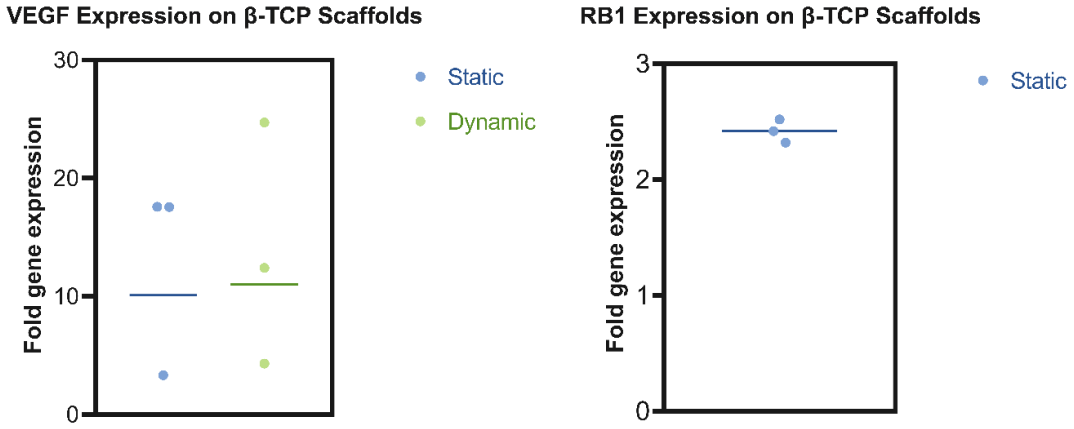

Figure 3-21 – Gene expression in the co-culture U2OS-EA.hy926 cell spheroids cultivated in static (flasks) and dynamic (Quasi Vivo®) conditions in relation to the initial 3-day cell-seeded scaffolds (well-plates).

3.4.5. Nanokicking study

This Chapter is mainly dedicated to the 3D-printed β-TCP scaffold as a basis for the creation of a bone-like environment. Thus, it is important to evaluate the scaffold's potential to modulate the fate and behaviour of MSCs, which, in turn, are able to differentiate along the osteoblast lineage when placed in the "right" conditions. In this part of the study, I benefited from the use of primary human bone-marrow-derive MSCs (pBMSCs) which might be more potent in terms of differentiation ability in comparison to the immortalized Y201 hBMSCs used earlier. Recently, it was shown in several studies, that the constant application of nanodisplacements to the cell-seeded structures may lead to osteoblastic differentiation of the cells in the absence of biochemical stimulation (Pemberton et al., 2015). In this section, I will present results obtained within the experiments carried out with the "nanokicker" – platform providing the nanodisplacements to the cell-seeded β-TCP scaffolds and discuss the possible potential of the scaffolds to trigger osteoblastic differentiation of pBMSCs and any other possible influence.

Metabolic activity of pBMSCs seeded on the scaffolds did not decrease after 3 weeks of cultivation in various conditions. There was only a slight decrease in metabolic activity on the 3rd day of cultivation on the scaffolds caused perhaps by the "adaptation" of the cells to a new environment. On a positive note, there was no severe drop in metabolic activity similar to the above-described observation of immortalized hBMSCs and endothelial cells. This supports the idea of enhancing the cells' viability on the scaffolds by preparatory immersing the scaffolds in a serum-rich medium. This step might have prevented possible excessive adsorption of the proteins from the culture medium which could lead to the lack of nutrients and cell starvation. After the start of stimulation – i.e., division of the scaffolds into two groups, one of which remained in standard conditions and another one was exposed to 1 kHz vertical oscillation on the nanokicking platform, – there was a gradual growth in metabolic activity of pBMSCs

(Figure 3-22). There was no significant difference observed between the group kept in standard conditions (Ctrl) and the group exposed to oscillation on the bioreactor (1 kHz).

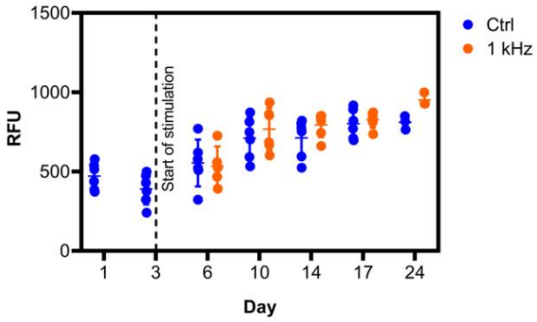

Figure 3-22 – Metabolic activity of pBMSCs seeded on β-TCP scaffolds. After 3 days of cultivation (marked with a dashed line), the scaffolds were divided into 2 groups, one of which was maintained in standard conditions (Ctrl) and the other one was kept on the nanovibrational bioreactor (1 kHz).

Cell viability analysis done by Calcein AM staining of live cells showed cell spreading over the scaffold's surfaces and the formation of dense cell mass covering the structures of the scaffolds and stretching between the neighbouring strings, in particular, visible after 2 weeks of cultivation regardless the culture conditions (Figure 3-23). As was predicted in the above sections, the prolonged cultivation of the MSCs on the β-TCP scaffolds leads to the proliferation of the cells and intensive ECM synthesis leading to the development of a more cell-friendly environment.

For SEM imaging, the scaffolds cultured for 3 weeks were cut perpendicular to the z-axis of printing. Along with the live observations, dense cell sheets were found to cover the surface of the material, and the intergranular space of β-TCP was rich in cell network. As was shown in the cytocompatibility experiments with hBMSCs (Figure 3-16), cell activity on the scaffolds leads to the degradation of the collagen matrix, used as a support for cell seeding. Thus, it is expected that the collagen would be fully degraded by 3 weeks of cultivation, meaning that the matrix observed on the SEM images in Figure 3-23 could be synthesised by pBMSCs cells. This may indicate the scaffold cytocompatibility and characterise it as a suitable basis for a cell-driven generation of an environment for an osteosarcoma model *in vitro*. However, it is yet to be defined, whether this cell-generated environment is a bone-like one. As for the nanokicking stimulation, visually, there was no difference between the cell-seeded scaffolds cultured in standard conditions (Control) and those stimulated by nanovibration (1 kHz).

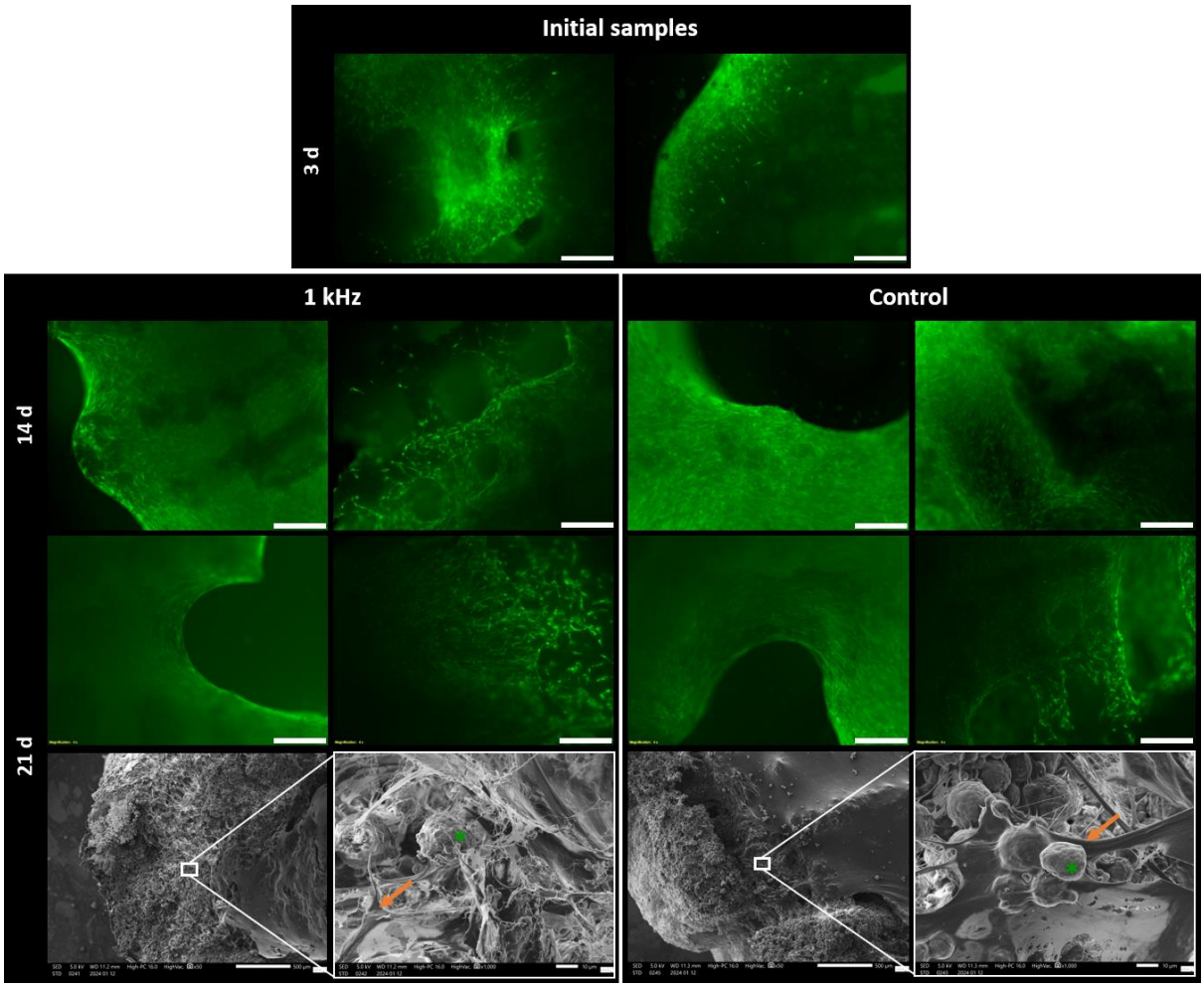

Figure 3-23 – Calcein AM staining of live pBMSCs cultured on ß-TCP scaffolds (green fluorescence microscopy images). Spread and proliferation of the cells covering and connecting structures of the scaffold are demonstrated. Scale bar 1 mm. Below: SEM images of the 21-d scaffolds are shown. Formation of cell sheets covering the scaffold, as well as filling the interspace between β-TCP granules (arrows mark the cells, asterisks mark β-TCP granules) are demonstrated at magnification ×50 (scale bar 500 µm) and ×1000 (framed images, scale bar 10 µm). No visual difference was observed between scaffolds in standard conditions (Control) and stimulated by nanovibration (1 kHz).

Alkaline phosphatase activity

Increased ALP activity is an early marker of osteogenic differentiation. To assess its intracellular level, pBMSCs cultured on the β-TCP scaffolds were lysed, and the obtained values of ALP activity were normalised by total protein concentration. In comparison to the initial scaffolds, there was an increase of ALP activity observed in both control and stimulated groups on the 7th day after the start of stimulation (10th day of overall culture). After the second week of culture, ALP activity decreased, still not showing any statistically significant difference between the compared groups (Figure 3-24). Usually, in studies related to the evaluation of osteogenic differentiation, ALP activity is evaluated primarily in the first week of osteogenic stimulation since it is an early marker of the osteoblast-like activity of the cells. Indeed, with the overall increase in the ALP activity in the present experiment, among the points analysed we can observe the peak of ALP activity on the earliest one, which may indicate the start of the osteoblastic differentiation.

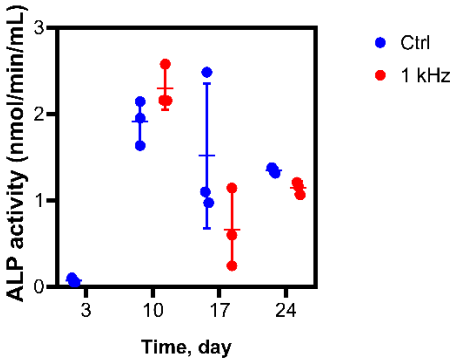

Figure 3-24 – Intracellular ALP activity in pBMSCs cultured on β-TCP scaffolds for 3, 10, 17 and 24 days in standard conditions (Ctrl) and stimulated by nanovibration (1 kHz).

3.4.6. Differential gene expression and enrichment analysis

3D-printed β-TCP scaffolds were employed as a platform to study the impact of nanokicking on the gene expression profile of pBMSCs. MSCs have the ability to differentiate into specialized tissues along the mesodermal lineage; typically including bone, cartilage and fat. As was mentioned earlier, lately, so-called nanokicking – constant nanodisplacements of cultured cells – was shown to be able to trigger MSCs differentiation along osteoblastic lineage (Campsie et al., 2019; Pemberton et al., 2015).

By performing an RNA-Seq analysis of pBMSCs cultured on standard polystyrene and the investigated scaffolds, I aimed to understand the impact of nanokicking in these two distinct conditions, as well as the impact of the scaffold itself. Both 2D and 3D models had a high number of differentially expressed genes (DEGs) in the nanokicking bioreactor (more than 400 in cells cultured on plastic, and more than 200 in cells cultured on the scaffolds, Figure 3-25), but not many of them were similar.

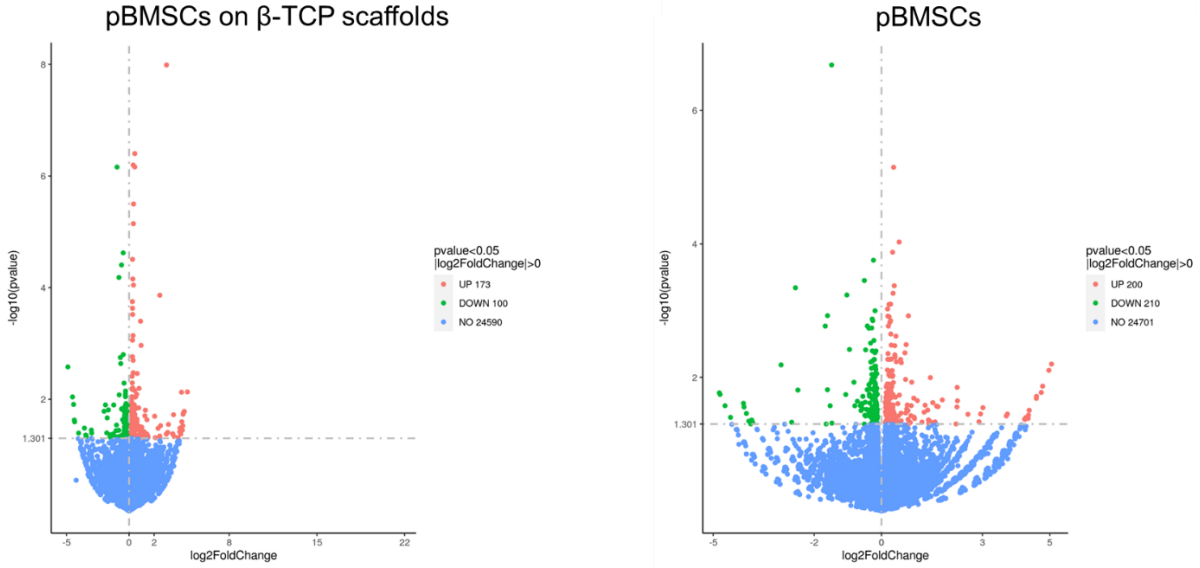

Figure 3-25 – Differentially expressed genes in the comparisons of standard conditions with nanokicking bioreactor.

Only 11 DEGs were common for 2D and 3D culture approaches, and so far, none of them is thought to be directly linked to the cues activated by nanokicking:

- ID1 - inhibitor of DNA binding 1;
- GASK1B - golgi associated kinase 1B;
- SRGN - serglycin;
- VMP1 - vacuole membrane protein 1;
- CDC42EP5 - CDC42 effector protein (Rho GTPase binding) 5;
- IFT140 - intraflagellar transport 140;
- GDF15 - growth differentiation factor 15;
- TRIM56 - tripartite motif containing 56;
- SOD2 - superoxide dismutase 2, mitochondrial;
- SMIM11 - small integral membrane protein 11;
- CA9 - carbonic anhydrase 9.

This part of the results indicates that there is an impact of the nanokicking on the cell response, but this response is activated and exhibited differently in the cells cultured as a monolayer and cells cultured on the scaffolds. Regarding the 11 "shared" DEGs, their expression should be analysed further and possibly undergo more complex and strict mathematical modelling to sort out non-significant (in a biological sense) DEGs.

Another way of the follow-up analysis of DEGs is the assessment of their involvement in various molecular signalling cascades. For instance, Reactome analysis of the common DEGs showed that the most significantly involved pathways (meaning that several of the listed DEGs are taking part in one pathway at the same time) are "Regulation of gene expression by Hypoxia-inducible Factor" and "Cellular response to hypoxia". At this moment, there is not much evidence of a connection between nanokicking stimulation and hypoxia response, and this peculiar part of the results needs further investigation.

Regarding the Gene Ontology (GO) pathway enrichment analysis, the pathways affected by nanokicking in cells cultivated in 2D (monolayer on plastic) and 3D (on the scaffolds) were also different in the majority. While pBMSCs on the scaffolds differentially expressed markers associated with respiratory chains in standard conditions in comparison to nanokicking, cells in monolayer differentially expressed genes connected with cell adhesion and cell-cell contacts (Figure 3-26).

Overall, RNA-Seq results at this stage of the analysis do not support the hypothesis that the nanokicking might be able to trigger osteogenic differentiation on the β-TCP scaffolds – at least, not within the 3 weeks of the described experiment. Interestingly, osteogenic differentiation was not observed either for the cells cultured on plastic. It is possible, that the absence of the effect is driven by the characteristics of the used substrates – culture plate and scaffolds – not fully providing the transduction of the nanodisplacements to pBMSCs. Nevertheless, the effect of nanokicking was present in both 2D and 3D models, and it is of great interest that it was affecting distinct pathways: while in the cells cultured on the scaffolds respiratory chain reactions on mitochondria were affected, in the cells cultured on plastic it was rather cell-cell cell-substrate interactions. In further steps, it is planned to analyse RNA-Seq outcome for different checkpoints of the experiment (1, 2 and 3 weeks) and to investigate the gene expression in the function of time.

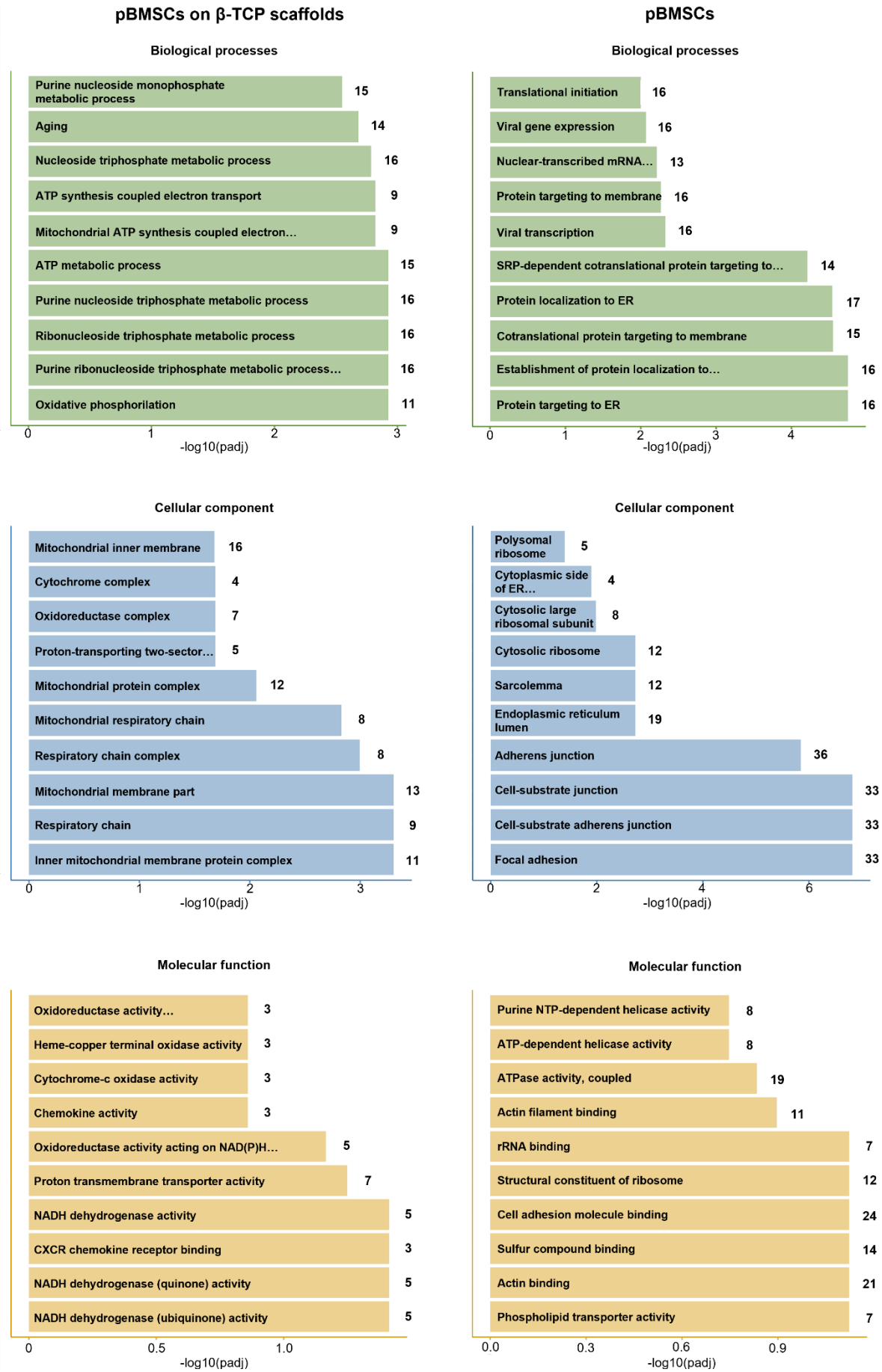

Figure 3-26 – Gene Ontology (GO) enrichment pathway analysis.

3.5. Conclusions

After making conclusions on the limitations of the alginate scaffolds in the context of cell culture in perfusion bioreactor in Chapter 2, in this Chapter, I moved to a distinct approach and used 3D-printed β-TCP scaffolds for developing the osteosarcoma model *in vitro*. For this, the scaffolds were analysed from the points of their stiffness, morphology and chemistry, and the results of nanoindentation, SEM-EDX, μ-CT, XRD and FTIR were presented. The chemical groups characteristic for β-TCP were present after sintering serving as evidence of the material features preservation during the scaffold production process. The element mapping of the scaffolds incubated in media for various periods also demonstrated the preservation of the material. The scaffolds were characterised by macro- and micro-porosity, with abundant inter- and intragranular pores, and a stiffness ranging from 0.5 to 2.5 GPa within one string of the printed scaffold. Based on the material characterisation outcomes, I could predict the response of the cells seeded on the β-TCP scaffolds. Indeed, the scaffolds proved to be cytocompatible towards osteosarcoma spheroids, MSCs, and endothelial cells. Cytocompatibility and preliminary perfusion bioreactor studies additionally demonstrated the need for scaffold immersion in a serum-rich medium as an additional step for *in vitro* biological studies. Yet another conclusion on optimisation was linked to the "adaptation" of the cells to the new environment: to ensure better attachment and integration of the cells into the scaffold structure, the initial culture of the cells on the scaffolds was extended from one to three days. With both optimisation steps considered, I observed the enhanced cell metabolic activity and viability and extensive ECM production during prolonged culturing of primary MSCs on the β-TCP scaffolds. The scaffold performance in dynamic conditions was tested in three different bioreactors and allowed to consider them as applicable to these needs from the point of their mechanical stability as well as their ability to serve as an environment for the selected cell lines, which was also supported by the gene expression analysis of the co-culture of osteosarcoma spheroids and endothelial cells. Additionally, β-TCP scaffolds were used as a platform for studying the impact of nanokicking stimulation on primary MSCs, and via RNA-Seq analysis it was revealed that the impact of nanokicking on the cells cultured in distinct conditions – standard culture on plastic and culture on the scaffolds – is different for these two conditions and triggers discrete molecular signalling pathways. This part of the thesis was done in close collaboration with PREMUROSA ESR Virginia Alessandra Gobbo, who developed and characterized (FTIR-ATR, XRD) 3D-printed scaffolds under the supervision of Prof. Jonathan Massera from Tampere University. The nanokicking experiment including the transcriptomic analysis was carried out during the secondment to CÚRAM under the supervision of Prof. Abhay Pandit (Galway, Ireland).

3.6. References

Baptista, D., Teixeira, L., van Blitterswijk, C., Giselbrecht, S., & Truckenmüller, R. (2019). Overlooked? Underestimated? Effects of Substrate Curvature on Cell Behavior. *Trends in Biotechnology*, *37*(8), 838–854. https://doi.org/10.1016/j.tibtech.2019.01.006

Bohner, M., Santoni, B. L. G., & Döbelin, N. (2020). β-tricalcium phosphate for bone substitution: Synthesis and properties. In *Acta Biomaterialia* (Vol. 113, pp. 23–41). Acta Materialia Inc. https://doi.org/10.1016/j.actbio.2020.06.022

Branca, C., Khouzami, K., Wanderlingh, U., & D'Angelo, G. (2018). Effect of intercalated chitosan/clay nanostructures on concentrated pluronic F127 solution: A FTIR-ATR, DSC and rheological study. *Journal of Colloid and Interface Science*, *517*, 221–229. https://doi.org/10.1016/j.jcis.2018.02.004

Campsie, P., Childs, P. G., Robertson, S. N., Cameron, K., Hough, J., Salmeron-Sanchez, M., Tsimbouri, P. M., Vichare, P., Dalby, M. J., & Reid, S. (2019). Design, construction and characterisation of a novel nanovibrational bioreactor and cultureware for osteogenesis. *Scientific Reports 2019 9:1*, *9*(1), 1–12. https://doi.org/10.1038/s41598-019-49422-4

Feng, J., Liu, J., Wang, Y., Diao, J., Kuang, Y., & Zhao, N. (2023). Beta-TCP scaffolds with rationally designed macro-micro hierarchical structure improved angio/osteo-genesis capability for bone regeneration. *Journal of Materials Science: Materials in Medicine*, *34*(7), 36. https://doi.org/10.1007/s10856-023-06733-3

Gibson, I. R., Rehman, I., Best, S. M., & Bonfield*, W. (2000). Characterization of the transformation from calcium-deficient apatite to β-tricalcium phosphate. *Journal of Materials Science: Materials in Medicine*, *11*(12), 799–804. https://doi.org/10.1023/A:1008905613182

Haugen, H. J., Lyngstadaas, S. P., Rossi, F., & Perale, G. (2019). Bone grafts: which is the ideal biomaterial? *Journal of Clinical Periodontology*, *46*(S21), 92–102. https://doi.org/10.1111/jcpe.13058

James, S., Fox, J., Afsari, F., Lee, J., Clough, S., Knight, C., Ashmore, J., Ashton, P., Preham, O., Hoogduijn, M., Ponzoni, R. D. A. R., Hancock, Y., Coles, M., & Genever, P. (2015). Multiparameter Analysis of Human Bone Marrow Stromal Cells Identifies Distinct Immunomodulatory and Differentiation-Competent Subtypes. *Stem Cell Reports*, *4*(6), 1004–1015. https://doi.org/10.1016/j.stemcr.2015.05.005

Kostov-Kytin, V. V., Dyulgerova, E., Ilieva, R., & Petkova, V. (2018). Powder X-ray diffraction studies of hydroxyapatite and β-TCP mixtures processed by high energy dry milling. *Ceramics International*, *44*(7), 8664–8671. https://doi.org/10.1016/j.ceramint.2018.02.094

Kwon, S.-H., Jun, Y.-K., Hong, S.-H., & Kim, H.-E. (2003). Synthesis and dissolution behavior of β-TCP and HA/β-TCP composite powders. *Journal of the European Ceramic Society*, *23*(7), 1039–1045. https://doi.org/10.1016/S0955-2219(02)00263-7

Paredes, C., Roleček, J., & Miranda, P. (2024). Improving the strength of β-TCP scaffolds produced by Digital Light Processing using two-step sintering. *Journal of the European Ceramic Society*, *44*(4), 2571–2580. https://doi.org/10.1016/J.JEURCERAMSOC.2023.11.028

Pemberton, G. D., Childs, P., Reid, S., Nikukar, H., Monica Tsimbouri, P., Gadegaard, N., Curtis, A. S. G., & Dalby, M. J. (2015). Nanoscale stimulation of osteoblastogenesis from mesenchymal stem cells: Nanotopography and nanokicking. *Nanomedicine*, *10*(4), 547–560. https://doi.org/10.2217/nnm.14.134

Rüdrich, U., Lasgorceix, M., Champion, E., Pascaud-Mathieu, P., Damia, C., Chartier, T., Brie, J., & Magnaudeix, A. (2019). Pre-osteoblast cell colonization of porous silicon substituted hydroxyapatite bioceramics: Influence of microporosity and macropore design. *Materials Science and Engineering: C*, *97*, 510–528. https://doi.org/10.1016/J.MSEC.2018.12.046

Szczodra, A., Houaoui, A., Salminen, T., Hannula, M., Gobbo, V. A., Ghanavati, S., Miettinen, S., & Massera, J. (2024). Pore graded borosilicate bioactive glass scaffolds: in vitro dissolution and cytocompatibility. Journal of Materials Science: Materials in Medicine, 35(1). https://doi.org/10.1007/s10856-024-06791-1

Surmenev, R. A., Surmeneva, M. A., & Ivanova, A. A. (2014). Significance of calcium phosphate coatings for the enhancement of new bone osteogenesis – A review. *Acta Biomaterialia*, *10*(2), 557–579. https://doi.org/10.1016/j.actbio.2013.10.036

Tavares, D. dos S., Castro, L. de O., Soares, G. D. de A., Alves, G. G., & Granjeiro, J. M. (2013). Synthesis and cytotoxicity evaluation of granular magnesium substituted β-tricalcium phosphate. *Journal of Applied Oral Science*, *21*(1), 37–42. https://doi.org/10.1590/1678-7757201302138

Vetsch, J. R., Müller, R., & Hofmann, S. (2016). The influence of curvature on three-dimensional mineralized matrix formation under static and perfused conditions: an *in vitro* bioreactor model. *Journal of The Royal Society Interface*, *13*(123), 20160425. https://doi.org/10.1098/rsif.2016.0425

Vogel, J. P., Szalay, K., Geiger, F., Kramer, M., Richter, W., & Kasten, P. (2006). Platelet-rich plasma improves expansion of human mesenchymal stem cells and retains differentiation capacity and *in vivo* bone formation in calcium phosphate ceramics. *Platelets*, *17*(7), 462–469. https://doi.org/10.1080/09537100600758867

Wang, C. X., Zhou, X., & Wang, M. (2004). Influence of sintering temperatures on hardness and Young's modulus of tricalcium phosphate bioceramic by nanoindentation technique. *Materials Characterization*, *52*(4–5), 301–307. https://doi.org/10.1016/j.matchar.2004.06.007

4. Tri-culture on 3D-printed β-TCP scaffolds as a model for testing anticancer drug activity

4.1. Introduction

Co-culture *in vitro* models present an attempt to recapitulate complex interactions known to take place in the tumour microenvironment. In the previous chapters, it was already mentioned that co-culturing bone cancer cells with MSCs poses a promising approach to developing advanced *in vitro* models of osteosarcoma and bone metastases. In other cases, co-culture may be focused on enhancing angiogenesis and vascularization and, thus, employs endothelial cells. For instance, in one study, microvascular endothelial cells were co-cultured with adipose-derived MSCs on poly-L-lactic acid/polylactic-co-glycolic acid (PLLA/PLGA) scaffolds. This resulted in the formation of mature vessel-like structures – not only expressing central markers such as CD31 (also called PECAM-1 – platelet/endothelial cell adhesion molecule-1) and alpha-smooth muscle actin (α-SMA) but also oriented and organized in a complex network (Freiman et al., 2016). The comparison was made to other combinations of cells including human neonatal dermal fibroblasts and human umbilical vein endothelial cells (HUVECs). Another interesting example of using endothelial cells for creating a co-culture is the work of Chaddad and co-authors (Chaddad et al., 2017). In their study, they combined a 2D and 3D approach by placing an osteosarcoma cell spheroid (MG-63) on top of the endothelial (HUVECs) cell monolayer. They observed the formation of oriented tubule-like structures by endothelial cells towards the osteosarcoma spheroid and confirmed the interplay by checking the expression of the CD31 marker.

Considering the above-mentioned examples and overall evidence of the benefits of co-culturing multiple cell lines, what could be the strategy for combining three cell types in one model? Technically, the task of setting up a co-culture, especially consisting of more than two types of cells, is challenging. While aiming to co-culture cells in direct contact (same scaffold, same chamber of the bioreactor, same compartment of a microfluidic chip, etc.), one can encounter obstacles on the way to downstream analysis – for instance, gene expression analysis. How to analyse gene expression in each cell type contained in a model? Frequently, the only option is total RNA extraction and following analysis, but even in this case, it is possible to design the initial experiment to get an understanding of cell-cell crosstalk. In the study by Pagani and co-authors, a simple multiwell plate insert model was used to co-culture osteoblasts, osteoclasts, and endothelial cells (Pagani et al., 2018). To understand the interactions between cells, the researchers incubated three different cell types in different combinations – and analysed the total markers (ALP, Collagen type I (COLL1), VEGFA, Osteoprotegerin (OPG), RANKL, Interleukin 6 (IL6), Transforming Growth Factor β1 (TGFβ1) and Cathepsin K (CATK)) by ELISA and RT-qPCR. Eventually, by observing the upregulation and downregulation patterns for the used cell types (monocultures), bi-cultures and tri-cultures, they were able to conclude the influence of cells on each other.

Another way to analyse gene expression in a co-culture is using transfected cells stably expressing a fluorescent protein or applying a cell tracker – live-compatible staining that can be retained in the cell throughout a limited (yet sufficient for an experiment) period. The latter

was used in the previously mentioned work of Freeman et al. where co-culture spheroids were created and simulated different stages of osteosarcoma (Freeman et al., 2022). However, both techniques require dissociation of the models which can be challenging due to cells forming strong cell-cell and cell-material contacts, and other technical obstacles.

As we already mentioned, the bone microenvironment in a pathological state is characterized above all by imbalanced bone remodelling. Several studies tried to reconstruct such conditions *in vitro*. Villasante et al., for example, implicated osteoclasts in the model already containing Ewing's sarcoma spheroids and MSC-derived osteoblasts. They observed several features connected to the progression of the tumour: degradation of trabecular structure and decrease of bone sialoprotein (Villasante et al., 2017).

Yet another example of a tri-culture model of bone cancer – a model consisting of MG-63 osteosarcoma cell spheroids embedded in platelet lysate-derived hydrogel, osteoblasts, and MSCs. It was utilized to reveal the influence of the osteoblasts and MSCs on the invasive behaviour of the tumour spheroid. In addition to the demonstration of the tumour-stromal cell interaction, the authors showed that the developed model responds differently to the tested anticancer drug in comparison to hydrogel-embedded spheroids without co-culture with osteoblasts and MSCs and freely cultured spheroid (C. F. Monteiro et al., 2021).

4.2. Aim

In this Chapter, I aim to combine the "components" described in the previous chapters in an advanced 3D model *in vitro*. To recapitulate the key features of osteosarcoma microenvironment, I am assembling the following constituents: stable cell spheroids obtained from the optimal ratio of osteosarcoma cells and MSCs, 3D-printed tricalcium phosphate scaffold pre-cultured with primary MSCs, and endothelial cells. The spheroids, in this case, represent a tumour-like unit, MSCs-seeded scaffolds represent a bone-like environment, and endothelial cells hold the potential to form vessel-like structures necessary for favourable tumour development. Last but not least, I provide the resulting model with efficient transport of nutrients and the source of mechanical stimuli by employing a perfusion bioreactor. Concluding this part of the work, as a preliminary validation of the developed model, I am using it to test a well-known and widely used anticancer drug.

4.3. Materials and Methods

4.3.1. Materials

Low-glucose, as well as high-glucose Dulbecco's modified Eagle's medium (DMEM), Minimum Essential Medium (MEM, GlutaMAX™ Supplement) α, fetal bovine serum (FBS), trypsin EDTA 1X, ethanol (EtOH, BioUltra, ≥ 99.8%, molecular biology grade, CAS: 64-17-5), phosphate-buffered saline (PBS, ready-to-use tablets, Ref. N. P4417-100TAB) were purchased from Sigma-Aldrich, USA. Vascular Cell Basal Medium (PCS-100-030) and Microvascular Endothelial Cell Growth Kit-BBE (PCS-110-040) were purchased from the

American Type Culture Collection, Manassas, VA, USA. RoosterNourish™-MSC-XF media (KT-016) was purchased from RoosterBio, USA. Blasticidin S HCl (10 mg/mL, Ref. A1113903), Geneticin™ Selective Antibiotic (G418 Sulfate) (50 mg/mL, Ref. 10131035), and Human Heat Stable bFGF Recombinant Protein (FGF2, Ref. PHG0360) was purchased from Gibco, USA. LIVE/DEAD™ Viability/Cytotoxicity Kit, for mammalian cells (Ref. L3224), Vybrant™ Multicolor Cell-Labeling Kit (DiO, DiI, DiD Solutions, Ref. V22889), Low-Density Lipoprotein From Human Plasma, Acetylated, Alexa Fluor™ 488 Conjugate (Ref. L23380), NucBlue™ Live ReadyProbes™ Reagent (Hoechst 33342, Ref. R37605), Penicillin-streptomycin (PS), alamarBlue™ HS Cell Viability Reagent (Ref. A50100), CyQUANT™ LDH Cytotoxicity Assay, fluorescence (Ref. C20303) and TRIzol™ were purchased from Invitrogen, USA. Doxorubicin hydrochloride (Ref. J64000.MA) was acquired from Thermo Scientific Chemicals, USA. Agarose (Certified Molecular Biology Agarose, Ref. 1613100), iScript™ cDNA Synthesis Kit and master mix for quantitative real-time PCR (SsoAdvanced Universal SYBR Green Supermix) were purchased from Bio-Rad Laboratories, USA. Primers for qPCR were designed using PrimerQuest™ Tool and synthesized by Integrated DNA Technologies (IDT, USA). Cell lines used for the research have the following specifications: human bone marrow-derived stem cells (hBMSCs, hTERT-BMSC clone Y201, isolated from bone marrow and immortalized through hTERT lentiviral vectors (James et al., 2015)) were kindly provided by Prof. P. Genever, University of York; human dermal microvascular endothelial cell line (TIME-GFP, CRL-4045) and human osteosarcoma cell line (U2OS, HTB96) were purchased in American Type Culture Collection, Manassas, VA, USA; primary human bone marrow-derived stem cells (pBMSCs) were purchased from RoosterBio, USA.

4.3.2. Pre-culture of pBMSCs on the 3D-printed β-TCP scaffolds

Primary human bone marrow-derived stem cells (pBMSCs) were first expanded in the specialised xeno-free expansion media RoosterNourish™, and then cultivated in MEM-α supplemented with 10 % FBS, 1 % PS, and 10 ng/mL FGF2, and maintained at 37 ºC in the humidified atmosphere containing 5 % CO_2. Before cell seeding, β-TCP scaffolds were sterilized by heating at 140 ^{0}C for 3 h, quickly washed in sterile PBS and immersed overnight in an FBS-enriched culture medium. PBMSCs were trypsinized, suspended in a 1:1 mixture of media and 5 mg/mL collagen and seeded on β-TCP scaffolds in the number of 3×10^5 cells per scaffold. After 3 h of collagen solidifying, 1.5 mL of the culture media was added to each well containing cell-seeded scaffold. To estimate cell seeding efficiency and metabolic activity on the 1st day of culture, the scaffolds were transferred to a clean 24-well plate, and alamarBlue™ reagent was added to the wells – both in the plate used for cell seeding and the clean plate with newly transferred scaffolds – and the fluorescence was read after 2 h of incubation at 560/590 nm. Metabolic activity of the pBMSCs on the scaffold, as well as their viability, was also assessed on the 3rd and 6th days of culture – by resazurin reduction assay (alamarBlue™) and fluorescence microscopy with live & dead staining (Calcein AM and Etidium homodimer-1), respectively, following manufacturer's instructions.

4.3.3. Tri-culture on the 3D-printed β-TCP scaffolds

Prior to the use in experiments, cell lines were cultured in standard conditions (37 ºC in the humidified atmosphere containing 5 % CO_2) in relevant media: high-glucose DMEM with 10 % FBS and 1 % PS (U2OS), low-glucose DMEM with 10 % FBS and 1 % PS (hBMSCs Y201), and Vascular Cell Basal Medium with the addition of Microvascular Endothelial Cell Growth Kit-BBE, 200 μg/mL G418 and 12.5 μg/mL Blasticidin (TIME-GFP). U2OS and hBMSCs cells were harvested and seeded in a 3 to 1 ratio for generating cell spheroids using the agarose-coated plate, as was described in the chapters above, and cultured in a 1:1 mixture of relevant media. TIME-GFP cells were harvested and used as a cell suspension.

One day before assembling the tri-culture on the scaffolds, all three components were stained with Vybrant™ Multicolor Cell-Labeling Kit: co-culture spheroids were stained with DiD, TIME-GFP – with DiO, and pBMSCs-seeded scaffolds – with DiI. On the day of the tri-culture assembling, both co-culture U2OS:hBMSCs (3:1) spheroids and TIME-GFP single-cell suspension were seeded on the 7-day precultured pBMSCs-seeded scaffolds in 100 μL of a collagen-medium mix. After 3 h of collagen solidifying, 1.5 mL of a medium composed of a 1:1:1 mixture of media for pBMSCs, U2OS and TIME-GFP was added per scaffold. Scaffolds seeded with co-culture spheroids only were used as a control and incubated in a 1:1 mix of media for U2OS and hBMSCs Y201.

For metabolic activity assay, the tri-culture scaffolds were transferred to a clean multiwell plate, and alamarBlue™ reagent was used as described above. For the morphological analysis, the scaffolds were observed with the use of a fluorescence microscope equipped with a humidified chamber with 37 ºC and 5 % CO_2 – THUNDER Imager Live Cell & 3D Assay (Leica, Japan). To enhance the visibility of the live cells, Calcein AM staining was used. Additionally, acetylated LDL was used to label endothelial TIME-GFP cells aiming to enhance and specify the signal during the imaging.

4.3.4. Tri-culture in dynamic conditions

To create dynamic conditions for the tri-culture scaffolds, the Quasi Vivo® (QV900, Kirkstall, Ltd, UK) perfusion system was used. For this, the scaffolds were placed in the chambers of the Quasi Vivo® system, and the chambers were sequentially connected to the pump and media reservoir and placed in the incubator. The peristaltic pump parameters were set with respect to media superficial velocity of 40 μm/s. The required volumetric flow rate was calculated using the cross-sectional area of the chamber as follows:

$$\text{Volumetric flow rate (mL/min)} = \frac{\text{Superficial velocity (cm/h)}}{60} \times \text{column cross-sectional area (cm}^2\text{)}$$

It should be noted, that in the context of the Quasi Vivo® system, this volumetric flow rate calculation is approximate due to the position of the inlet and outlet in the chambers. To understand the actual superficial velocity in the chambers, mathematical modelling is required.

In total, 50 mL of 1:1:1 mixture medium was used for the perfusion system containing 6 scaffolds. In the case of static culture, the scaffolds were placed in the T-75 flasks and immersed in medium – with the volume equal to the volume used in the dynamic system. Half of the culture medium was changed every two or three days. On the 3rd and 6th days, the

scaffolds were inspected through metabolic activity assay and fluorescence imaging. At the end of the one-week culture period, the scaffolds were collected for RNA extraction using the RNeasy Plus Mini Kit (Qiagen, Hilden, Germany). The expression of the genes of interest in tri-culture models in dynamic and static conditions was analysed on the synthesized cDNA with a SYBR Green mix via quantitative real-time PCR. The sequences of forward and reverse primers are listed in Table 4-1.

Table 4-1 – Sequences of forward and reverse primers.

Gene	Forward primer	Reverse primer
ACTB	5'- GCA CCA CAC CTT CTA CAA T -3'	5'- CAT GAT CTG GGT CAT CTT CTC -3'
TP53	5'- TGT ACC ACC ATC CAC TAC A -3'	5'- TGT TCC GTC CCA GTA GAT TA -3'
RB1	5'- AGC CTA TCT CCG GCT AAA TA -3'	5'- GTC CAA ATG CCT GTC TCT C -3'
KDR	5'- CCT CAC CTG TTT CCT GTA TG -3'	5'- GCT CTT TCG CTT ACT GTT CT -3'
VEGF	5'- ACC AGA GGA AAG TGG TGT -3'	5'- CAT GAG CTC CAC AGT CAA G -3'

4.3.5. Application of tri-culture model in cytotoxicity test

To preliminary evaluate the tri-culture model's performance in anticancer drug cytotoxicity applications, doxorubicin (DOX) was chosen. First, to assess the sensitivity of osteosarcoma cells to the chosen agent, U2OS cells were routinely seeded as a monolayer in a 48-well plate and incubated overnight. The tested compound was added in concentrations of 20, 40 and 80 μg/mL in culture medium. After 24 h of incubation, 50 μL of media was transferred to a clear 96-well plate, and lactate dehydrogenase (LDH) activity was assessed. LDH is an essential enzyme involved in anaerobic metabolic pathway, and its presence in cell culture medium indicates the loss of cell membrane integrity. Briefly, 50 μL reaction mix from CyQUANT™ LDH Cytotoxicity Fluorescent Assay kit was added to the wells containing medium, followed by 50 μL of stop solution after 10 min incubation in the dark, and finally, the fluorescence was read in the plate reader (Spark®, Tecan Trading AG, CH) with excitation and emission set to 560 and 590 nm, respectively.

Following the evaluation of U2OS sensitivity and the concentration of the anti-cancer agent, DOX was added to the culture medium of the scaffolds cultured for 1 week in static and dynamic conditions. In the case of the dynamic system, the additional reservoir bottle was added, and the chambers were divided into two separate sequences – with the tested compound and without, – as shown in Figure 4-1.

Figure 4-1 – Perfusion bioreactor system with two separate reservoir bottles – with and without doxorubicin. Three chambers are sequentially connected to each bottle. Both groups of chambers are connected to the peristaltic pump operating at 3.8 rpm (calculated following the recommended 40 μm medium superficial velocity).

After 24 hours, alamarBlue™ assay, LDH activity assay and fluorescent microscopy imaging were performed on the tri-culture scaffolds incubated in static and dynamic conditions with or without the tested anticancer drug.

4.3.6. Statistical analysis

Each group of samples was represented by three replicates. Results are shown as mean value ± standard deviation, where applicable. Comparison between groups within experimental time points was performed in Prism (v8, GraphPad Software, USA) using one-way ANOVA with Tukey correction for multiple comparisons, preceded by normal distribution Shapiro–Wilk's test and homoscedasticity Levene's median test. For each comparison performed, the difference was determined as significant for $p < 0.05$.

4.4. Results and Discussion

4.4.1. Pre-culture of pBMSCs on the 3D-printed β-TCP scaffolds

In line with the results of the above-described application of primary human bone-marrow-derived MSCs for culturing on the 3D-printed scaffolds, resazurin reduction assay demonstrated, firstly, high cell seeding efficiency of 87.4 ± 5 %. Secondly, the metabolic activity of the cells raised on the 3rd day of culture and decreased on the 6th day, with overall positive growth (Figure 4-2). A similar drop in cell metabolic activity was observed in the previous Chapter in the context of a 3-week pBMSCs culture on the β-TCP scaffolds and is thought to be linked to the adaptation of the cells to the scaffold.

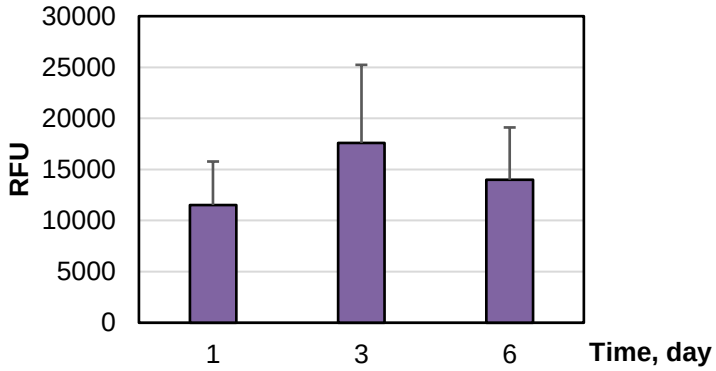

Figure 4-2 – Resazurin reduction assay of pBMSCs cultured on the 3D-printed β-TCP scaffolds. Metabolic activity is presented as an average of relative fluorescent units (RFU) ± standard deviation.

The viability of the cells on the scaffolds was confirmed by fluorescent microscopy observation with live/dead staining on the 3rd and the 6th days of culture (Figure 4-3). It can be seen that in comparison to the earlier time point, cells are more oriented and elongated on the images of the later time point. Moreover, in the areas between structures of the scaffolds – neighbouring strings, small holes or sharp corners – the cells produced a more organized and abundant ECM. As previously, the channel of the Ethidium homodimer-1 ("dead") is not presented here due to the absence of signal and "pollution" of the image by the background noise. The inability to find dead cells might be due to the removal of them by regular medium exchange or due to the large volume of the scaffolds and technical limitations of the imaging system. The observations of the pBMSCs cell morphology on the scaffolds are in agreement with the experiments described in the previous Chapter, supporting the reproducibility of the cell-seeding method as well as batch-to-batch uniformity of the 3D-printed scaffolds.

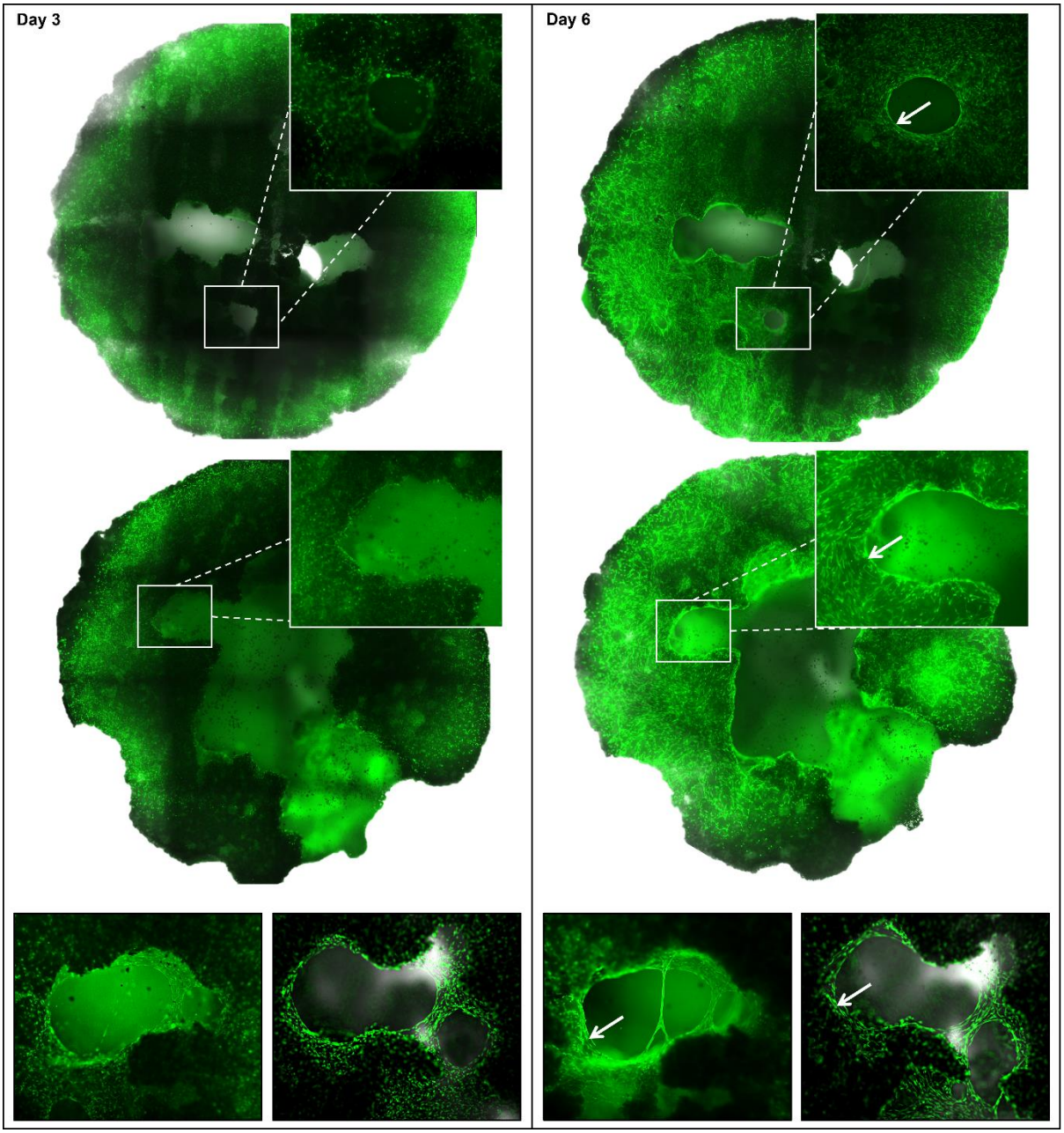

Figure 4-3 – Live/dead staining of pBMSCs cultured on the 3D-printed β-TCP scaffolds. Only the green ("live", Calcein AM) channel is presented due to the absence of the signal in the red ("dead", Ethidium homodimer-1) channel. On the left panel (*3 d*), the images collected on the 3rd day are presented, while on the right panel (*7 d*) the images taken on the 7th day are presented, with white arrows indicating regions with more elongated, oriented pBMSCs and/or evidence of abundant ECM synthesis.

4.4.2. Tri-culture on the 3D-printed β-TCP scaffolds

The developed *in vitro* model design implies the use of several "building blocks" representing the key features of the osteosarcoma microenvironment. In detail, the tri-culture described in this section contains the tumour unit represented by co-culture spheroid of osteosarcoma and MSCs cells; bone-like environment represented by the 3D-printed β-TCP scaffolds seeded with primary MSCs; and endothelial cells serving as a source of vascularization. Additionally, to provide the resulting system with efficient mass transport and

mechanical stimuli driven by fluid flow, the scaffolds with three cellular components were placed into the chambers of the perfusion bioreactor.

Metabolic activity and viability analysis

The analysis of the U2OS:MSC spheroids cultured on the scaffolds taken as a control revealed that the cells had a metabolic activity pattern similar to pBMSCs shown previously – rising on the 3rd day of culture and slightly decreasing on the 6th day, with an overall positive growth (Figure 4-4, *a*, left panel). In comparison to pBMSCs, the fluorescent signal was expectedly lower due to the fact that the spheroids were seeded in a number of 3 spheroids per scaffold and had comparably lower penetration ability owing to their compactness and development of ECM. Tri-culture, in turn, also demonstrated sufficient metabolic activity – slightly higher in the scaffolds cultivated in dynamic conditions (Figure 4-4, *a*, right panel).

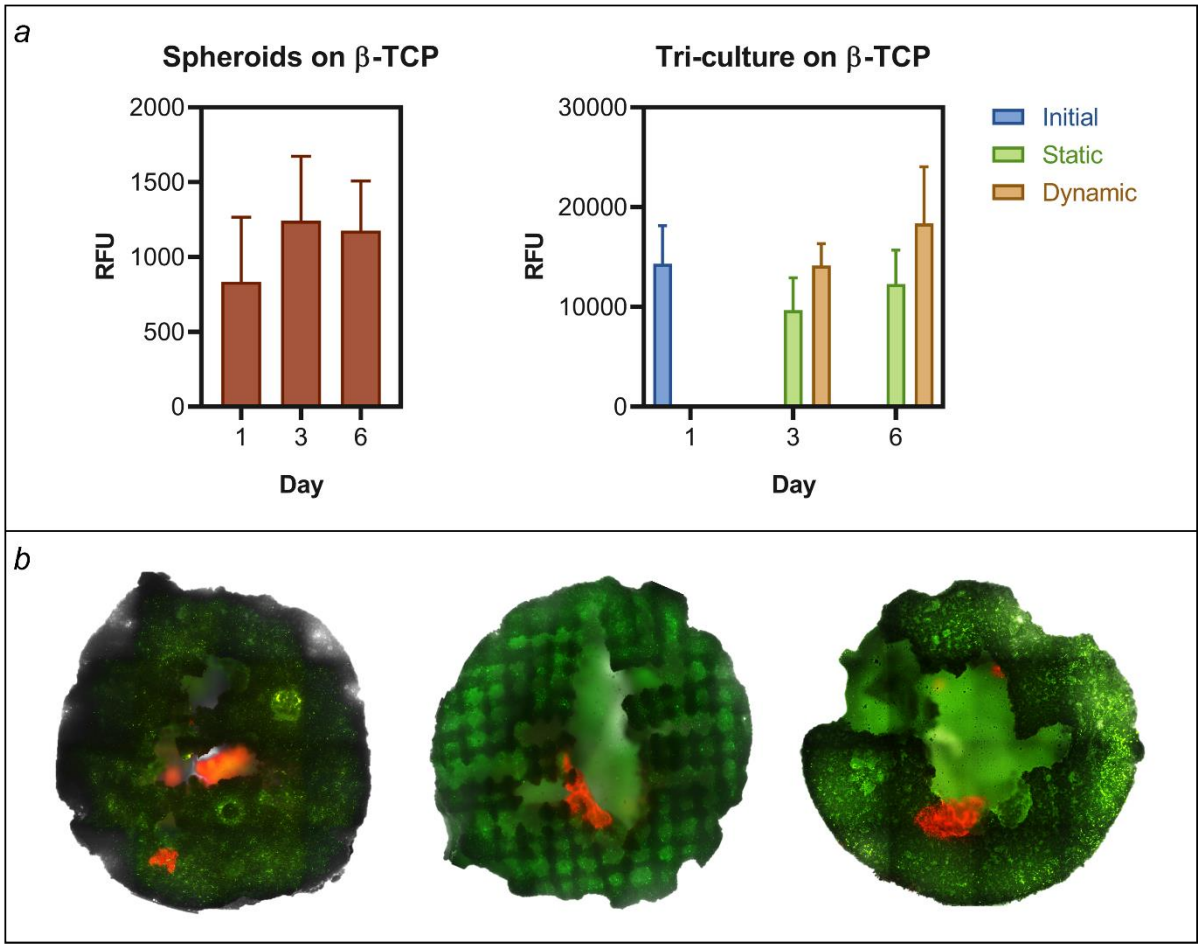

Figure 4-4 – Metabolic activity (a) and fluorescent microscopy (b) of co-culture U2OS-MSC spheroids and tri-culture (spheroids + pBMSCs + endothelial cells) on β-TCP scaffolds. Panel *a*: the values are presented as an average of RFU ± SD. Panel *b*: co-culture U2OS-MSC spheroids are stained with cell tracker and are visible in red, and pBMSCs and endothelial cells are stained with Calcein AM and are visible in green.

Regarding fluorescent microscopy observations, it was possible to distinguish between osteosarcoma spheroids (Figure 4-4, *b*, red) and cells seeded in suspension – pBMSCs and endothelial cells (Figure 4-4, *b*, green). The spheroids were found to be compact, and there

were almost no floating cells observed indicating the integrity of the spheroids. Green-stained cells were found to be homogeneously spread all over the scaffolds and attached to their surface. Unfortunately, due to too weak and overlapping signals of the DiO and DiI cell tracking agents in the used 3D model, it was impossible to distinguish between pBMSCs and endothelial cells at this time point. Together, the results of cell metabolic activity and cell viability analyses of both spheroid monoculture on the scaffolds and tri-culture on scaffolds allowed me to make an intermediate conclusion of the positive progress of the 3D *in vitro* model assembling – and to introduce dynamic culture conditions to the system by means of perfusion bioreactor (Quasi Vivo® system).

The fluorescence imaging after the division of the cell-seeded scaffolds into static (cultivated in standard conditions) and dynamic (cultivated in perfusion bioreactor) groups did not reveal any visible differences between these conditions (Figure 4-5). In both conditions, the spheroids were found to be securely arranged within the scaffolds, and the cells seeded in suspension (pBMSCs and endothelial cells) were evenly distributed and presented in comparably similar numbers in static cultures and bioreactor cultures. With the help of acetylated LDL-based staining, it was also possible to define endothelial cells (Figure 4-5, upper row, magnified image). Endothelial cells were found to be distributed as single cells all over the scaffold and there was no network formation observed neither between endothelial cells nor between other cell types. Endothelial cell network formation in 3D *in vitro* models is frequently stimulated by the addition of either matrix components such as fibronectin or growth factors such as vascular endothelial growth factor (VEGF), and these measures might help in facilitating the formation of the network in the present model. Even though the VEGF expression was demonstrated in the previous chapter in the context of a co-culture experiment, this might be not sufficient for triggering the growth of the vessel-like structure.

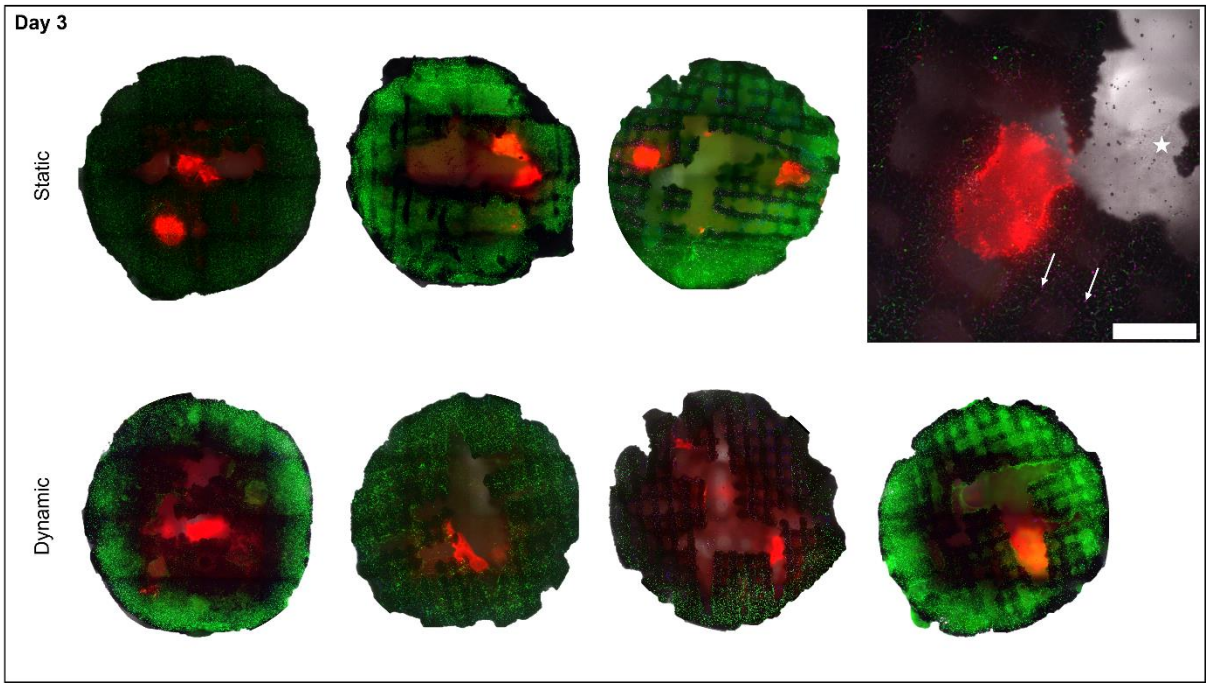

Figure 4-5 – Fluorescent microscopy of and tri-culture (spheroids + pBMSCs + endothelial cells) on β-TCP scaffolds. Co-culture U2OS-MSC spheroids are stained with a cell tracker and are visible in red, and pBMSCs and endothelial cells are stained with Calcein AM and are visible in green. On the magnified image, endothelial

cells are additionally stained with acetylated LDL and visible in magenta (marked with arrows). The cell-produced collagen is slightly visible as semi-transparent fibres stretched between the scaffold's structures (marked with a star). Scale bar 650 μm.

Gene expression analysis

Gene expression analysis in co-culture *in vitro* models may be challenging. However, gene expression in the model as a whole unit is of great interest. For example, both osteosarcoma cells and MSCs may express VEGF, which is involved in the development of endothelial cells, vasculogenesis, and angiogenesis. When creating a model that is susceptible to vascularization, overall VEGF expression is just as significant as the expression of VEGF in different cell types. In one co-culture investigation with osteoblasts and endothelial cells, gene expression from total RNA was used to compare the expression of co-culture spheroids to that of monoculture spheroids. Thus, the authors looked at the regulation of genes associated with cell interaction from both osteoblasts and an endothelial cells perspective (Casbas-Hernandez et al., 2011).

VEGF is known to be linked to the advancement of cancer because it stimulates endothelial cell proliferation, encourages cell migration, suppresses apoptosis, and causes blood vessel permeabilization. Targeting VEGF is not the main therapeutic strategy, despite clinical case studies showing a poor association between VEGF expression and osteosarcoma stage classification; still, this marker has a significant potential in the prognosis of treated cancer survival (Assi et al., 2021; Bajpai et al., 2009; Yu et al., 2014). VEGF overexpression would function as an early marker of the cell-seeded scaffold's propensity to become possibly vascularized in the context of our osteosarcoma model. KDR gene encodes a protein tightly connected with VEGF – its receptor (kinase insert domain receptor or VEGFR). KDR expression is elevated in endothelial cells which are recruited in the sites of VEGF-mediated angiogenesis. Both circulating VEGF and KDR are used as markers of efficacy of anticancer drugs targeting angiogenesis (Kerbel, 2008). Tumour suppressor protein p53, the cellular tumour antigen, is encoded by the TP53 gene. In response to various cellular stressors, the p53 protein modulates target gene expression, consequently triggering various biological processes such as cell cycle arrest, apoptosis, senescence, DNA repair, or metabolic alterations. Upregulation of TP53 is associated in the context of osteosarcoma with a decreased 3-year disease-free survival as well as a shorter 3-year overall survival (Zamborsky et al., 2019). The retinoblastoma-associated protein (RB1 gene) is a tumour suppressor and a major modulator of the G1/S phase of the cell cycle. Owing to its roles, RB1 is anticipated to be either downregulated or mutated in a broad range of malignancies, including OS. Additionally, RB1 seems to be a possible indicator of osteosarcoma metastasis (Ren & Gu, 2017).

Analysis of the total gene expression in the tri-culture on β-TCP in comparison to the spheroids on β-TCP, it was observed that VEGF was slightly upregulated (Figure, left). It was also noted that VEGF was expressed higher in the tri-culture models incubated in a perfusion bioreactor (dynamic) than in standard conditions (static) (Figure, right). The difference in the gene expression between spheroids and tri-culture was highlighted especially in the case of KDR gene (2^{-ddCT} around 5000) – expectedly, due to the fact that KDR is specific for endothelial cells, which were not present in the spheroid models. Interestingly, KDR was upregulated in static tri-culture in relation to dynamic tri-culture, which may indicate the better

survival of endothelial cells in static conditions, inhibition of their activity in perfusion conditions, or both. TP53 was found to be upregulated in tri-culture, with a prevalence of expression in dynamic conditions. Finally, RB1 was also upregulated, with a prevalence in static tri-culture. Considering the above-listed evidence of correlation of marker expression with invasiveness of the tumour, it appears that tri-culture is beneficial for approximating the tumour-like behaviour of the osteosarcoma spheroids – at least, judging from VEGF, KDR and TP53 expression. It is not clear whether the upregulation of RB1 should be considered as a "negative" characteristic of the developed model, and further investigation should be performed.

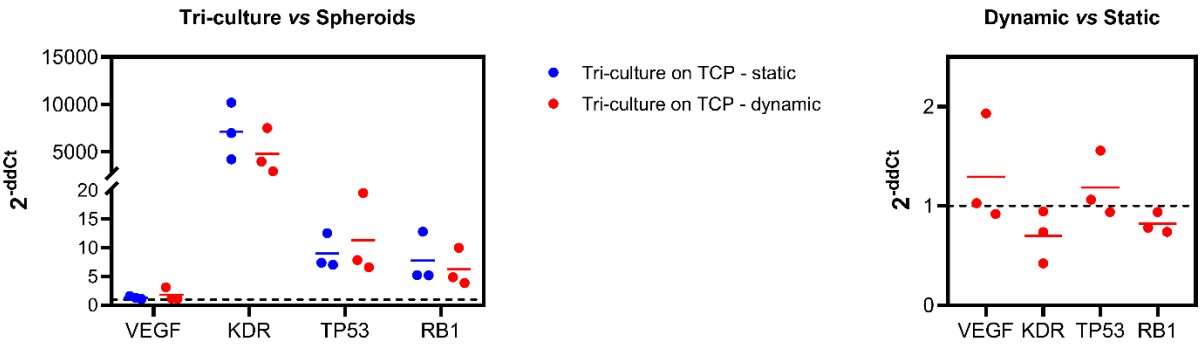

Figure 4-6 – Normalized gene expression in tri-cultures on β-TCP scaffolds in relation to osteosarcoma spheroids on β-TCP scaffolds (left) and dynamic tri-cultures in relation to static tri-cultures (right). ACTB was used as a housekeeping gene. The data is presented as 2^{-ddCt} for each sample and their means.

4.4.3. Application of tri-culture model in cytotoxicity test

For a preliminary assessment of the tri-culture model suitability for anticancer drug cytotoxicity applications, doxorubicin (DOX) was chosen. DOX, also known as adriamycin, is frequently used for the post- or pre-surgical treatment of osteosarcoma patients in the context of a chemotherapy course known as MAPi – a combination of methotrexate, adriamycin, cisplatin and ifosfamide (Tippett et al., 2023). Thus, knowing also that U2OS cells in monolayer are sensitive to DOX as will be shown later, this anticancer drug was selected for this preliminary cytotoxicity trial.

As was demonstrated in the LDH activity assay, osteosarcoma U2OS cells seeded in a monolayer are sensitive to DOX in all three tested concentrations – 20, 40 and 80 μg/mL – demonstrating LDH activity at least 50% higher than the control group within 24 hours of incubation (cells cultivated without the addition of DOX) (Figure 4-7). For the application in the advanced 3D *in vitro* model, the DOX concentration of 50 μg/mL was selected due to the fact that the osteosarcoma cells are organized as spheroids and are arranged in the complex 3D structure of the β-TCP scaffold.

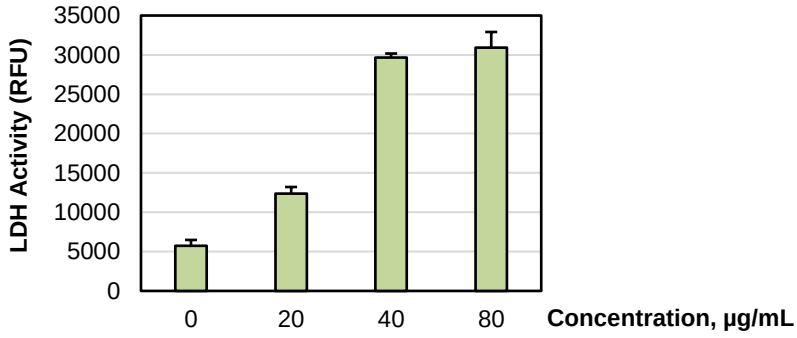

Figure 4-7 – LDH activity of U2OS cells incubated with various concentrations of doxorubicin (DOX) for 24 h. Control is represented by a "0" bar. Values are presented as average relative fluorescent units (RFU) ± standard deviation.

In the tri-culture on the scaffolds, 24-h incubation with 50 µg/mL of DOX did not occur to cause any effect on the cell viability detectable by resazurin reduction (alamarBlue™), LDH (CyQUANT™) or visual observation via fluorescent microscopy. Interestingly, such exposure to anticancer agents did not even alter the activity of the U2OS:MSC spheroids seeded on β-TCP (Figure 4-8). Additionally, there was no significant difference in metabolic activity and LDH activity of tri-culture in static or dynamic conditions.

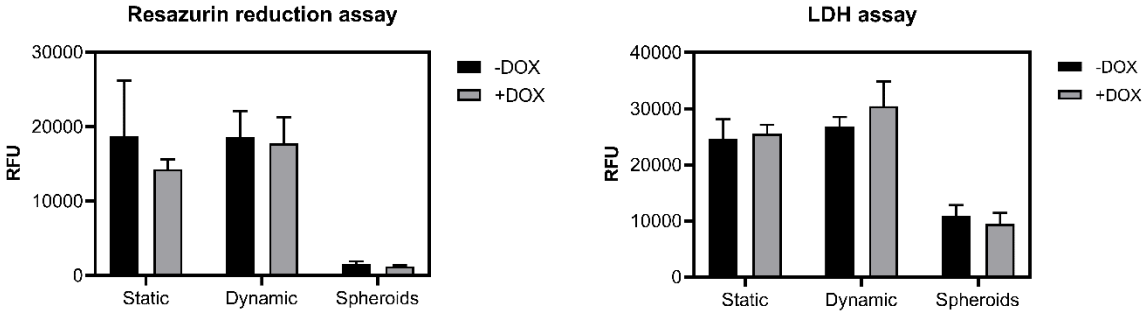

Figure 4-8 – Metabolic activity and LDH activity of U2OS:MSC co-culture spheroids on β-TCP (*Spheroids*) and tri-cultures (spheroids + pBMSCs + endothelial cells) on β-TCP in standard (*Static*) and perfusion (*Dynamic*) conditions incubated for 24 h with 50 µg/mL of doxorubicin (*+DOX*) and in usual culture media (*-DOX*). The values are presented as an average of RFU ± SD.

Fluorescence microscopy observation of the tri-cultures in various conditions did not reveal any alterations in cell or cell spheroid morphology and presence (Figure 4-9). Both tri-culture models cultivated with or without doxorubicin had fluorescent compact spheroids arranged within the scaffolds, as well as pBMSCs and endothelial cells evenly distributed throughout the volume of the scaffold. There was also no difference noted in comparison to the previous time point of 6 days (Figure 4-5).

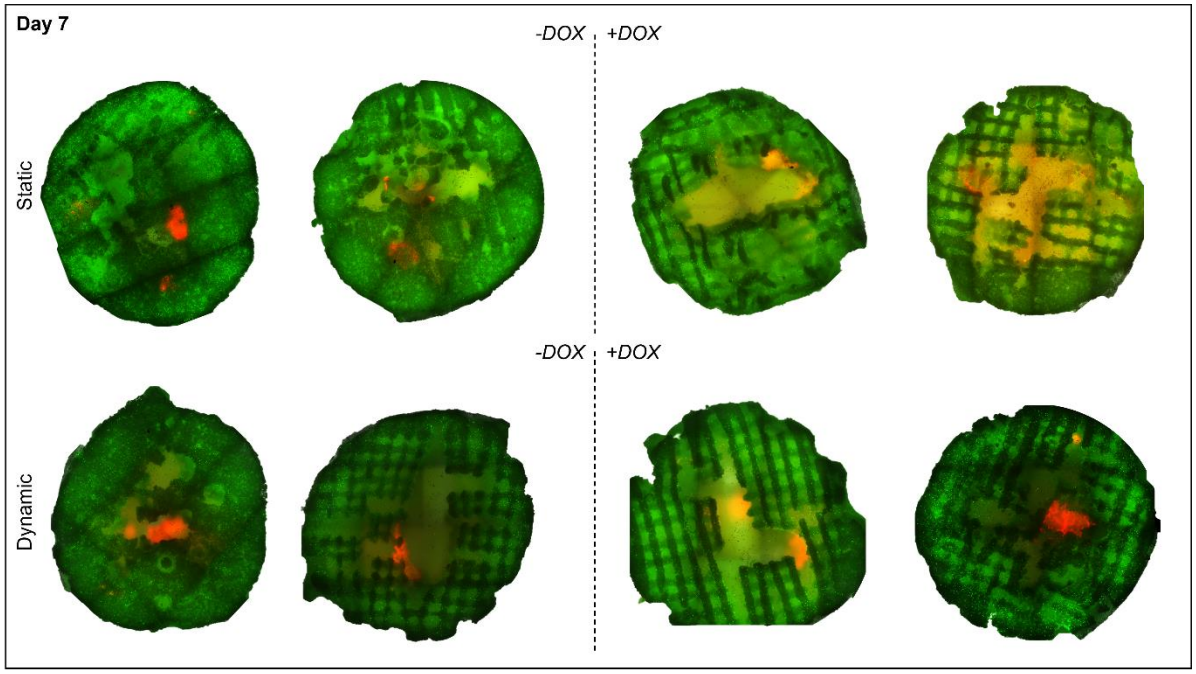

Figure 4-9 – Fluorescent microscopy imaging of tri-culture on β-TCP scaffolds cultivated for 7 days in static or dynamic (perfusion) conditions with (+DOX) or without (-DOX) the addition of doxorubicin. Co-culture U2OS:MSC spheroids are stained with cell tracker visible in red, and pBMSCs and endothelial cells are stained with Calcein AM and are visible in green.

Overall, the cytotoxicity results indicate that both the exposure time and the concentration of DOX are to be adjusted. The contrasting features of the cell spheroids in comparison to cell monolayers have been extensively discussed in the context of the present study, thus, it is expected that the concentration of any tested compound as well as the incubation time is to be optimized accordingly. There are numerous studies investigating the various drug cytotoxicity on the spheroid-based models. Indeed, the exposure periods usually exceed 24 hours: spheroids grown from 1×10^4 ovarian cancer cells were incubated with DOX for 72 hours (Świerczewska et al., 2023); spheroids formed from 2×10^4 cells (osteosarcoma and adipose-derived MSCs) – for 96 hrs (Cortini et al., 2023); spheroids from 1×10^4 osteosarcoma cells – for up to 5 days (Baek et al., 2016). It is also important to optimize the monitoring of the effect caused by DOX. The compound exhibits fluorescence, and its accumulation may be tracked via microscopy. Thus, in the next steps, the choice of the cell tracker agents should be reconsidered to allow the live monitoring of the accumulation of DOX in the osteosarcoma co-culture spheroids.

4.5. Conclusion

In this Chapter, I made an attempt to create a tri-culture containing key components of a 3D osteosarcoma model *in vitro*: osteosarcoma cell spheroid with optimized stability gained by co-culturing it with MSCs; primary MSCs pre-cultured on the 3D-printed β-TCP scaffolds and representing bone-like environment; and endothelial cells with a potential of forming vessel-like structures. From the technical point of view, there were several obstacles in establishing a tri-culture. Firstly, it was necessary to distinguish between the cell types visually

during fluorescent microscopy imaging. For this, cell tracking agents were used; however, due to the close peaks of emission and excitation coupled with small dimensions of single cells on the scaffolds in relation to the whole scaffold and weak signal, it was difficult to detect visually primary MSCs and endothelial cells, as well as distinguish between them. U2OS-MSC spheroids – being relatively large and compact – were visible even when resting in the deep layers of the scaffolds. Second, the extraction of only the total RNA of the tri-culture was possible, and not RNA from each cell type separately. Even having the cells stained differently, due to the nature of the used material – sintered β-TCP – it would not be feasible to separate cells from the β-TCP granules and sort them in a flow cytometer. Lastly, the cytotoxicity test of anticancer agent doxorubicin should have been better optimized (increased) for tri-culture conditions – both from the point of exposure time and concentration. Nevertheless, the results of metabolic activity, morphological analysis and gene expression analysis are promising, and with longer incubation periods in standard and perfusion conditions, as well as with an adapted cytotoxicity assay, the developed tri-culture model may serve as a worthy approach to establishing an osteosarcoma 3D model *in vitro*.

4.6. References

Assi, T., Watson, S., Samra, B., Rassy, E., Le Cesne, A., Italiano, A., & Mir, O. (2021). Targeting the VEGF Pathway in Osteosarcoma. *Cells 2021, Vol. 10, Page 1240*, *10*(5), 1240. https://doi.org/10.3390/CELLS10051240

Baek, N., Seo, O. W., Kim, M., Hulme, J., & An, S. S. A. (2016). Monitoring the effects of doxorubicin on 3D-spheroid tumor cells in real-time. OncoTargets and Therapy, 9, 7207–7218. https://doi.org/10.2147/OTT.S112566

Bajpai, J., Sharma, M., Sreenivas, V., Kumar, R., Gamnagatti, S., Khan, S. A., Rastogi, S., Malhotra, A., & Bakhshi, S. (2009). VEGF expression as a prognostic marker in osteosarcoma. *Pediatric Blood & Cancer*, *53*(6), 1035–1039. https://doi.org/10.1002/PBC.22178

Casbas-Hernandez, P., Fleming, J. M., & Troester, M. A. (2011). Gene Expression Analysis of In Vitro Cocultures to Study Interactions between Breast Epithelium and Stroma. *Journal of Biomedicine and Biotechnology*, *2011*. https://doi.org/10.1155/2011/520987

Chaddad, H., Kuchler-Bopp, S., Fuhrmann, G., Gegout, H., Ubeaud-Sequier, G., Schwinté, P., Bornert, F., Benkirane-Jessel, N., & Idoux-Gillet, Y. (2017). Combining 2D angiogenesis and 3D osteosarcoma microtissues to improve vascularization. *Experimental Cell Research*, *360*(2), 138–145. https://doi.org/10.1016/j.yexcr.2017.08.035

Cortini, M., Macchi, F., Reggiani, F., Vitale, E., Lipreri, M. V., Perut, F., Ciarrocchi, A., Baldini, N., & Avnet, S. (2023). Endogenous Extracellular Matrix Regulates the Response of Osteosarcoma 3D Spheroids to Doxorubicin. Cancers, 15(4), 1221. https://doi.org/10.3390/cancers15041221

Freeman, F. E., Burdis, R., Mahon, O. R., Kelly, D. J., & Artzi, N. (2022). A Spheroid Model of Early and Late-Stage Osteosarcoma Mimicking the Divergent Relationship between Tumor Elimination and Bone Regeneration. *Advanced Healthcare Materials*, *11*(7). https://doi.org/10.1002/adhm.202101296

Freiman, A., Shandalov, Y., Rozenfeld, D., Shor, E., Segal, S., Ben-David, D., Meretzki, S., Egozi, D., & Levenberg, S. (2016). Adipose-derived endothelial and mesenchymal stem cells enhance vascular network formation on three-dimensional constructs in vitro. *Stem Cell Research & Therapy*, *7*(1), 5. https://doi.org/10.1186/s13287-015-0251-6

James, S., Fox, J., Afsari, F., Lee, J., Clough, S., Knight, C., Ashmore, J., Ashton, P., Preham, O., Hoogduijn, M., Ponzoni, R. D. A. R., Hancock, Y., Coles, M., & Genever, P. (2015). Multiparameter Analysis of Human

Bone Marrow Stromal Cells Identifies Distinct Immunomodulatory and Differentiation-Competent Subtypes. *Stem Cell Reports*, *4*(6), 1004–1015. https://doi.org/10.1016/j.stemcr.2015.05.005

Kerbel, R. S. (2008). Tumor Angiogenesis. *New England Journal of Medicine*, *358*(19), 2039–2049. https://doi.org/10.1056/NEJMra0706596

Monteiro, C. F., Custódio, C. A., & Mano, J. F. (2021). Bioengineering a humanized 3D tri-culture osteosarcoma model to assess tumor invasiveness and therapy response. *Acta Biomaterialia*, *134*, 204–214. https://doi.org/10.1016/j.actbio.2021.07.034

Pagani, S., Torricelli, P., Veronesi, F., Salamanna, F., Cepollaro, S., & Fini, M. (2018). An advanced tri-culture model to evaluate the dynamic interplay among osteoblasts, osteoclasts, and endothelial cells. *Journal of Cellular Physiology*, *233*(1), 291–301. https://doi.org/10.1002/jcp.25875

Ren, W., & Gu, G. (2017). Prognostic implications of RB1 tumour suppressor gene alterations in the clinical outcome of human osteosarcoma: a meta-analysis. *European Journal of Cancer Care*, *26*(1), e12401. https://doi.org/10.1111/ECC.12401

Świerczewska, M., Sterzyńska, K., Ruciński, M., Andrzejewska, M., Nowicki, M., & Januchowski, R. (2023). The response and resistance to drugs in ovarian cancer cell lines in 2D monolayers and 3D spheroids. Biomedicine & Pharmacotherapy, 165, 115152. https://doi.org/10.1016/j.biopha.2023.115152

Tippett, V. L., Tattersall, L., Ab Latif, N. B., Shah, K. M., Lawson, M. A., & Gartland, A. (2023). The strategy and clinical relevance of in vitro models of MAP resistance in osteosarcoma: a systematic review. *Oncogene*, *42*(4), 259–277. https://doi.org/10.1038/s41388-022-02529-x

Villasante, A., Marturano-Kruik, A., Robinson, S. T., Liu, Z., Guo, X. E., & Vunjak-Novakovic, G. (2017). Tissue-Engineered Model of Human Osteolytic Bone Tumor. *Tissue Engineering - Part C: Methods*, *23*(2), 98–107. https://doi.org/10.1089/ten.tec.2016.0371

Yu, X. W., Wu, T. Y., Yi, X., Ren, W. P., Zhou, Z. Bin, Sun, Y. Q., & Zhang, C. Q. (2014). Prognostic significance of VEGF expression in osteosarcoma: A meta-analysis. *Tumor Biology*, *35*(1), 155–160. https://doi.org/10.1007/S13277-013-1019-1/METRICS

Zamborsky, R., Kokavec, M., Harsanyi, S., & Danisovic, L. (2019). Identification of Prognostic and Predictive Osteosarcoma Biomarkers. *Medical Sciences 2019, Vol. 7, Page 28*, *7*(2), 28. https://doi.org/10.3390/MEDSCI7020028

Conclusions and Future Prospective

The research work presented in this **thesis aimed** to develop a robust, tuneable and reproducible *in vitro* model of osteosarcoma that would mimic the bone tumour and its complex microenvironment and implement the mechanical stimuli essential for the normal functioning of the skeletal system.

To approximate this goal in a step-by-step approach, in each chapter, I focused on one "component" of the future *in vitro* model following the main objectives of the thesis. In **Chapter 1**, I elucidated the technical and functional aspects of spheroids as fundamental "building blocks" in 3D *in vitro* models. To overcome challenges in generating osteosarcoma cell spheroids, I employed a co-culture with MSCs and defined a co-culture ratio which proved to be optimal in terms of the spheroid mechanical properties and functionality. Additionally, a batch analysis method for live & dead assay quantification was established and demonstrated on the example of the spheroids.

The next two objectives of the thesis were dedicated to finding and characterization of an optimal bone-like environment for the developed *in vitro* model. I had an opportunity to evaluate two distinct approaches to creating such an environment – based on a soft scaffold and based on a rigid scaffold. In **Chapter 2**, I optimized the production of freeze-dried alginate-bioactive glass scaffolds with controllable pore size, evaluating their material characteristics and cytocompatibility. While microstructurally similar to trabecular bone and suitable for culture in static conditions, these scaffolds lacked mechanical stability under dynamic conditions, limiting their use. Thus, in **Chapter 3** I introduced 3D-printed β-TCP which exhibited macro- and micro-porosity, cytocompatibility with cell lines-representatives of bone tumour environment and promoted ECM production by MSCs. Importantly, their performance in dynamic conditions was validated in various bioreactors, making them suitable for the study's needs.

Finally, in **Chapter 4**, a tri-culture incorporating key components of the osteosarcoma model was attempted, employing the results obtained in the previous chapters – stable osteosarcoma cell spheroids, extensively characterized MSCs-seeded β-TCP scaffolds, and endothelial cells providing a source of future model vascularization. Despite the technical obstacles naturally coming along the co-culture of multiple cell types, promising results in metabolic activity, morphology, and gene expression analyses, as well as the preliminary assessment of the model's application for testing anti-cancer drug doxorubicin, suggest the potential of this tri-culture model with further optimization.

One of the **future steps** is to focus on a deeper understanding of cell-cell interactions within the developed 3D *in vitro* tri-culture model and optimize the system accordingly. In such a complex system, every parameter matters, and by varying cell seeding ratio, culture medium contents, and biochemical stimulation of the "players" of the model it is possible to move the fragile balance between the components of the model. It is also planned to apply mathematical modelling to the perfusion system and to understand how exactly the medium flows and which stimuli are applied to the cell-seeded scaffolds in the chambers. Additionally, mimicking tumour interactions with immune cells such as tumour-associated macrophages might assist in understanding these important and yet not entirely untangled relationships and

the role of immune cells in osteosarcoma development. Lastly, it would be of great interest and importance to extend the application of the model and to adapt it for the needs of metastatic bone tumour engineering.

Personal Bibliography

Three first-author publications in peer-reviewed journals:

• Menshikh, K., Reddy, A. K., Cochis, A., Fraulini, F., Zambon, A., Lusvardi, G., & Rimondini, L. (2024). Bifunctional Mesoporous Glasses for Bone Tissue Engineering: Biological Effects of Doping with Cerium and Polyphenols in 2D and 3D In Vitro Models. Biomaterials and Biosystems, 100095. https://doi.org/10.1016/j.bbiosy.2024.100095

• Kovrlija, I., Menshikh, K. (shared 1st author), Abreu, H., Cochis, A., Rimondini, L., Marsan, O., Rey, C., Combes, C., Locs, J., & Loca, D. (2024). Challenging applicability of ISO 10993- 5 for calcium phosphate biomaterials evaluation: Towards more accurate in vitro cytotoxicity assessment. Biomaterials Advances, 160, 213866. https://doi.org/10.1016/J.BIOADV.2024.213866

• Menshikh, K., Banicevic, I., Obradovic, B., & Rimondini, L. (2023). Biomechanical Aspects in Bone Tumor Engineering. Tissue Engineering Part B: Reviews. https://doi.org/10.1089/ten.teb.2023.0106

Three co-author publications:

• Minaychev, V., Teterina, A., Smirnova, P., Menshikh, K., Senotov, A., Kobyakova, M., Smirnov, I., Pyatina, K., Krasnov, K., Fadeev, R., Komlev, V., & Fadeeva, I. (2024). Composite Remineralization of Bone-Collagen Matrices by Low-Temperature Ceramics and Serum Albumin: A New Approach to the Creation of Highly Effective Osteoplastic Materials. Journal of Functional Biomaterials, 15(2), 27. https://doi.org/10.3390/jfb15020027

• Kovrlija, I., Menshikh, K., Marsan, O., Rey, C., Combes, C., Locs, J., & Loca, D. (2023) Exploring the Formation Kinetics of Octacalcium Phosphate from Alpha-Tricalcium Phosphate: Synthesis Scale-Up, Determination of Transient Phases, Their Morphology and Biocompatibility. Biomolecules, 13(3), 462. https://doi.org/10.3390/biom13030462

• Bonartsev, A. P., Lei, B., Kholina, M. S., Menshikh, K. A., Svyatoslavov, D. S., Samoylova, S. I., Sinelnikov, M. Y., Voinova, V. V., Shaitan, K. V., Kirpichnikov, M. P., & Reshetov, I. V. (2022) Models of head and neck squamous cell carcinoma using bioengineering approaches. 4 Critical Reviews in Oncology/Hematology, 175, 103724. https://doi.org/10.1016/j.critrevonc.2022.103724

Funding

This work got support from the European Union’s Horizon 2020 research and innovation programme under grant agreement No. under the Marie Skłodowska-Curie Grant Agreement No. 860462 (PREMUROSA).

Acknowledgements

I express my deepest gratitude to my supervisor, Professor Lia Rimondini, whose leadership, support, and provision of resources and collaborations have been invaluable throughout this journey. I am truly grateful for her guidance and encouragement. I would like to express my sincere appreciation to Professor Andrea Cochis for his tutelage and constant presence, always ready to offer assistance and wisdom. My appreciation extends to my colleagues Farah Daou, Alessandro Scalia, Ajay Kumar, Ziba Najmi, and Jamil Kandalaft, I owe a debt of gratitude for their generous assistance and acceptance. Their collaboration and friendship have enriched this experience immeasurably. I am indebted to all the professors of PREMUROSA for their guidance, invaluable advice, and timely support, with special mention to my co-supervisor Professor Janis Locs, collaborators Professor Dagnija Loca and Professor Jonathan Massera for their expertise, and Professors Bojana Obradovic and Abhay Pandit for their guidance and support during the secondments. A special acknowledgement goes to the PREMUROSA Early Stage Researchers, particularly with whom I closely collaborated: Ilijana Kovrlija, Ivana Banicevic, and Virginia Alessandra Gobbo. Their dedication and partnership have been influential in the success of our endeavours.

To my family and friends, I am deeply grateful for their support and encouragement throughout this journey. Their love and belief in me sustained me through the challenges and triumphs of this fellowship.